

**Master-slave Force-reflecting Resolved Motion
Control of Hydraulic Mobile Machines**

by
Ming Zhu

B.Sc., Shanghai Jiao Tong University, China, 1987

A THESIS SUBMITTED IN PARTIAL FULFILLMENT OF
THE REQUIREMENTS FOR THE DEGREE OF
MASTER OF APPLIED SCIENCE

in

THE FACULTY OF GRADUATE STUDIES
DEPARTMENT OF ELECTRICAL ENGINEERING

We accept this thesis as conforming
to the required standard

THE UNIVERSITY OF BRITISH COLUMBIA

April 1994

© Ming Zhu, 1994

In presenting this thesis in partial fulfilment of the requirements for an advanced degree at the University of British Columbia, I agree that the Library shall make it freely available for reference and study. I further agree that permission for extensive copying of this thesis for scholarly purposes may be granted by the head of my department or by his or her representatives. It is understood that copying or publication of this thesis for financial gain shall not be allowed without my written permission.

Department of Electrical Engineering

The University of British Columbia
Vancouver, Canada

Date November 29, 84

Abstract

Issues concerning the design and implementation of master-slave force-reflecting resolved motion control of hydraulic mobile machines are addressed in this thesis.

Network concepts and linear system theory are used to design and analyze general force-reflecting teleoperator systems to achieve high performance while maintaining stability. A new control structure is proposed to achieve "transparency" for teleoperator systems under rate control. A novel approach to stability analysis of the stiffness feedback strategy proposed in previous work is provided which, under certain condition, guarantees global asymptotic stability of the teleoperator system. The system could be either under rate or position control and could be subject to time-delays, nonlinearities or active environments.

The closed-form inverse kinematics solutions of an excavator and a feller-buncher, which are four and five degree-of-freedom manipulators respectively, are provided to achieve resolved-motion of the manipulator's end-effector.

Using the UBC magnetically levitated joystick, the master-slave force-reflecting resolved motion control has been successfully implemented on a CAT-215 excavator and a CAT-325 feller-buncher. Machine experiments demonstrate the effectiveness of this control strategy in improving productivity and safety of general hydraulic mobile machines.

Table of Contents

Abstract	ii
List of Tables	vi
List of Figures	vii
Acknowledgments	x
1 Introduction	1
1.1 Motivation	3
1.2 Previous Work	6
1.3 Thesis Overview	9
2 Resolved Motion	10
2.1 Overview	10
2.2 Inverse Kinematics of an Excavator	12
2.3 Inverse Kinematics of a Feller-buncher	16
2.3.1 Inverse Kinematics: Approach 1	18
2.3.2 Inverse Kinematics: Approach 2	20
2.3.3 Some Comments on the Inverse Kinematics	24
3 Force Reflection	25
3.1 Network Representation of Teleoperator System	26
3.2 General Teleoperator Structure	28
3.3 Force-reflecting Control	32
3.3.1 Coordinating Force	32

3.3.2	Force Feedback	34
3.4	Transparency	37
3.4.1	Achieving Transparency Under Position Control	37
3.4.2	Achieving Transparency Under Rate Control	43
3.4.3	Achieving Transparency Via Impedance Identification	48
4	Stiffness Feedback	50
4.1	Principle	50
4.2	Stability	52
5	System Overview	62
5.1	Master — Maglev Joystick	63
5.1.1	System Configuration	64
5.1.2	Sensor and actuator	65
5.1.3	Control about the Remote Center of Compliance	66
5.2	Slave — Hydraulic Mobile Machines	69
5.3	Computing System	70
6	Machine Experiments	72
6.1	Endpoint Force Sensing	72
6.1.1	Modeling	72
6.1.2	Torque Computations	78
6.1.3	Recursive Least-squares Link Parameter Estimation	81

6.2	Excavator Experiments	90
6.2.1	Resolved Motion Control	91
6.2.2	Applying a Desired Force	96
6.3	Feller–buncher Experiments	99
6.3.1	Desired Force Tracking	102
6.3.2	Complete Tree Cutting Process	105
6.3.3	Practical Issues	107
7	Conclusions	111
7.1	Thesis Contributions	111
7.2	Further Work	112
	References	113

List of Tables

2.1	Excavator link Denavit–Hartenberg parameters	13
2.2	Feller–buncher link Denavit–Hartenberg parameters	17
6.3	Piston geometry of the excavator	78
6.4	Piston geometry of the feller-buncher	78
6.5	Joint linkage geometry of the excavator	80
6.6	Joint Linkage geometry of the feller-buncher	80
6.7	Gain selections for the excavator experiments	90
6.8	Maximum feedback force for the excavator experiments	91
6.9	Gain selections for the feller-buncher experiments	99
6.10	Maximum feedback force for the feller-buncher experiments	100
6.11	Detent parameters for the feller-buncher experiments	102

List of Figures

1.1	Kinematically similar master-slave system	1
1.2	Kinematically dissimilar master-slave system	2
1.3	Excavator schematic	4
1.4	Photograph of a typical excavator	4
1.5	Feller-buncher schematic	5
1.6	Photograph of a typical feller-buncher	5
2.7	Excavator configuration	13
2.8	Projection of excavator onto plane	14
2.9	Feller-buncher configuration	16
3.10	Ideal teleoperator system	25
3.11	Network concepts	26
3.12	Network representation of teleoperator system	27
3.13	General teleoperator structure: After Lawrence, 1992	29
3.14	Closed-loop stability analysis	31
3.15	Position-position structure	32
3.16	Network representation of position-position structure	33
3.17	Mechanical equivalence of position-position structure	33
3.18	Rate-position structure	34
3.19	Position-force structure	35
3.20	Intervient impedance	40
3.21	Achieving transparency under rate control	44
3.22	Achieving transparency via parameter identification	49

4.23	Comparison of two rate control structures	50
4.24	Stiffness adjustment scheme	51
4.25	Stiffness feedback control block diagram	52
4.26	Trajectory in phase plane	57
4.27	Trajectory in phase plane	58
4.28	Trajectory in phase plane	60
4.29	Trajectory in phase plane	61
5.30	Overall system configuration	62
5.31	Maglev Joystick system configuration	64
5.32	Maglev Joystick assembly	65
5.33	Frame assignment	67
5.34	VME cage configuration	70
6.35	Two-bar mechanical linkage	79
6.36	Four-bar mechanical linkage	79
6.37	Excavator link parameter identification	82
6.38	Excavator link parameter identification	83
6.39	Excavator link parameter identification	84
6.40	Excavator link parameter identification	85
6.41	Feller-buncher link parameter identification	86
6.42	Feller-buncher link parameter identification	87
6.43	Feller-buncher link parameter identification	88
6.44	Feller-buncher link parameter identification	89
6.45	Excavator resolved motion control: bucket straight up	92
6.46	Excavator resolved motion control: bucket straight down	93

6.47	Excavator resolved motion control: bucket straight out	94
6.48	Excavator resolved motion control: bucket straight in	95
6.49	Excavator stiffness control: applying a desired force	97
6.50	Excavator force control: applying a desired force	98
6.51	Detent implementation	100
6.52	Conventional position control	101
6.53	Feller-buncher stiffness control: force tracking	103
6.54	Feller-buncher control without force-reflection: force tracking	104
6.55	Feller-buncher stiffness control: tree cutting process	106
6.56	Feller-buncher step response: boom	108
6.57	Feller-buncher step response: stick	109
6.58	Feller-buncher step response: tilt	110

Acknowledgments

I would like to thank my supervisor Tim Salcudean for his support and guidance in my thesis work. I wish to thank Peter Lawrence and Dan Chan for their invaluable assistance and encouragement during the enduring machine experiments. I would also like to thank Niall Parker and Tim Vlaar for their helpful discussions and advice.

Special thanks to my wife Jane Zhang for her support and understanding.

Chapter 1 Introduction

Due to the fact that fully autonomous robots could not be realized using the latest technology, researchers began to concentrate on combining human versatility and expertise with machines. In some applications such as microsurgery, perhaps it will never be possible to have a robot acting alone.

The idea of using a master manipulator to command a slave manipulator can be traced back to the pioneering work by Goertz and his colleagues in the late 1940s when the first recognizable mechanical master-slave manipulator was built. Later in the early 1950s, the electrical servo was introduced. Most of these early designs exploit a kinematically similar master and slave because of the simplicity of the required controller, see Figure 1.1. Corresponding joint servos between the master and slave are tied together through electrical means. As a result, only position control in which the position of the master is interpreted as a position command to the slave, can be used.

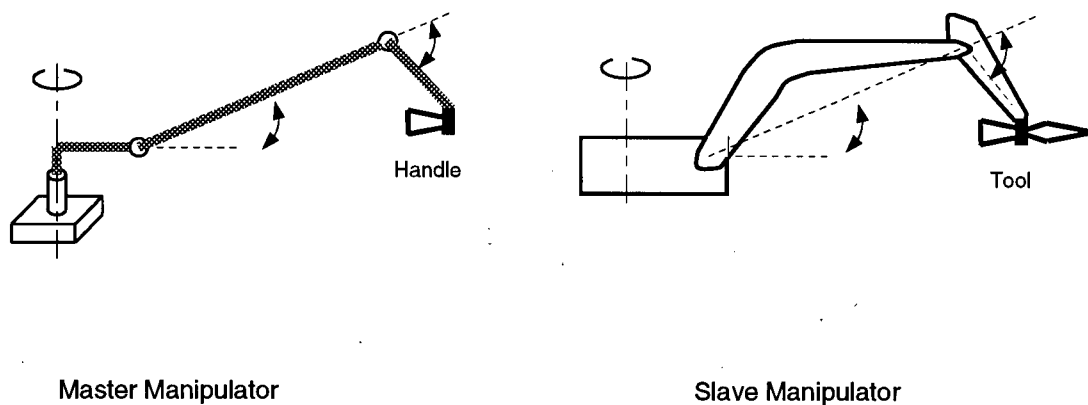


Figure 1.1 Kinematically similar master-slave system

Later, multi-degree-of-freedom joysticks were used as the input device to command the slave manipulator (see Figure 1.2). This structure soon gained its popularity due to the fact that the joystick can be used universally and usually takes less space. Rate control, in which the position of the master is interpreted as a velocity command to the slave, combined with conventional position control can be realized. For example, the space shuttle remote manipulator system is provided with both position and rate control modes [1]. When the joystick controls the motion of the endpoint of the slave directly, we call it resolved motion control.

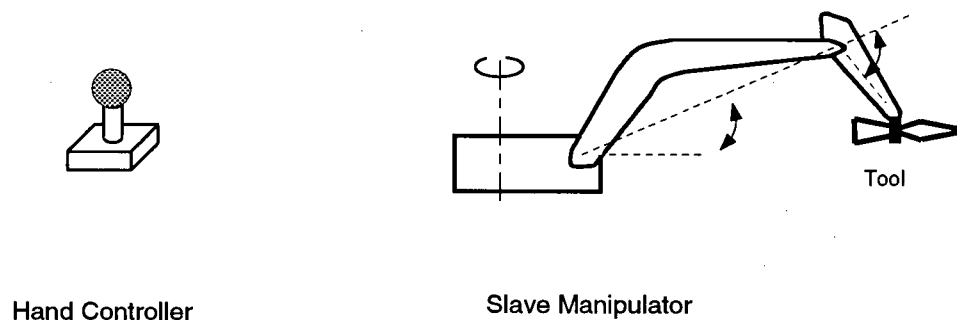


Figure 1.2 Kinematically dissimilar master-slave system

Contact information is helpful to the operator in reducing contact force, therefore reducing damages to the remote object. It also helps an operator probing in an uncertain environment, and reduces task completion time. Although this information can be provided by visual display, the most natural and efficient way is to transmit it directly to the operator's hand. In the case of multiaxial operation, a visual display is not acceptable to the user. When the contact force is reflected via the master actuator to the operator's hand, the teleoperator system is said to be controlled bilaterally, and the operator is said to be kinesthetically coupled to the environment.

The early application of teleoperator systems were mainly in the nuclear industry to remove radioactive materials without involving the human in the hazardous environment. The original

idea of manipulating objects remotely was soon broadened to include working on a different power scale, for instance, as a “man-amplifier” [2]. Teleoperator systems have the potential to play an important role in future remote or hazardous operations, such as space servicing, undersea exploration, and mining and in delicate operations such as microsurgery, microassembly and microchemistry.

1.1 Motivation

Hydraulic mobile machines can be found in various industries including forestry, mining and construction. To operate a conventional hydraulic mobile machine such as an excavator (Figure 1.3) or a feller-buncher (Figure 1.5), an operator uses two joysticks to control the individual displacements of the hydraulic cylinders of the machine in an uncoordinated way. In order to achieve a desired end-effector motion, e.g. a straight line motion, a complicated two-handed maneuver must be executed. It usually takes a few months to train an operator.

The advantages of applying resolved motion control to these machines are the following:

1. Simple, intuitive, single-hand operation.
2. High performance, since accurate motion, such as a straight line, can be obtained.
3. Reduced machine wear, since unnecessary joint motion is reduced to a minimum.
4. Increased productivity and safety, since the machine moves in an intuitive way.

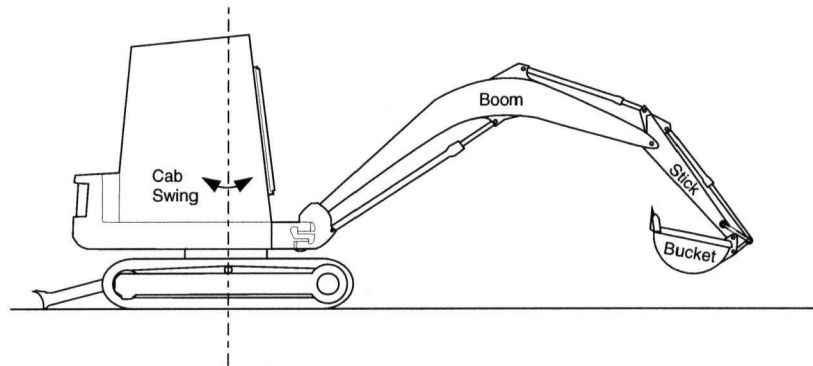


Figure 1.3 Excavator schematic¹



Figure 1.4 Photograph of a typical excavator

¹ Drawing by S. Tafazoli

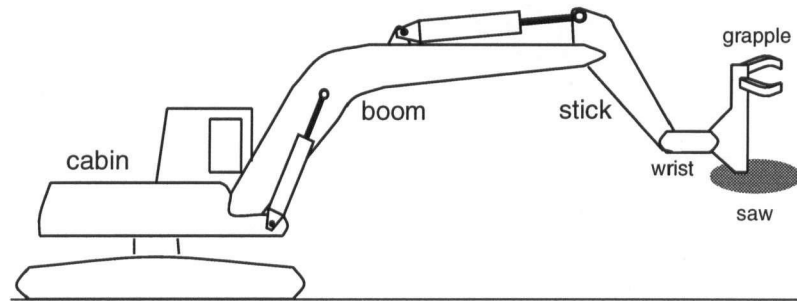


Figure 1.5 Feller-buncher schematic²



Figure 1.6 Photograph of a typical feller-buncher

² Drawing by N. Parker

Currently, an experienced operator depends solely on cues such as engine noise and machine motion to determine its load. High contact force can easily cause damage to the task, even to the machine itself.

The advantages of applying force reflection to the control of these machines are the following:

1. Improved performance, as more delicate tasks can be achieved.
2. Improved safety, since machine tip-over can be avoided by pushing the joystick back to the center under computer control.
3. Reduced machine wear, as the operator is more able to determine the machine load.

For a detailed description of applications of these hydraulic mobile machines in construction and forestry industry, refer to [3].

The application of resolved motion control to general hydraulic machines was first investigated by Lawrence *et al.* [4]. Later, force-reflecting resolved control was applied by Parker [3] to a three degree-of-freedom log-loader. Our goal in this project was focusing on the application of force-reflecting resolved control to a wider variety of machines such as excavators and feller-bunchers and addressing related issues.

1.2 Previous Work

The first recognizable mechanical master-slave manipulator was built in the late 1940s by Goertz and his colleagues. Later in the early 1950s, an electric servomanipulator system with force reflection capacity was introduced [5].

A survey on different universal joysticks can be found in [6].

A dissimilar master and slave teleoperator system was studied by Jansen *et al.* [7] in which force-reflection based on the master and slave Jacobians was proposed to control a 7-DOF slave manipulator.

A comparison between position and rate control was done by Kim *et al.* [8]. Position control is recommended for small workspaces with fast manipulators, while rate control is recommended for large workspaces with slow manipulators.

The design of force-reflecting teleoperator systems for robot surgery were reported by Sabatini *et al.*[9]. A mini six-degree-of-freedom magnetically levitated wrist designed for microsurgery experiments was designed by Yan [10].

The human dynamics in response to visual and force feedback was modelled and incorporated into the controller design and evaluation by Lee *et al.* [11]. The role of the controller was defined as modifying the dynamic characteristics of the master and slave arms to achieve a desirable one.

In [12], the force applied by the operator was used locally at the master side to modify its dynamics so that a “heavier” or a “lighter” master can be easily realized.

Hard contact with direct force feedback was examined by Hannaford *et al.* [13]. The effect of the operator in stabilizing the system was reported as in much the same manner as local damping feedback of the hand controller. It was suggested that the human operator impedance be estimated on-line in order to find the minimum necessary damping for the system. Salcudean and Wong [14] added damping which is proportional to the amount of contact force to the system to maintain hard contact stability, therefore avoiding “sluggishness” during free motion.

Force reflection under time delay was investigated by Spong and Anderson [15], via scattering theory. Stability was achieved by introducing a control law that prevents the communication block from generating energy. However, Lawn and Hannaford [16] reported a 50% increase of task

completion time with these passivity based methods. Kim *et al.* [17] proposed compliant control in which the feedback of the contact force is done locally at the slave side without kinesthetic force feedback so that the force feedback loop does not include a long communication time delay. Hannaford [18] argued that local force feedback reduces stability problem at the price of telemanipulation fidelity.

Bilateral impedance control was proposed by Hannaford [19], in which force and velocity sensing were used at both the master and slave side to identify the impedances of the operator and environment to make the system transparent. Raju *et al.* [20] introduced a teleoperator structure in which with velocity sensing the gains of the controller are selected based on the knowledge of the human operator and the task impedance. In order to achieve “transparency”, infinite gains are required.

It has been suggested by authors such as Salcudean [21], Lawrence [22] and Yokokohji [23] that the operator hand force should be fed forward to the slave side in order to achieve transparency. Salcudean and Wong applied this approach to a master-slave manipulator system with identical six-degree-of-freedom magnetically levitated wrists. Yokokohji and Yoshikawa reported similar work on a single degree of freedom system.

Force reflection based on a kinematically similar master-slave teleoperator structure was proposed for the control of excavators by Ostoja-Starzewski and Skibniewski [24]. A “Smart Shovel” which can be controlled remotely to remove hazardous waste with force reflection capability was reported in [25].

The application of teleoperation ideas to general hydraulic machines was investigated by Lawrence *et al.* [4]. Resolved motion control of such machines was found to be useful in reducing operator training time [26]. Force-reflection for hydraulic machines was previously treated by

Parker *et al.* [3]. A three degree-of-freedom log-loader was controlled by a magnetically levitated joystick; a stiffness adjustment scheme was used for force reflection under rate control to realize stable operation.

1.3 Thesis Overview

The remainder of this thesis is divided into 7 chapters. Resolved motion control of hydraulic mobile machines is treated in Chapter 2. Transparency and stability issues related to force reflecting control of teleoperator system are investigated in Chapter 3. The analysis of stiffness feedback control is provided in Chapter 4. Chapter 5 gives an overview of the entire system which includes the master, slave and computing system. Chapter 6 presents results of machine experiments. Finally Chapter 7 draws a conclusion and makes some suggestions for future work.

Chapter 2

Resolved Motion

Resolved motion control requires on-line computation of inverse kinematics. In this chapter, closed-form inverse kinematics solutions are provided for typical hydraulic mobile machines, excavators and feller-bunchers, which are four and five DOF manipulators respectively.

2.1 Overview

There are two types of problems in the kinematic analysis of manipulators. The first type is forward kinematics, in which the endpoint location has to be found given the joint displacement. The second type is inverse kinematics, which is the other way around. For serial manipulators, the forward kinematics can be easily carried out by a matrix recursion while the inverse kinematics is complicated because the governing equations are highly nonlinear. In the case of rate control, one approach is to transform the manipulator velocity from Cartesian space to joint space via an inverse Jacobian mapping, that is

$$\dot{q} = J^{-1}(q)V \quad (2.1)$$

where V and \dot{q} are the manipulator's velocities in Cartesian space and joint space respectively and J is the manipulator's Jacobian. Since position error can accumulate, the inverse Jacobian method suffers from low accuracy.

It is known that in order to place an endpoint frame freely in three dimensional space, the manipulator must have at least 6 DOF. For manipulators with 6 or more DOF, the inverse kinematics problem can be formulated as follows: given the endpoint frame position and orientation, find the joint displacements.

The methods of solving the inverse kinematics problem fall into two categories:

1. Closed-form solution, *i.e.* an algebraic equation relating the given position and orientation of the endpoint to only joint displacements (see [27]).
2. Numerical solution, *i.e.* an iterative algorithm for solving a system of six nonlinear equations (see [28, 29, 30, 31]).

When the manipulator has 6 DOF, the system of six nonlinear equations has a solution. When the manipulator has more than 6 DOF, the system of six nonlinear equations is underdetermined, thus there may be multiple solutions. In this case, an objective function can be used to select a “best” solution among them.

When the manipulator has less than 6 DOF, the system of six nonlinear equations is overdetermined, so there may be no solution at all. Instead of solving a system of nonlinear equations, one approach is to solve an optimization problem, that is, find a “best” fit in some sense. This usually requires an iterative procedure. Another approach is to carefully formulate the problem with some constraint in mind so that the solutions can be guaranteed (hopefully a closed-form solution). The philosophy behind this is never to force a manipulator to do anything beyond its capacity while, at the same time, fully utilizing the degrees of freedom the manipulator provides. For a simple example, we should not expect a planar manipulator to go out of that plane. The inverse kinematics problem can be easily formulated and solved in this manner for a manipulator with few degrees of freedom, but as the number of degrees of freedom increases, the problem becomes more difficult.

A few comments about closed-form solutions versus numerical solutions are in order. Generally speaking, closed-form solutions are preferred. There are two major reasons. First, most of the iterative algorithms are considered “local methods” which requires an initial close guess to

the exact solution; they may lack stability and reliability. Numerical solution can not find multiple solutions. Second, iterative algorithms usually require more time to compute a solution, so they are used mainly for off-line applications. The disadvantage of closed-form solutions are their dependence on manipulator structure, that is only certain classes of manipulators allow closed-form solutions. For example, it was found that a sufficient condition for a closed-form solution for a six DOF manipulator is to have three adjacent joint axes intersecting at a common point or any three adjacent joints axes parallel to each other. The problem becomes more critical for kinematically redundant robots, for which the number of DOF exceeds the required six coordinates necessary to attain arbitrary location in the three-dimensional work space. In comparison, many iterative algorithms can treat general manipulators without special considerations.

2.2 Inverse Kinematics of an Excavator

An excavator schematic is shown in Figure 2.7. Considering the four DOF nature of excavator, the inverse kinematics problem can be formulated as follows: given the endpoint frame position and its rotation angle along Z_1 of frame C_1 , find the four joint angles. The endpoint frame position is given in cylindrical coordinates, that is (z_e, r_e, θ_e) ; the rotation angle is expressed as θ_{Z_1} .

The relationship between Cartesian coordinates and cylindrical coordinates is

$$\begin{aligned}x &= r_e \cos \theta_e \\y &= r_e \sin \theta_e \\z &= z_e\end{aligned}\tag{2.2}$$

There are two reasons for using cylindrical coordinates: first, as we will see later, it is easier to solve the inverse kinematics using cylindrical coordinates; second, it is more natural to map the hand control command into cylindrical coordinates since the operator moves with the cabin.

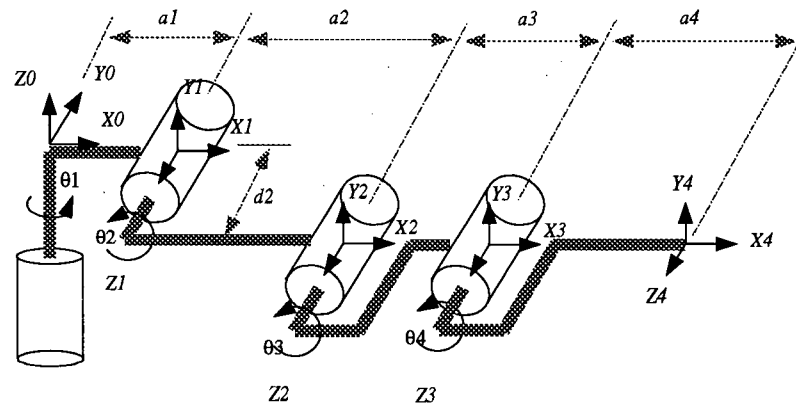


Figure 2.7 Excavator configuration

Index	θ_i	d_i	a_i	α_i
1	θ_1	0	a_1	$\frac{\pi}{2}$
2	θ_2	d_2	a_2	0
3	θ_3	0	a_3	0
4	θ_4	0	a_4	0

Table 2.1 Excavator link Denavit-Hartenberg parameters

Figure 2.8 shows the projection of excavator onto a plane. There are many ways in solving this inverse kinematics problem. Here we use a geometrical method. First we examine the case when endpoint frame is at the end of stick, that is, the origins of frame three and frame four coincide. Due to the physical constraint, only the right and above arm configuration is considered.

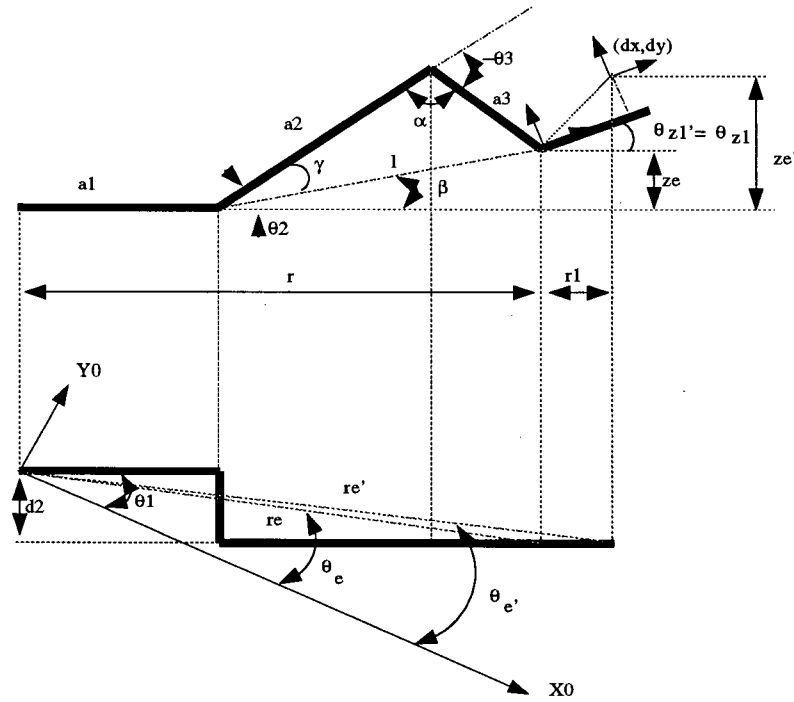


Figure 2.8 Projection of excavator onto plane

Given (z_e, r_e, θ_e) , after a few algebraic manipulations [3], it is easy to derive the following

$$\begin{aligned}
 \theta_1 &= \theta_e + \tan^{-1}\left(\frac{d_2}{r}\right) \\
 \theta_3 &= -(\pi - \alpha) \\
 \alpha &= \cos^{-1}\left(\frac{a_2^2 + a_3^2 - l^2}{2a_2a_3}\right) \\
 l &= \sqrt{z_e^2 + (r - a_1)^2} \\
 r &= \sqrt{r_e^2 - d_2^2} \\
 \theta_2 &= \beta + \gamma \\
 \beta &= \tan^{-1}\left(\frac{z_e}{r - a_1}\right) \\
 \gamma &= \sin^{-1}\left(\frac{a_3 \sin \alpha}{l}\right)
 \end{aligned} \tag{2.3}$$

and

$$\theta_4 = \theta_{Z_1} - \theta_2 - \theta_3 \quad (2.4)$$

If the endpoint frame is not at the end of stick, the following procedure can be used. Let the position and orientation of the endpoint frame be $C'_4: (z'_e, r'_e, \theta'_e, \theta'_{Z_1})$. Define the origins of frame C_4 and C'_4 as O_4 and O'_4 respectively. If the relation between the two origins is

$$O'_4 = C_4 [d_x, d_y, 0]' + O_4 \quad (2.5)$$

the inverse kinematics solution becomes

$$\begin{aligned} \theta_1 &= \theta'_e + \tan^{-1} \left(\frac{d_2}{r + r_1} \right) \\ \theta_3 &= -(\pi - \alpha) \\ \alpha &= \cos^{-1} \left(\frac{a_2^2 + a_3^2 - l^2}{2a_2a_3} \right) \\ l &= \sqrt{z_e'^2 + (r - a_1)^2} \\ r &= \sqrt{r_e'^2 - d_2^2} - r_1 \\ r_1 &= \sqrt{d_x^2 + d_y^2} \cos \left(\tan^{-1} \frac{d_y}{d_x} + \theta'_{Z_1} \right) \\ z_e &= z'_e - \sqrt{d_x^2 + d_y^2} \sin \left(\tan^{-1} \frac{d_y}{d_x} + \theta'_{Z_1} \right) \\ \theta_2 &= \beta + \gamma \\ \beta &= \tan^{-1} \left(\frac{z_e}{r - a_1} \right) \\ \gamma &= \sin^{-1} \left(\frac{a_3 \sin \alpha}{l} \right) \\ \theta_4 &= \theta'_{Z_1} - \theta_2 - \theta_3 \end{aligned} \quad (2.6)$$

assuming the specified endpoint frame is within the manipulator's work space; Otherwise, solution does not exist.

2.3 Inverse Kinematics of a Feller-buncher

The feller-buncher is a five DOF manipulator which is mainly used for forestry harvesting. Figure 2.9 shows its schematic. The additional degree of freedom makes its inverse kinematics problem more difficult to handle than the excavator. In the following, we introduce two closed-form solutions for which one is preferred to the other depending on operation situation. We will

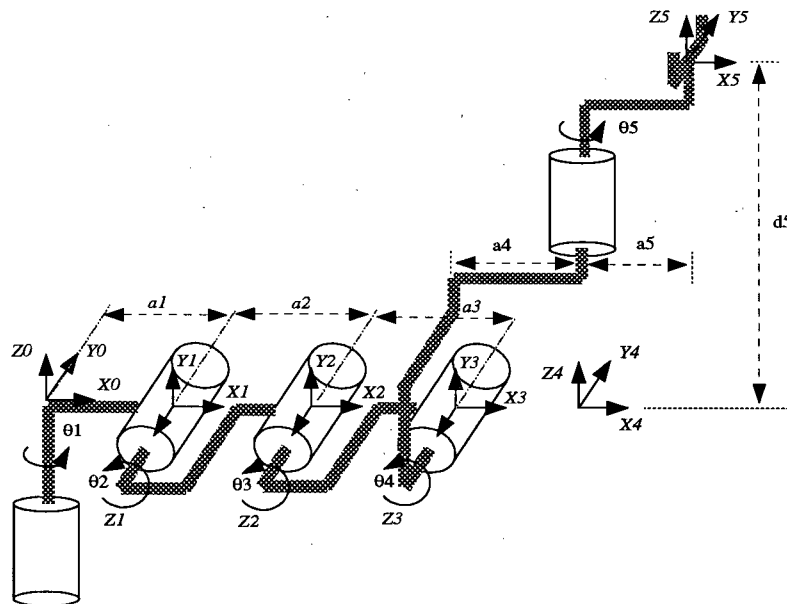


Figure 2.9 Feller-buncher configuration

show how the inverse kinematics problem should be formulated so that a closed-form solution is guaranteed.

We add a frame C'_5 attached to the feller-buncher head, such that its initial position coincides with C_4 (see Figure 2.7).

Define

$$\begin{bmatrix} C'_5 & O'_5 \\ 0 & 1 \end{bmatrix} = \begin{bmatrix} C_0 & O_0 \\ 0 & 1 \end{bmatrix} {}^5_0T \quad (2.7)$$

where 5_0T is the homogeneous transformation, having the following special structure

$${}^5_0T = \begin{bmatrix} e^{\phi k \times} e^{\theta j \times} e^{\psi k \times} & \begin{bmatrix} x \\ y \\ z \\ 1 \end{bmatrix} \\ 0 & \end{bmatrix} \quad (2.8)$$

where $(\phi \ \theta \ \psi)$ are Euler angles w.r.t. \underline{C}_0 . We observe that $\phi = \text{atan2}(y, x)$, but θ, ψ, x, y, z are independent variables.

Index	θ_i	d_i	a_i	α_i
1	θ_1	0	a_1	$\frac{\pi}{2}$
2	θ_2	0	a_2	0
3	θ_3	0	a_3	0
4	θ_4	0	a_4	$-\frac{\pi}{2}$
5	θ_5	d_5	a_5	0

Table 2.2 Feller–buncher link Denavit–Hartenberg parameters

The introduction of frame \underline{C}'_5 is important in solving the inverse kinematics of feller-buncher.

Assume the relationship between \underline{C}_5 and \underline{C}'_5 is

$$\begin{bmatrix} \underline{C}_5 & O_5 \\ 0 & 1 \end{bmatrix} = \begin{bmatrix} \underline{C}'_5 & O'_5 \\ 0 & 1 \end{bmatrix} \begin{bmatrix} I & d_o \\ 0 & 1 \end{bmatrix} \quad (2.9)$$

where d_o is a arbitrarily chosen constant vector. This assumption indicates that \underline{C}_5 can be positioned arbitrarily on the feller-buncher head. With \underline{C}'_5 , we can conclude that the homogeneous transformation between \underline{C}_o and \underline{C}_5 is in the following special form

$${}^5_0T = {}^5_0T \begin{bmatrix} I & d_o \\ 0 & 1 \end{bmatrix} = \begin{bmatrix} e^{\phi k \times} e^{\theta j \times} e^{\psi k \times} & e^{\phi k \times} e^{\theta j \times} e^{\psi k \times} d_o + \begin{bmatrix} x \\ y \\ z \end{bmatrix} \\ 0 & 1 \end{bmatrix} \quad (2.10)$$

where d_o is a constant vector, and $\phi = \text{atan2}(y, x)$. Note θ, ψ, x, y, z are independent variables.

Since the manipulator only has five DOF, we can not achieve arbitrary position with arbitrary orientation. Hence the target frame should be specified to be within the manipulator subspace; otherwise the solution may not exist at all. Here we propose two approaches.

2.3.1 Inverse Kinematics: Approach 1

Generally, if the operator specifies

$${}^5_0T_d = \begin{bmatrix} e^{\phi_a k \times} e^{\theta_a j \times} e^{\psi_a k \times} & \begin{bmatrix} x_d \\ y_d \\ z_d \end{bmatrix} \\ 0 & 1 \end{bmatrix} \quad (2.11)$$

there may be no solution at all. On the other hand, in some applications, it may not be crucial to specify ϕ_d , for instance, when the operator moves with the cabin. Thus, one solution is given by:

$$\begin{cases} \theta = \theta_d \\ \psi = \psi_d \\ e^{\phi k \times} e^{\theta j \times} e^{\psi k \times} d_o + \begin{bmatrix} x \\ y \\ z \end{bmatrix} = \begin{bmatrix} x_d \\ y_d \\ z_d \end{bmatrix} \\ \phi = \text{atan2}(y, x) \end{cases} \quad (2.12)$$

Define

$$e^{\theta_a j \times} e^{\psi_a k \times} d_o \equiv d_1 \equiv [d_{1x} \ d_{1y} \ d_{1z}]^T \quad (2.13)$$

to obtain that

$$\begin{cases} e^{\phi k \times} d_1 + \begin{bmatrix} x \\ y \\ z \end{bmatrix} = \begin{bmatrix} x_d \\ y_d \\ z_d \end{bmatrix} \\ \phi = \text{atan2}(y, x) \end{cases} \quad (2.14)$$

Since we have

$$e^{\phi k \times} d_1 = \begin{bmatrix} \cos\phi & -\sin\phi & 0 \\ \sin\phi & \cos\phi & 0 \\ 0 & 0 & 1 \end{bmatrix} \begin{bmatrix} d_{1x} \\ d_{1y} \\ d_{1z} \end{bmatrix} = \begin{bmatrix} \cos\phi d_{1x} - \sin\phi d_{1y} \\ \sin\phi d_{1x} + \cos\phi d_{1y} \\ d_{1z} \end{bmatrix} \quad (2.15)$$

thus the equation set (2.14) is equivalent to

$$\begin{cases} \cos\phi d_{1x} - \sin\phi d_{1y} + x = x_d \\ \sin\phi d_{1x} + \cos\phi d_{1y} + y = y_d \\ d_{1z} + z = z_d \\ \phi = \text{atan2}(y, x) \end{cases} \quad (2.16)$$

Substituting $\phi = \text{atan2}(y, x)$ into the second equation of equation set (2.16), we get

$$\begin{cases} \cos\phi d_{1x} - \sin\phi d_{1y} + x = x_d \\ \sin\phi d_{1x} + \cos\phi d_{1y} + \tan\phi x = y_d \end{cases} \quad (2.17)$$

Multiplying the first equation in (2.17) by $\sin\phi$ and the second by $\cos\phi$, we obtain that

$$x_d \sin\phi - y_d \cos\phi = -d_{1y} \quad (2.18)$$

Define

$$\begin{aligned} a^* &= -y_d \\ b^* &= x_d \\ c^* &= -d_{1y} \end{aligned} \quad (2.19)$$

thus we have

$$a^* \cos\phi + b^* \sin\phi = c^* \quad (2.20)$$

The solution for this equation is

$$\phi = \text{atan2}(b^*, a^*) \pm \text{atan2}\left(\sqrt{a^{*2} + b^{*2} - c^{*2}}, c^*\right) \quad (2.21)$$

Finally we have

$$\begin{cases} x = x_d - \cos\phi d_{1x} + \sin\phi d_{1y} \\ y = y_d - \sin\phi d_{1x} - \cos\phi d_{1y} \\ z = z_d - d_{1z} \\ \theta = \theta_d \\ \psi = \psi_d \end{cases} \quad (2.22)$$

Here we have located the position and orientation of C'_5 . We can see there are at most two possible solutions. Equations (2.14) should be checked to eliminate any extraneous solutions.

It is clear that

$$\theta_5 = \psi \quad (2.23)$$

Solving for $\theta_1, \theta_2, \theta_3, \theta_4$ is equivalent to the inverse kinematics problem of the excavator we have seen before.

Define

$$\begin{aligned}
 z'_e &= z \\
 r'_e &= \sqrt{x^2 + y^2} \\
 \theta'_e &= \phi \\
 \theta'_{Z_1} &= -\theta
 \end{aligned}
 \tag{2.24}$$

the solution can be summarized as following

$$\begin{aligned}
 \theta_1 &= \theta'_e \\
 \theta_3 &= -(\pi - \alpha) \\
 \alpha &= \cos^{-1} \left(\frac{a_2^2 + a_3^2 - l^2}{2a_2a_3} \right) \\
 l &= \sqrt{z_e^2 + (r - a_1)^2} \\
 r &= r'_e - r_1 \\
 r_1 &= a_4 \cos(\theta'_{Z_1}) \\
 z_e &= z'_e - a_4 \sin(\theta'_{Z_1}) \\
 \theta_2 &= \beta + \gamma \\
 \beta &= \tan^{-1} \left(\frac{z_e}{r - a_1} \right) \\
 \gamma &= \sin^{-1} \left(\frac{a_3 \sin \alpha}{l} \right) \\
 \theta_4 &= \theta'_{Z_1} - \theta_2 - \theta_3
 \end{aligned}
 \tag{2.25}$$

2.3.2 Inverse Kinematics: Approach 2

A five DOF manipulator can easily be found in applications such as welding or spray painting. Since the rotation along the gun axis direction is not important in these applications, five DOF is enough to do the job. In [27], the author joined the end effector to the grounded joint of the arm by a pair of hypothetical joints and links, then a complicated procedure was required to solved this hypothetical closed-loop spatial mechanism for joint displacements. Here we propose

an algebraic method. The inverse kinematics problem can be formulated as follows: given the position of frame C_5 and direction of X_5 , find the corresponding joint angles, that is, given

$${}^5_0T_d = \begin{bmatrix} m_1 & n_1^* & o_1^* & p_1 \\ m_2 & n_2^* & o_2^* & p_2 \\ m_3 & n_3^* & o_3^* & p_3 \\ 0 & 0 & 0 & 1 \end{bmatrix} \quad (2.26)$$

where only (m_1, m_2, m_3) and (p_1, p_2, p_3) are user specified. Compared with approach 1, this method is desirable in the case where the operator controls the machine from a fixed ground-based location.

As before, we have

$${}^5_0T = {}^5_0T' \begin{bmatrix} I & d_o \\ 0 & 1 \end{bmatrix} = \begin{bmatrix} e^{\phi k \times} e^{\theta j \times} e^{\psi k \times} & e^{\phi k \times} e^{\theta j \times} e^{\psi k \times} d_o + \begin{bmatrix} x \\ y \\ z \end{bmatrix} \\ 0 & 1 \end{bmatrix} \quad (2.27)$$

where d_o is a constant vector, $\phi = \text{atan2}(y, x)$ and θ, ψ, x, y, z are independent variables.

Since we have

$$d_o = [a_5 \quad 0 \quad d_5]^T \quad (2.28)$$

and

$$e^{\phi k \times} e^{\theta j \times} e^{\psi k \times} = \begin{bmatrix} c_\phi c_\theta c_\psi - s_\phi s_\psi & -c_\phi c_\theta s_\psi - s_\phi c_\psi & c_\phi s_\theta \\ s_\phi c_\theta c_\psi + c_\phi s_\psi & -s_\phi c_\theta s_\psi + c_\phi c_\psi & s_\phi s_\theta \\ -s_\theta c_\psi & s_\theta s_\psi & c_\theta \end{bmatrix} \quad (2.29)$$

where $c_\phi = \cos\phi$, $s_\phi = \sin\phi$ etc., we obtain

$$\begin{cases} c_\phi c_\theta c_\psi - s_\phi s_\psi = m_1 \\ s_\phi c_\theta c_\psi + c_\phi s_\psi = m_2 \\ -s_\theta c_\psi = m_3 \end{cases} \quad (2.30)$$

and

$$\begin{bmatrix} m_1 a_5 + d_5 c_\phi s_\theta \\ m_2 a_5 + d_5 s_\phi s_\theta \\ m_3 a_5 + d_5 c_\theta \end{bmatrix} + \begin{bmatrix} x \\ y \\ z \end{bmatrix} = \begin{bmatrix} p_1 \\ p_2 \\ p_3 \end{bmatrix} \quad (2.31)$$

$$\phi = \text{atan2}(y, x) \quad (2.32)$$

Now we have six unknowns $(x, y, z, \phi, \theta, \psi)$ and six equations (only two of (2.30) are independent).

The procedure to solve these equations is given by the following steps:

Step (A) If $s_\theta \neq 0$, from (2.31), we have that

$$\tan\phi = \frac{\sin\phi}{\cos\phi} = \frac{p_2 - m_2 a_5 - y}{p_1 - m_1 a_5 - x} = \frac{y}{x} \quad (2.33)$$

Solving for y/x , we get

$$\frac{y}{x} = \frac{p_2 - m_2 a_5}{p_1 - m_1 a_5} \quad (2.34)$$

thus we have

$$\phi = \text{atan2}(p_2 - m_2 a_5, p_1 - m_1 a_5) \quad \text{or} \quad \phi = \phi + \pi \quad (2.35)$$

If $s_\theta = 0$, from (2.31) we get

$$\begin{cases} y = p_2 - m_2 a_5 \\ x = p_1 - m_1 a_5 \end{cases} \quad (2.36)$$

we have the similar result

$$\phi = \text{atan2}(p_2 - m_2 a_5, p_1 - m_1 a_5) \quad (2.37)$$

We conclude that there are at most two solutions for ϕ , that is

$$\phi = \text{atan2}(p_2 - m_2 a_5, p_1 - m_1 a_5) \quad \text{or} \quad \phi = \phi + \pi \quad (2.38)$$

Step (B) If $s_\psi \neq 0$, from (2.30), we can get

$$\theta = \text{atan2}(-m_3, m_1 c_\phi + m_2 s_\phi) \quad \text{or} \quad \theta = \theta + \pi \quad (2.39)$$

If $s_\psi = 0$ then

$$\psi = \pm \frac{\pi}{2} \quad (2.40)$$

From (2.30) we have

$$\begin{cases} y/x = s_\phi/c_\phi = -m_1/m_2 \\ m_3 = 0 \end{cases} \quad (2.41)$$

From (2.31) we have

$$\begin{cases} m_1^2 a_5 + d_5 m_1 m_2 s_\theta + m_1 x = m_1 p_1 \\ m_2^2 a_5 - d_5 m_1 m_2 s_\theta + m_2 y = m_2 p_2 \end{cases} \quad (2.42)$$

Note the fact that

$$m_1^2 + m_2^2 + m_3^2 = 1 \quad (2.43)$$

Adding the two equations in (2.42), we get

$$a_5 = m_1 p_1 + m_2 p_2 \quad (2.44)$$

We conclude that there are infinite number of solutions for θ if $s_\psi = 0$. The necessary condition for $s_\psi = 0$ is

$$a_5 = m_1 p_1 + m_2 p_2 \quad (2.45)$$

and

$$m_3 = 0 \quad (2.46)$$

Step (C) From (2.30) we have

$$\begin{cases} -s_\theta c_\psi = m_3 \\ c_\theta c_\psi = m_1 c_\phi + m_2 s_\phi \\ s_\psi = c_\phi m_2 - s_\phi m_1 \end{cases} \quad (2.47)$$

Multiplying the first equation in (2.30) by $-s_\theta$ and the second by c_θ , we have

$$\begin{cases} s_\psi = c_\phi m_2 - s_\phi m_1 \\ c_\psi = -m_3 s_\theta + c_\theta (m_1 c_\phi + m_2 s_\phi) \end{cases} \quad (2.48)$$

thus

$$\psi = \text{atan2}(c_\phi m_2 - s_\phi m_1, -m_3 s_\theta + c_\theta (m_1 c_\phi + m_2 s_\phi)) \quad (2.49)$$

Step (D) The solutions for x , y , z can be obtained as

$$\begin{bmatrix} x \\ y \\ z \end{bmatrix} = \begin{bmatrix} p_1 \\ p_2 \\ p_3 \end{bmatrix} - \begin{bmatrix} m_1 a_5 + d_5 c_\phi s_\theta \\ m_2 a_5 + d_5 s_\phi s_\theta \\ m_3 a_5 + d_5 c_\theta \end{bmatrix} \quad (2.50)$$

From the above procedure, we can see that there are at most four solutions to this problem, but (2.30) and (2.32) should be checked to eliminate extraneous solutions if any. Now that we have ϕ , θ , ψ , x , y , z , the next step to find the required joint angles is the same as seen in Approach 1.

It is clear that approach 1 is easier than approach 2, and introduces fewer extraneous solutions.

2.3.3 Some Comments on the Inverse Kinematics

If we know that the target frame is within the manipulator subspace, namely

$${}^5_0T_d = \begin{bmatrix} e^{\phi_a k \times} e^{\theta_{aj} \times} e^{\psi_{ak} \times} & \begin{bmatrix} x_d \\ y_d \\ z_d \\ 1 \end{bmatrix} \\ 0 & \end{bmatrix} \quad (2.51)$$

satisfies the constraint, then the inverse kinematics is straightforward, that is

$$\begin{aligned} \phi &= \phi_d \\ \theta &= \theta_d \\ \psi &= \psi_d \end{aligned} \quad (2.52)$$

and

$$\begin{bmatrix} x \\ y \\ z \end{bmatrix} = \begin{bmatrix} x_d \\ y_d \\ z_d \end{bmatrix} - e^{\phi_a k \times} e^{\theta_{aj} \times} e^{\psi_{ak} \times} d_0 \quad (2.53)$$

In practice, it is very difficult, if at all possible, to obtain the desired 5_0T_d within the manipulator subspace without first solving the inverse kinematics. In fact, the two methods we propose here amount to avoid using this assumption.

Chapter 3 Force Reflection

Two fundamental issues in force-reflection control of master-slave teleoperator system are stability and transparency. In fact, the stability problem is common for almost any closed-loop system. An ideal teleoperator system should be “transparent”; in other words, the operator should feel as if the task object were being handled directly.

Yokokhoji and Yoshikawa [23] define an ideal response of master-slave system is that the position and force responses of the master and slave arms are absolutely equal respectively. Similarly, Handlykken suggests that an ideal teleoperator system should be represented by an infinitely stiff and weightless mechanical connection between the end-effector of the master arm and the slave arm (Figure 3.10).

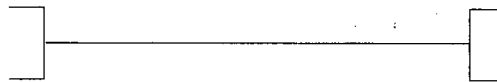


Figure 3.10 Ideal teleoperator system

Clearly, this definition only applies to those teleoperator systems in which slaves are controlled to follow the motion of the masters faithfully. In a lot of applications, the position mapping between the master and slave needs to be scaled either down or up. In some applications, for instance if the master has limited workspace, the slave is often controlled in rate mode; that is, the position of the master is interpreted as a velocity instead of position command to the slave.

What is a more general performance measure for teleoperator system? Generally speaking, the “feel” of an object can be characterized by the object’s smoothness and stiffness (or impedance in the dynamic case). However when a tool is used, it is the impedance of the task which becomes the major perception for the human operator. Naturally, we can define a teleoperator system to be

“transparent” if the impedance “felt” by the operator, or in other words transmitted to the operator via the master-slave system, equals that of the task [22]. Of course, in certain applications, such as microsurgery dealing with human tissue, it would be desirable to have a scaled version of the task impedance [32].

3.1 Network Representation of Teleoperator System

In network theory, an n-port is characterized by the relationship between effort, f (force, voltage) and flow, v (velocity, current). For a linear time-invariant (LTI) lumped one port network, this relationship is specified by its impedance, $Z(s)$, according to

$$Z(s) = \frac{F(s)}{V(s)} \quad (3.1)$$

where $F(s)$ and $V(s)$ are the Laplace transforms of f and v respectively. A LTI lumped two-port network can be represented by its hybrid matrix which is defined as

$$\begin{bmatrix} F_1 \\ -V_2 \end{bmatrix} = H(s) \begin{bmatrix} V_1 \\ F_2 \end{bmatrix} = \begin{bmatrix} h_{11} & h_{12} \\ h_{21} & h_{22} \end{bmatrix} \begin{bmatrix} V_1 \\ F_2 \end{bmatrix} \quad (3.2)$$

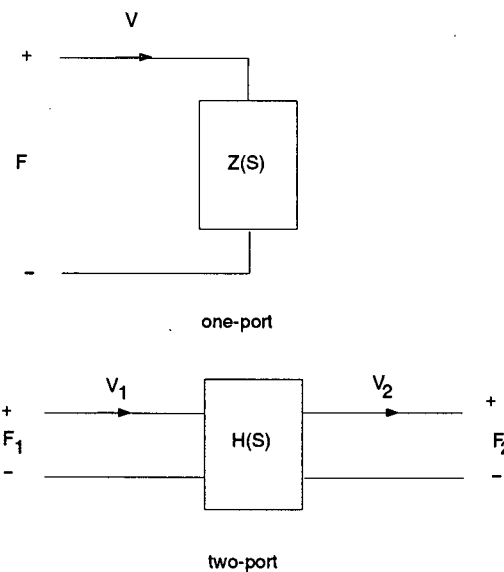


Figure 3.11 Network concepts

A suggested network representation of a master and slave telemanipulation system is a two-port connected between two one-ports, the operator and the environment [15, 19], see Figure 3.12.

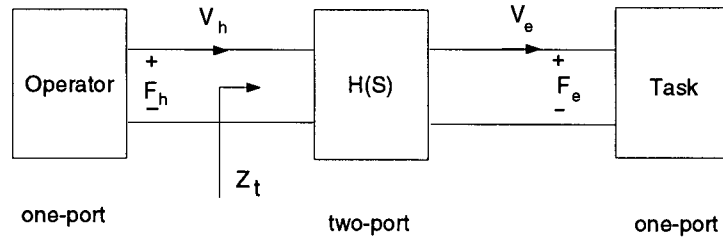


Figure 3.12 Network representation of teleoperator system

Using the hybrid matrix of the two-port and the task impedance

$$Z_e = \frac{F_e}{V_e} \quad (3.3)$$

we can express the impedance “felt” by the operator as

$$Z_t = \frac{F_h}{V_h} = \frac{h_{11}(1 + h_{22}Z_e) - h_{21}h_{12}Z_e}{1 + h_{22}Z_e} \quad (3.4)$$

Thus we have the following necessary and sufficient condition for transparency:

$$h_{11} = h_{22} = 0 \quad (3.5)$$

$$h_{12}h_{21} = -1$$

Another useful concept in network theory is passivity. In the case of master-slave systems, the condition for the total system to be stable is that the system itself must be passive if the operator and environment can be regarded as passive system [23]. One useful tool in determining passivity of a network is scattering theory .

Theorem [15]: A system is passive if and only if the norm of its scattering operator is less than or equal to one, that is

$$\|S(jw)\| = \sup \lambda^{\frac{1}{2}}[S^*(jw)S(jw)] \leq 1 \quad (3.6)$$

where $*$ denotes complex conjugate transpose and $\lambda^{\frac{1}{2}}(\cdot)$ denotes the square root of the maximum eigenvalue.

For a two-port network, the scattering operator can be related to its hybrid matrix as follows:

$$S(s) = \begin{bmatrix} 1 & 0 \\ 0 & -1 \end{bmatrix} (H(s) - I) (H(s) + I)^{-1} \quad (3.7)$$

Anderson etc. [15] apply the scattering theory to the two-port time delayed communication circuit which has the following hybrid matrix

$$H(s) = \begin{bmatrix} 0 & e^{-sT} \\ -e^{-sT} & 0 \end{bmatrix} \quad (3.8)$$

where T is the time delay in the communication line. It can be shown that the standard method of communicating forces and velocity between the master and slave in a teleoperator system leads to a nonpassive system for any time delay. This is the major cause of instability for position-position architecture. Traditionally, a large amount of damping is added to the system to deal with this problem. This in turn degrades the system performance making it feel "sluggish". The authors thus introduce an active control law to make the communication block identical to a two-port lossless transmission line.

Passivity is a sufficient, but not necessary condition for stability. Quite often the two-port master-slave subsystem is nonpassive while the entire system is stable. The passivity of the master-slave system guarantee the stability when connected to any passive load. However this guaranteed stability does not come without price. Lawn and Hannaford [16] reported a 50% increase of task completion time with the above passivity based methods.

3.2 General Teleoperator Structure

In a conventional position control teleoperator system, either the contact force or the slave position is fed back to the master to provide force reflection. The first is called direct force

feedback method, and the second is called coordinating force method. From the network point of view, there are no specific reasons for not using the position and force information bilaterally. The four-channel communication scheme gives us more freedom to achieve the desired hybrid matrix which fulfill the requirement for transparency. Here, we adopt much of the formalism presented in the earlier work by Lawrence [22]. A block diagram of a general teleoperator structure is shown in Figure 3.13.

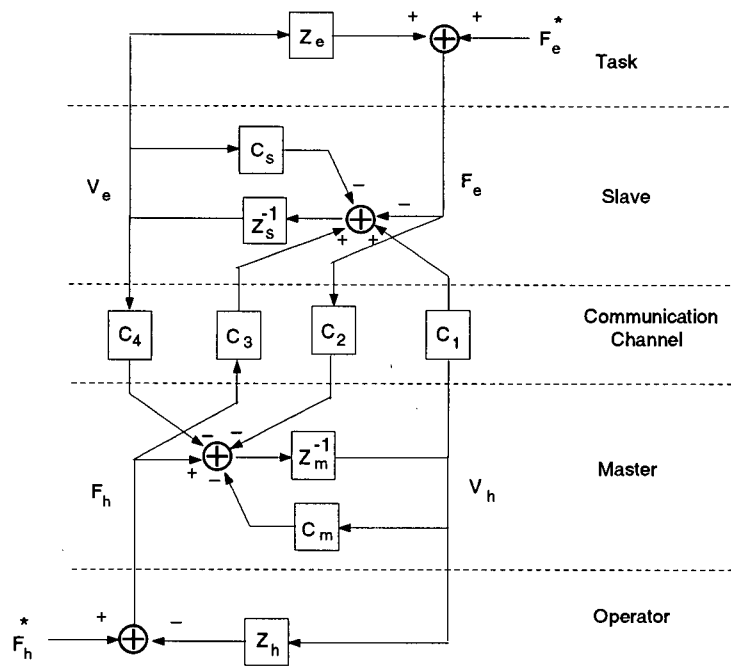


Figure 3.13 General teleoperator structure: After Lawrence, 1992

The symbols are defined as follow:

$$\begin{aligned}
 Z_m &= M_m s \\
 C_m &= B_m + K_m/s \\
 Z_s &= M_s s \\
 C_s &= B_s + K_s/s \\
 Z_h &= \text{the impedance of the operator's hand} \\
 &= M_h s + B_h + K_h/s \\
 Z_e &= \text{the impedance of the environment} \\
 &= M_e s + B_e + K_e/s
 \end{aligned} \tag{3.9}$$

where M_m and M_s are the masses of the master and the slave respectively; C_m and C_s are the transfer functions of the controllers; Assuming the operator's hand is a mass, damper and spring system, M_h , B_h , and K_h are the mass, damper and spring coefficients; M_e , B_e , and K_e are the mass, damper and spring coefficients of the task.

We can see the position-position and position-force structure are just two special cases of this general structure.

The hybrid matrix of this two-port teleoperator system can be easily derived as

$$\begin{aligned}
 h_{11} &= \frac{(Z_m + C_m)(Z_s + C_s) + C_1 C_4}{D} \\
 h_{12} &= \frac{C_2(Z_s + C_s) - C_4}{D} \\
 h_{21} &= -\frac{C_3(Z_m + C_m) + C_1}{D} \\
 h_{22} &= \frac{1 - C_2 C_3}{D}
 \end{aligned} \tag{3.10}$$

where

$$D = Z_s + C_s - C_3 C_4 \tag{3.11}$$

The transmitted impedance felt by the operator can be derived in terms of the block transfer functions as

$$Z_t = \frac{[(Z_m + C_m)(Z_s + C_s) + C_1C_4] + Z_e(Z_m + C_m + C_1C_2)}{(Z_s + C_s - C_3C_4) + Z_e(1 - C_2C_3)} \quad (3.12)$$

Z_t can be thought as the measure of transparency.

In linear control theory, stability of a closed-loop system can be checked by applying Nyquist criterion to its loop transfer function $LG = G(s)H(s)$. Thus LG can be regarded as the measure of stability. Assuming the task is just a passive impedance and reorganizing the block diagram of the general teleoperator system, we have the following for stability analysis.

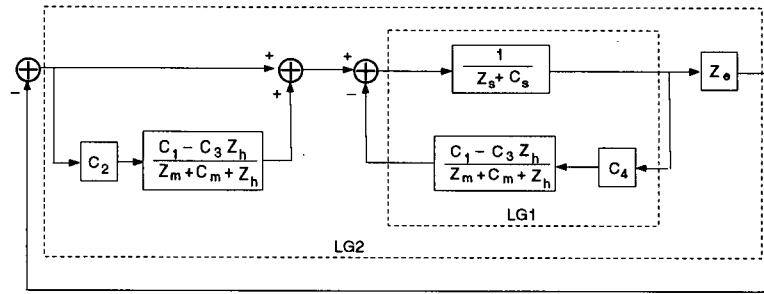


Figure 3.14 Closed-loop stability analysis

Assume that the individual master and slave control system are stable. C_1, C_2, C_3 and C_4 are user specified transfer functions which should also be designed to be stable. In order to ensure stability of the entire system, the Nyquist plot of the inner loop transfer function LG_1 and the outer loop transfer function LG_2

$$LG_1 = \frac{C_4(C_1 - Z_h C_3)}{(Z_m + C_m + Z_h)(Z_s + C_s)} \quad (3.13)$$

$$LG_2 = \frac{Z_e(Z_m + C_m + Z_h(1 - C_2C_3) + C_1C_2)}{(Z_m + C_m + Z_h)(Z_s + C_s) - C_4(Z_h C_3 - C_1)}$$

can not encircle the critical point $(-1 + j0)$ on the Nyquist plot.

3.3 Force-reflecting Control

3.3.1 Coordinating Force

The position error between the desired and actual machine positions is usually proportional to the contact force; therefore it is often used for force reflection instead of direct force feedback. Other reasons for its popularity are: position sensing is much easier and less expensive to implement than direct force measuring, and secondly coordinating force (position error) method can be shown to be passive under position control. A block diagram of a position-position structure is shown in Figure 3.15.

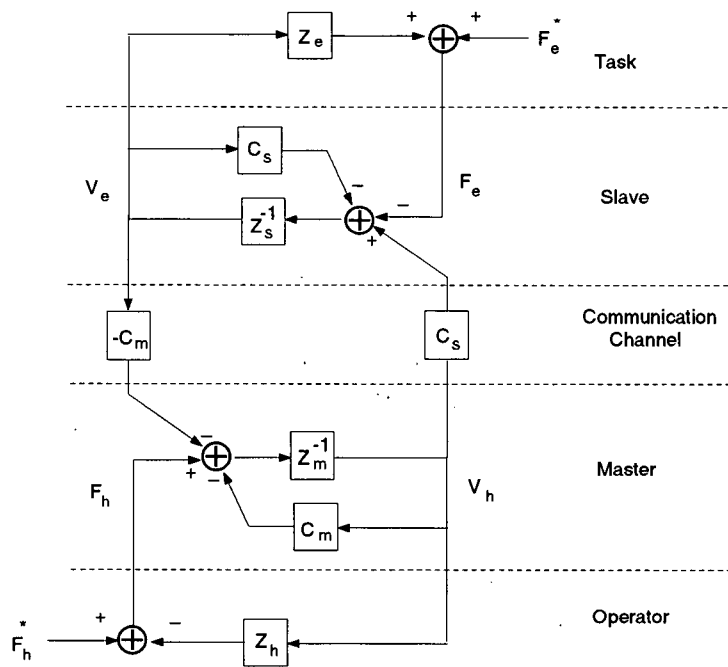


Figure 3.15 Position-position structure

If we choose $C_m = C_s$, the position-position structure can be reformulated using the network

concept, see Figure 3.16. It is known that any circuit network made up of strictly passive

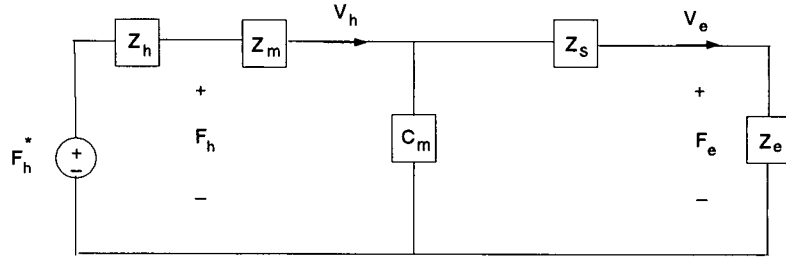


Figure 3.16 Network representation of position-position structure

components is itself passive, thus the system can not go unstable. The mechanical equivalent of the above two-port teleoperator system is shown in Figure 3.17.

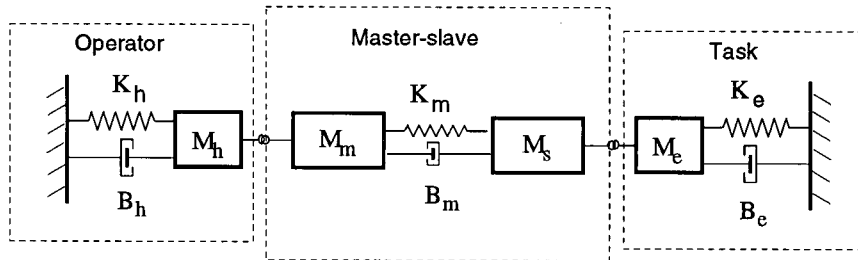


Figure 3.17 Mechanical equivalence of position-position structure

It is quite often that the slave is controlled by the master under rate mode, that is the slave velocity is proportional to the master position. For position servo, this is realized by adding an integrator to the position forward channel, that is

$$C_1 = \frac{C_s}{K_v s} = \frac{B_s + \frac{K_v}{s}}{K_v s} \quad (3.14)$$

where K_v is the velocity gain.

The coordinating force method can be easily adapted to rate control. A block diagram of such a rate-position structure is shown in Figure 3.18. However, a “stiff” controller (high

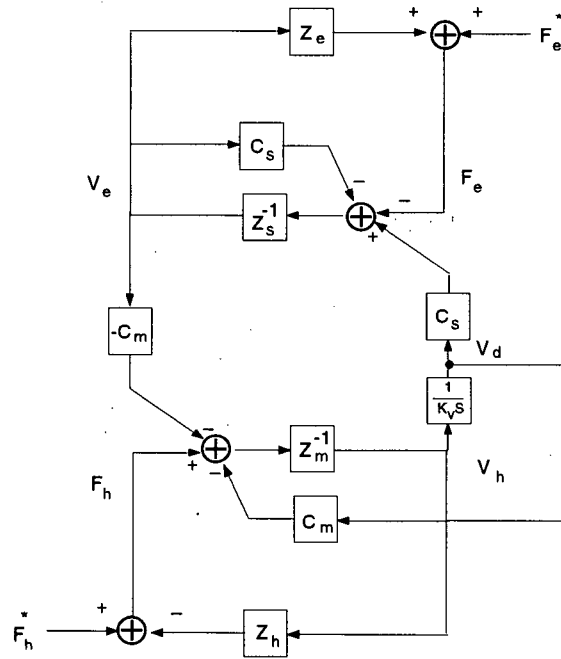


Figure 3.18 Rate-position structure

position gain) can make the position error smaller than noise. Therefore it is not always possible to implement this method in practice. For instance, the position gain is so high for hydraulic mobile machines such as excavators and feller-bunchers that there is virtually no position error for feedback considering the noise.

3.3.2 Force Feedback

It is well known that direct force feedback with position control can cause instability. Parker [3] pointed out that stability problem is even more serious when direct force feedback is used

for rate control.

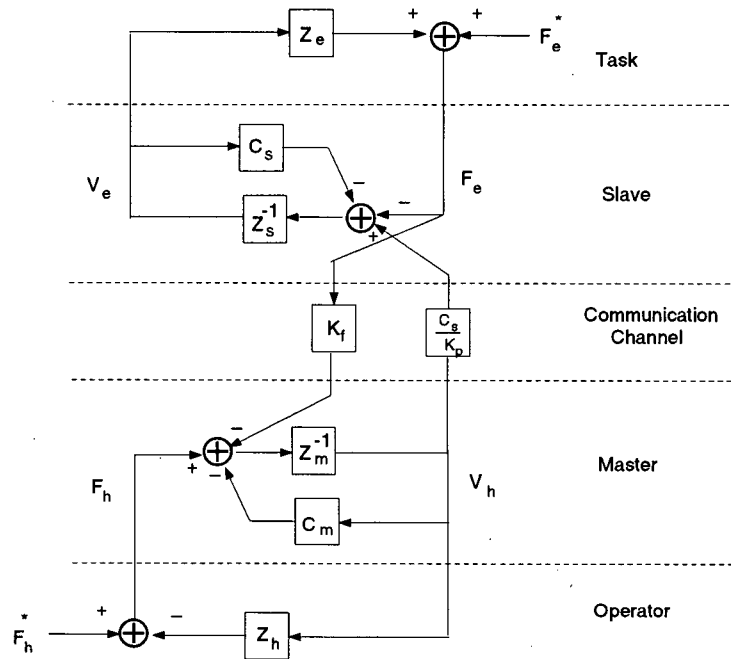


Figure 3.19 Position-force structure

For general position control with direct force feedback, we have the following block transfer functions (see Figure 3.19)

$$\begin{aligned}
 C_1 &= \frac{C_s}{K_p} \\
 C_2 &= K_f \\
 C_3 &= C_4 = 0
 \end{aligned}
 \tag{3.15}$$

where K_p , K_f are the position gain and force feedback gain respectively. The inner loop does not appear in this structure. The outer loop transfer function becomes

$$LG_2 = \frac{Z_e \left(Z_m + C_m + Z_h + \frac{K_f}{K_p} C_s \right)}{(Z_s + C_s)(Z_m + C_m + Z_h)}
 \tag{3.16}$$

The corresponding characteristic equation is

$$1 + LG_2 = 1 + \frac{Z_e \left(Z_m + C_m + Z_h + \frac{K_t}{K_p} C_s \right)}{(Z_s + C_s)(Z_m + C_m + Z_h)} = 0 \quad (3.17)$$

which can be rewritten as

$$1 + \frac{\frac{K_t}{K_p} C_s Z_e}{(Z_s + C_s + Z_e)(Z_m + C_m + Z_h)} = 0 \quad (3.18)$$

For stability analysis, it is equivalent to use the following loop transfer function:

$$LG = \frac{\frac{K_t}{K_p} C_s Z_e}{(Z_s + C_s + Z_e)(Z_m + C_m + Z_h)} \quad (3.19)$$

For position control with direct force feedback, stability can be achieved by reducing the loop gain $\frac{K_p}{K_f}$, but at the cost of reduced sensitivity.

For general rate control with direct force feedback, we have the following block transfer functions

$$\begin{aligned} C_1 &= \frac{C_s}{K_v s} \\ C_2 &= K_f \\ C_3 &= C_4 = 0 \end{aligned} \quad (3.20)$$

where K_v , K_f are the velocity and force feedback gain respectively. Compared with position control, the difference is that the position gain K_p is replaced by $K_v s$. For stability analysis, we have the following loop transfer function:

$$LG = \frac{\frac{K_t}{K_v s} C_s Z_e}{(Z_s + C_s + Z_e)(Z_m + C_m + Z_h)} \quad (3.21)$$

It is well known from linear system theory, that the addition of pole at $s = 0$ to the transfer function has an adverse effect on the system stability. In general, the result is to push the original root loci toward the right-half plane. On the Nyquist plot, adding a pole at $s = 0$ causes the original Nyquist locus of $G(jw)H(jw)$ to be rotated by -90 degree making it easy for it to cross

the critical point $(-1, 0)$ on the complex plane. Therefore rate control with direct force feedback tends to be unstable even without time-delay in the system.

Therefore it is not trivial to develop a scheme in which contact information is transmitted to the operator while keeping the system stable under rate control. As we pointed out before, the coordinating force method may be one option. However, as we discussed before, it might not be possible in some applications where there are almost no position errors at all.

3.4 Transparency

3.4.1 Achieving Transparency Under Position Control

As Lawrence [22] pointed out, the position-position structure does not provide transparency, nor does the position-force structure if the dynamics of the system can not be neglected.

It has been suggested by authors such as Salcudean [14], Lawrence [22] and Yokokohji [23] that operator hand applied force should be fed forward to achieve transparency. Salcudean and Wong applied this approach to a master-slave teleoperator system which consists of two identical six DOF magnetically levitated wrist. Yokokohji and Yoshikawa reported similar work on a single degree of freedom system.

It is clear that from the structure of the transmitted impedance

$$Z_t = \frac{[(Z_m + C_m)(Z_s + C_s) + C_1C_4] + Z_e(Z_m + C_m + C_1C_2)}{(Z_s + C_s - C_3C_4) + Z_e(1 - C_2C_3)} \quad (3.22)$$

that in order to make system fully transparent, i.e.,

$$Z_t = Z_e \text{ for any } Z_e \quad (3.23)$$

the following conditions must be satisfied:

$$\begin{aligned}(Z_m + C_m)(Z_s + C_s) + C_1 C_4 &= 0 \\ 1 - C_2 C_3 &= 0\end{aligned}\tag{3.24}$$

$$Z_m + C_m + C_1 C_2 = Z_s + C_s - C_3 C_4$$

For position control, if we set

$$C_1 = Z_s + C_s\tag{3.25}$$

Solving the above system of equations, we have two possible solutions

$$\begin{aligned}C_2 &= 1 \\ C_3 &= 1 \\ C_4 &= -(Z_m + C_m)\end{aligned}\tag{3.26}$$

and

$$\begin{aligned}C_2 &= -\frac{Z_m + C_m}{Z_s + C_s} \\ C_3 &= -\frac{Z_s + C_s}{Z_m + C_m} \\ C_4 &= -(Z_m + C_m)\end{aligned}\tag{3.27}$$

where the second solution results in $Z_e = \frac{0}{0}$, and therefore it should be eliminated.

The hybrid matrix for this “transparent” telemanipulator system can be derived as

$$H = \begin{bmatrix} 0 & 1 \\ -1 & 0 \end{bmatrix}\tag{3.28}$$

Remarks:

1. It is interesting to note that the end point impedance of the system viewed from the slave side equals:

$$Z_{end} = -\frac{F_e}{V_e} = Z_h\tag{3.29}$$

which is the impedance of the human hand. In robotics control, the goal of impedance control of a manipulator is to create a desired impedance at its end-effector. However, in practice, it is not very clear what the best impedance for the manipulator to contact its tasks is. Experiences show human hands offer an adjustable impedance, which makes them ideal for manipulating almost any object without encountering stability problem. Thus, from the impedance control point of view, the above fully transparent teleoperator structure provides a way to reconstruct the human impedance at the manipulator end-effector.

2. We have

$$\begin{aligned} F_h - F_e &= (Z_m + C_m)(V_h - V_e) \\ F_h - F_e &= (Z_s + C_s)(V_e - V_h) \end{aligned} \quad (3.30)$$

the position error dynamics can be formed as

$$s(Z_m + C_m + Z_s + C_s)(x_h - x_e) = 0 \quad (3.31)$$

where x_h and x_e are the positions of the master and slave respectively. Thus the slave tracks the master position asymptotically. Therefore we indeed have realized the ideal weightless infinitely stiff bar asymptotically.

Applying Scattering Theory, we can compute the scattering matrix of the two-port as follows

$$S(s) = \begin{bmatrix} 1 & 0 \\ 0 & -1 \end{bmatrix} (H(s) - I) (H(s) + I)^{-1} = \begin{bmatrix} 0 & 1 \\ 1 & 0 \end{bmatrix} \quad (3.32)$$

The norm of this scattering matrix is

$$\|S(j\omega)\| = \sup \lambda^{\frac{1}{2}}[S^*(j\omega)S(j\omega)] = 1 \quad (3.33)$$

Therefore, from the network point of view, this two-port is passive ("lossless" to be exact). Hence when it is connected to any strictly passive load, the system stability is ensured. Let's assume

the system is connected to two passive one-ports with impedance Z_h (operator's hand) and Z_e (payload). The inner and outer loop transfer functions become

$$\begin{aligned} LG_1 &= \frac{-(Z_m + C_m)(Z_s + C_s - Z_h)}{(Z_m + C_m + Z_h)(Z_s + C_s)} \\ LG_2 &= \frac{Z_e(Z_m + C_m + Z_s + C_s)}{Z_h(Z_m + C_m + Z_s + C_s)} \end{aligned} \quad (3.34)$$

The corresponding characteristic equations are

$$\begin{aligned} LG_1 + 1 &= \frac{Z_h(Z_m + C_m + Z_s + C_s)}{(Z_m + C_m + Z_h)(Z_s + C_s)} = 0 \\ LG_2 + 1 &= \frac{(Z_e + Z_h)(Z_m + C_m + Z_s + C_s)}{Z_h(Z_m + C_m + Z_s + C_s)} = 0 \end{aligned} \quad (3.35)$$

Any mass-damper-spring system is stable if the mass, damping and spring coefficients are all positive. Thus, the inner loop and outer loop are stable; therefore, the entire system is stable.

The above teleoperator control strategy requires acceleration measurement. Furthermore, it needs accurate knowledge of the mass of master and slave in order to completely compensate for their dynamics. This makes it difficult to implement in practice. On the other hand, complete transparency might not be desirable since an infinitely stiff and weightless mechanical bar would drift around if it is not connected to a load and an operator. As it is suggested by Salcudean and Wong [21], a small centering force is desirable to "fix" the master and slave system to prevent drifting. This, in fact, can be interpreted as an intervenient impedance [23] added to the ideal mechanical bar as shown in Figure 3.20.

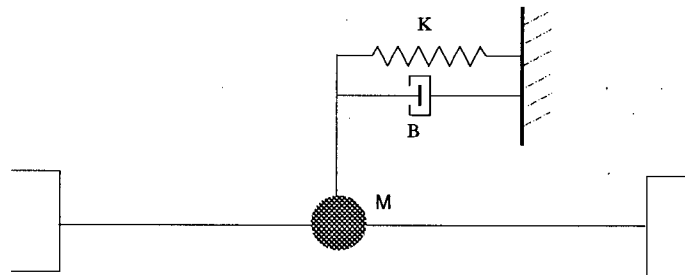


Figure 3.20 Intervient impedance

Consequently, a small force is always needed to move the telemanipulator even without payload. As we will see that the adding of intervenient impedance makes it unnecessary to measure accelerations.

First let us add some damping and spring term to the master-slave subsystems

$$Z_m = M_m s + B_{mc} + K_{mc}/s \quad (3.36)$$

$$Z_s = M_s s + B_{sc} + K_{sc}/s$$

and set the block transfer function as

$$C_1 = C_s$$

$$C_2 = C_3 = 1 \quad (3.37)$$

$$C_4 = -C_m$$

Thus the corresponding transmitted impedance becomes

$$\begin{aligned} Z_t &= \frac{[(Z_m + C_m)(Z_s + C_s) + C_1 C_4] + Z_e(Z_m + C_m + C_1 C_2)}{(Z_s + C_s - C_3 C_4) + Z_e(1 - C_2 C_3)} \\ &= \frac{(Z_m C_s + Z_s C_m + Z_m Z_s) + Z_e(Z_m + C_m + C_s)}{(Z_s + C_s + C_m)} \end{aligned} \quad (3.38)$$

If we have identical master and slave subsystem, that is $Z_m = Z_s$, the transmitted impedance becomes

$$Z_t = Z_m + Z_e \quad (3.39)$$

Thus the operator indeed feels the object's impedance and an intervenient impedance as we expected.

The hybrid matrix for this telemanipulator structure becomes

$$H = \begin{bmatrix} Z_m & 1 \\ -1 & 0 \end{bmatrix} \quad (3.40)$$

The end point impedance of the system viewed from the slave side equals:

$$Z_{end} = -\frac{F_e}{V_e} = Z_m + Z_h \quad (3.41)$$

which is the impedance of the human hand plus an intervenient impedance.

Since we have

$$\begin{aligned} F_h - F_e &= Z_m V_h + C_m (V_h - V_e) \\ F_h - F_e &= Z_s V_e + C_s (V_e - V_h) \end{aligned} \quad (3.42)$$

In case of identical master and slave, that is $Z_m = Z_s$, the position error dynamics can be formed as

$$s(Z_m + C_m + C_s)(x_h - x_e) = 0 \quad (3.43)$$

thus the slave tracks the master's position asymptotically. Therefore, we indeed have asymptotically realized the ideal weightless infinitely stiff bar with an intervenient impedance.

The stability can be checked as before, starting from inner loop transfer function,

$$LG_1 = \frac{-C_m(C_s - Z_h)}{(Z_m + C_m + Z_h)(Z_s + C_s)} \quad (3.44)$$

The characteristic equation is

$$LG_1 + 1 = \frac{(Z_s + C_s + C_m)(Z_h + Z_m)}{(Z_m + C_m + Z_h)(Z_s + C_s)} = 0 \quad (3.45)$$

Clearly the inner loop is stable.

For the outer loop

$$LG_2 = \frac{Z_e(Z_m + C_m + C_s)}{(Z_s + C_s)(Z_m + C_m + Z_h) + C_m(Z_h - C_s)} \quad (3.46)$$

Again if we assume the master and slave subsystems are identical $Z_m = Z_s$, then

$$LG_2 + 1 = \frac{(Z_h + Z_m + Z_e)(Z_m + C_m + C_s)}{(Z_m + Z_h)(Z_s + C_s + C_m)} = 0 \quad (3.47)$$

Therefore, the outer loop is stable.

However, the above stability analysis is based on the assumption that the master subsystem is exactly the same as the slave subsystem, and the force feedback and feed-forward is accurate. Salcudean [14] reported an error of only 5% in the force feed forward could drive the system unstable. In addition, as we discussed before, time delay is always a destabilizing factor in the system. The robust implementation of above scheme needs further study.

3.4.2 Achieving Transparency Under Rate Control

The position-force structure does not provide transparency nor does the rate-force structure. Let's have a look at what the operator feels if the slave is controlled in rate mode and direct force feedback is used. The block transfer functions for rate-force control are

$$C_1 = \frac{C_s}{K_v s} = \frac{B_s + \frac{K_s}{s}}{K_v s}$$

$$C_2 = K_f$$

$$C_3 = C_4 = 0$$
(3.48)

where K_v , K_f are the velocity gain and force feedback gain respectively.

The transmitted impedance becomes

$$Z_t = \frac{(Z_m + C_m)(Z_s + C_s) + Z_e \left(Z_m + C_m + \frac{K_f C_s}{K_v s} \right)}{Z_s + C_s + Z_e}$$
(3.49)

Therefore it is difficult to say what the operator could feel from this transmitted impedance. For large Z_e , the impedance can be approximated as

$$Z_t \rightarrow Z_m + C_m + \frac{K_f C_s}{K_v s}$$
(3.50)

For small Z_e ,

$$Z_t \rightarrow Z_m + C_m$$
(3.51)

At these extremes, the operator could only feel some dynamics of the master-slave system; it has nothing to do with the dynamics of the task.

As we discussed before, for position control, the bilateral communication of force information is important to achieve transparency. Here we can extend it to rate control.

In position control, a coordinating force is generated by the error between the desired and actual slave position according to

$$F_{co.} = C_m s(X_h - X_e) \tag{3.52}$$

where $C_m = B_m + \frac{K_m}{s}$. We can apply the same idea to rate control. However the coordinating force under rate control takes the form of (see Figure 3.18)

$$F_{co.} = C_m s\left(\frac{X_h}{K_v s} - X_e\right) \tag{3.53}$$

Therefore it is natural to replace the block transfer function C_m in the general teleoperator structure with $\frac{C_m}{K_v s}$ as shown in Figure 3.21.

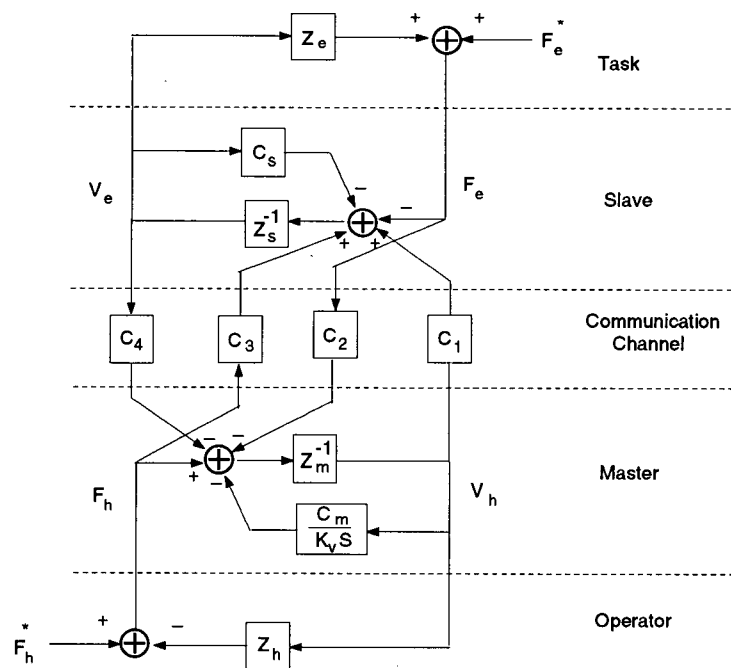


Figure 3.21 Achieving transparency under rate control

The transmitted impedance becomes

$$Z_t = \frac{\left[\left(Z_m + \frac{C_m}{K_v s} \right) (Z_s + C_s) + C_1 C_4 \right] + Z_e \left(Z_m + \frac{C_m}{K_v s} + C_1 C_2 \right)}{(Z_s + C_s - C_3 C_4) + Z_e (1 - C_2 C_3)} \quad (3.54)$$

In order to achieve complete transparency, the following constraints must be satisfied:

$$\begin{aligned} \left(Z_m + \frac{C_m}{K_v s} \right) (Z_s + C_s) + C_1 C_4 &= 0 \\ 1 - C_2 C_3 &= 0 \end{aligned} \quad (3.55)$$

$$Z_m + \frac{C_m}{K_v s} + C_1 C_2 = Z_s + C_s - C_3 C_4 \neq 0$$

For rate control, we set

$$C_1 = \frac{Z_s + C_s}{K_v s} \quad (3.56)$$

After a few algebraic manipulations, we have the following solutions

$$\begin{aligned} C_2 &= K_v s \\ C_3 &= \frac{1}{K_v s} \\ C_4 &= -K_v s \left(Z_m + \frac{C_m}{K_v s} \right) \end{aligned} \quad (3.57)$$

and

$$\begin{aligned} C_2 &= -K_v s \frac{Z_m + \frac{C_m}{K_v s}}{Z_s + C_s} \\ C_3 &= -\frac{1}{K_v s} \frac{Z_s + C_s}{Z_m + \frac{C_m}{K_v s}} \\ C_4 &= -K_v s \left(Z_m + \frac{C_m}{K_v s} \right) \end{aligned} \quad (3.58)$$

where the second solution results in $Z_e = \frac{0}{0}$, therefore it should be eliminated.

Unfortunately, the control law $C_4 = -K_v s \left(Z_m + \frac{C_m}{K_v s} \right)$ requires the measure of jerk which is impossible in practice. Instead, we can use the following simplified control law:

$$\begin{aligned} C_1 &= \frac{C_s}{K_v s} \\ C_2 &= K_v s \\ C_3 &= \frac{1}{K_v s} \\ C_4 &= -C_m \end{aligned} \quad (3.59)$$

The corresponding impedance felt by the operator is as follows

$$Z_t = \frac{\left(Z_m C_s + \frac{Z_s C_m}{K_{vs}} + Z_m Z_s \right) + Z_e \left(Z_m + C_s + \frac{C_m}{K_{vs}} \right)}{\left(Z_s + C_s + \frac{C_m}{K_{vs}} \right)} \quad (3.60)$$

If we have identical master and slave subsystem, that is $Z_m = Z_s$, the transmitted impedance becomes

$$Z_t = Z_m + Z_e \quad (3.61)$$

Thus we have the same impedance as for position control, which can be interpreted as the master impedance plus the task impedance. The teleoperator system is transparent.

The hybrid matrix of the master-slave system can be computed as

$$H = \begin{bmatrix} Z_m & K_{vs} \\ -\frac{1}{K_{vs}} & 0 \end{bmatrix} \quad (3.62)$$

The transfer function between the master and slave velocities can be derived. Since

$$\begin{bmatrix} F_h \\ -V_e \end{bmatrix} = H(s) \begin{bmatrix} V_h \\ F_e \end{bmatrix} \quad (3.63)$$

hence

$$\frac{V_e}{V_h} = \frac{1}{K_{vs}} \quad (3.64)$$

therefore the slave is indeed under rate control.

The stability can be checked as before, using the loop transfer functions,

$$LG_1 = \frac{-C_m \left(\frac{C_s}{K_{vs}} - \frac{Z_h}{K_{vs}} \right)}{\left(Z_m + \frac{C_m}{K_{vs}} + Z_h \right) (Z_s + C_s)} \quad (3.65)$$

$$LG_2 = \frac{Z_e \left(Z_m + \frac{C_m}{K_{vs}} + C_s \right)}{(Z_s + C_s) \left(Z_m + \frac{C_m}{K_{vs}} + Z_h \right) + C_m \left(\frac{Z_h}{K_{vs}} - \frac{C_s}{K_{vs}} \right)} \quad (3.66)$$

Under the assumption the master and slave are identical $Z_m = Z_s$, we have the following characteristic equations,

$$LG_1 + 1 = \frac{(Z_m + Z_h)\left(Z_s + C_s + \frac{C_m}{K_v s}\right)}{\left(Z_m + \frac{C_m}{K_v s} + Z_h\right)(Z_s + C_s)} \quad (3.67)$$

$$LG_2 + 1 = \frac{\left(Z_m + \frac{C_m}{K_v s} + C_s\right)(Z_h + Z_m + Z_e)}{(Z_m + Z_h)\left(Z_s + C_s + \frac{C_m}{K_v s}\right)} \quad (3.68)$$

In order to guarantee stability, we must choose a control law such that the zeros of

$$Z_m + \frac{C_m}{K_v s} + C_s = 0 \quad (3.69)$$

fall in the left half of the complex plane.

Compared with the position control, we have an additional feedback subsystem in this rate control structure which is no longer guaranteed to be stable. In other words, we also have to make the zeros of the following characteristic equations to be in the left half of the complex plane,

$$Z_m + \frac{C_m}{K_v s} + Z_h = 0 \quad (3.70)$$

$$Z_m + \frac{C_m}{K_v s} = 0 \quad (3.71)$$

which are related to the master subsystem.

Equation 3.71 can be written as

$$K_v M_m s^3 + B_{mc} K_v s^2 + (K_v K_{mc} + B_m)s + K_m = 0 \quad (3.72)$$

It is known that in order for a polynomial equation to have no roots with positive real part, it is necessary that

1. All the coefficients of the polynomial have the same sign
2. None of the coefficients vanishes.

Thus for stability reason, it is important to have $B_{mc} \neq 0$; otherwise, the system can not be stable.

During rate control, the position correspondence between the master and slave is lost. Therefore the increase of spring force will not be felt by the operator if he can only feel the impedance of the task. This can cause machine tip over (for instance, an excavator) or damage to the tool. For these applications, it is more important to transmit the contact force to the operator than to feel the task dynamics. However, as we discussed before, stability is still a problem.

3.4.3 Achieving Transparency Via Impedance Identification

As we discussed before, it is not necessary to cancel the dynamics of the master-slave system completely. Another interesting structure which could be used to make the system transparent is via parameter identification [19]. Assume the task is merely a linear mass-spring-damper, that is

$$Z_e = M_e s + B_e + \frac{K_e}{s} \quad (3.73)$$

A regression model can be formulated as

$$f_e = [\ddot{x}_e \quad \dot{x}_e \quad x_e][M_e \quad B_e \quad K_e]^T = \varphi^T \theta \quad (3.74)$$

where $\varphi = [\ddot{x}_e \quad \dot{x}_e \quad x_e]^T$ and $\theta = [M_e \quad B_e \quad K_e]^T$

On-line recursive least-squares estimation can be used to identify the task impedance parameters. In addition, the resetting and forgetting factor technique can be employed to deal with a changing environment. The estimated task impedance \hat{Z}_e then can be implemented in the master subsystem control as

$$F_h = Z_m V_h + \hat{Z}_e V_h \quad (3.75)$$

where $Z_m = M_m s + B_{mc} + \frac{K_{mc}}{s}$

Thus the impedance felt by the operator becomes

$$Z_t = Z_m + \hat{Z}_e \tag{3.76}$$

which makes the system transparent.

A block diagram of the rate control with impedance identification scheme is shown in Figure 3.22.

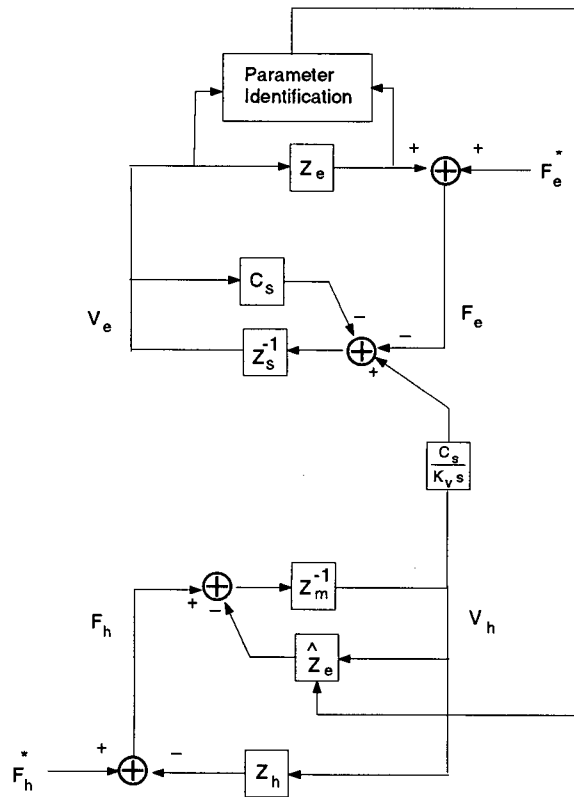


Figure 3.22 Achieving transparency via parameter identification

Chapter 4 Stiffness Feedback

4.1 Principle

It has been shown that direct force feedback under rate control can easily introduce instability. Parker [3] proposed a method in which the contact force is used to adjust the stiffness of the joystick instead of being applied directly to the operator's hand. A comparison of direct force feedback and stiffness feedback is shown in Figure 4.23.

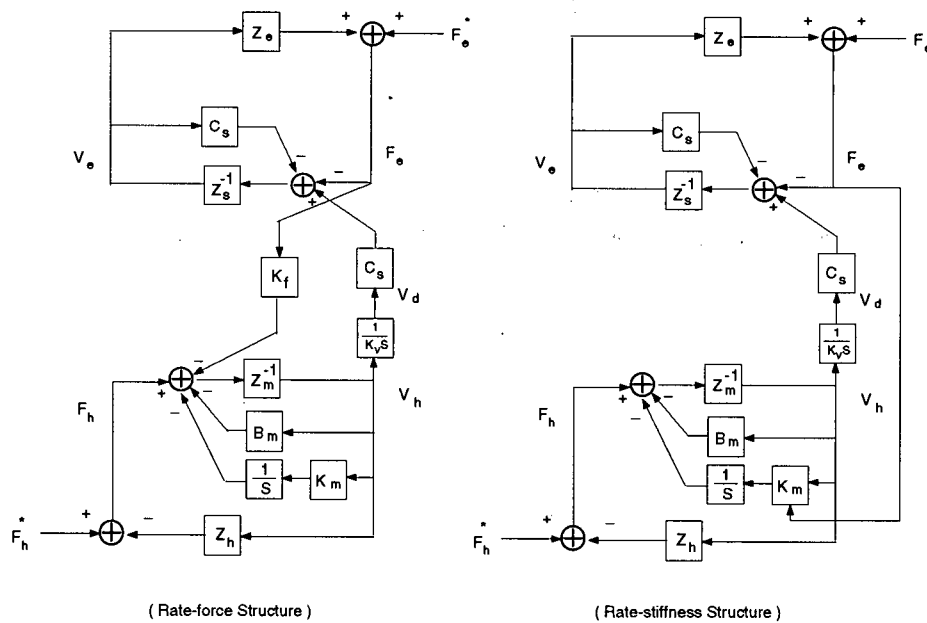


Figure 4.23 Comparison of two rate control structures

The stiffness of the joystick can be adjusted according to

$$K_m = K_{nom} + f_e K_r \text{sgn}(x_h) \tag{4.1}$$

K_m is bounded by $[K_{min}, K_{max}]$

where K_{nom} is a constant gain when there is no contact, K_r is the ratio of stiffness and contact force, see Figure 4.24.

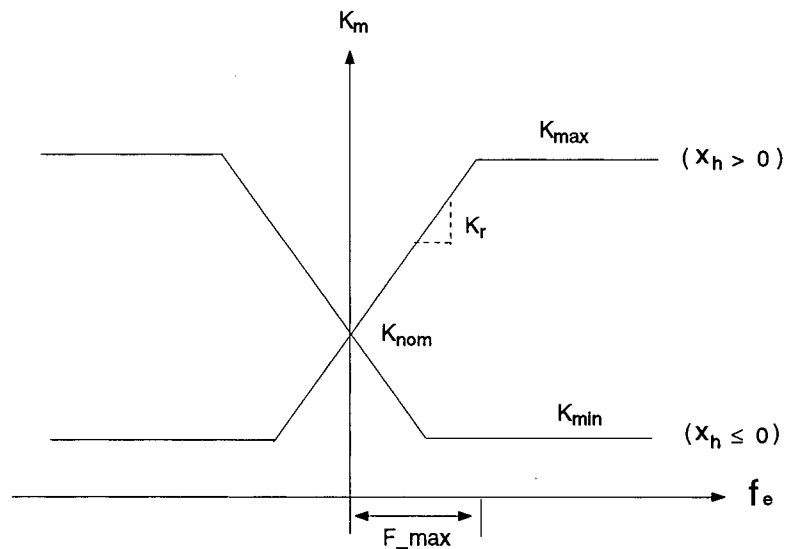


Figure 4.24 Stiffness adjustment scheme

Within the linear area, the operator hand applied force equals to

$$\begin{aligned}
 f_h &= M_m \ddot{x}_h + B_m \dot{x}_h + K_m x_h \\
 &= M_m \ddot{x}_h + B_m \dot{x}_h + K_{nom} x_h + f_e K_r |x_h|
 \end{aligned}
 \tag{4.2}$$

Thus, within this linear area, this stiffness adjustment scheme can be thought of as a special case of direct force feedback whose feedback gain is linearly proportional to the master position. In the case where the operator holds the master position constant, this gain is fixed; it is the same as direct force feedback.

Clearly, this stiffness adjustment scheme does deliver the contact force information to the operator to a certain extent. Numerical simulation and machine experiments show rate control with stiffness adjustment can easily make the system stable. However, a stability analysis is difficult to carry out for such a highly nonlinear system. The nonlinearity comes not only from the stiffness adjusting mechanism but also from the master position deadband since a position deadband is always needed for rate control. Stiffness feedback can be used for position control as well.

4.2 Stability

Rate control with stiffness adjustment makes the system highly nonlinear. Liapunov stability analysis seems elusive for such a system [3]. However, careful examination of this control structure reveals that the system can actually be divided into two separate second-order subsystems: a master system with a varying spring and a slave system which tracks a desired path set by the master (see Figure 4.25). We assume the operator's hand is modeled as a constant mass, damper

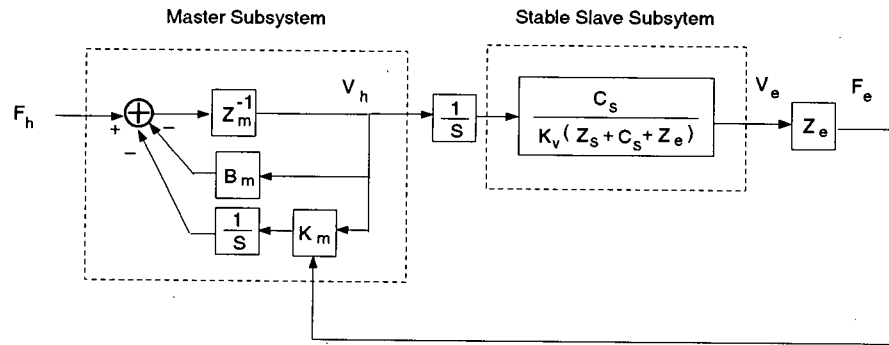


Figure 4.25 Stiffness feedback control block diagram

and spring system. Since the slave subsystem is stable, one only needs to be concerned about the stability of the master system (mass-damper-spring), that is

$$M_m \ddot{x}_h + B_m \dot{x}_h + K_m(f_e)x_h = f_h, \quad B_m > 0, K_m(f_e) > 0 \quad (4.3)$$

where $K_m(f_e)$ is only a function of the contact force f_e and bounded as $K_{max} \geq K_m(f_e) \geq K_{min} > 0$.

It is helpful to study the following time-varying system which is quite similar to our problem

$$\ddot{x} + B\dot{x} + K(t)x = 0, \quad B > 0, K(t) > 0 \quad (4.4)$$

where for simplicity we assume unit mass.

The behavior of a linear time-varying (LTV) system can be quite different from a LTI system. We know that a mass-damper-spring system with constant positive coefficients $\ddot{x} + B\dot{x} + Kx = 0$ ($B > 0$, $K > 0$) is always asymptotically stable. However as we will see, its time-varying counterpart $\ddot{x} + B(t)\dot{x} + K(t)x = 0$ ($B(t) > 0$, $K(t) > 0$) might be unstable. Special care should be taken when dealing with LTV system. Before we start, let us have a taste of such a difference. Consider the following second-order system

$$\ddot{x} + B(t)\dot{x} + Kx = 0, \quad B(t) > 0, K > 0 \quad (4.5)$$

Instead of having a time-varying spring coefficient, the above system has a time-varying damping coefficient. One might conclude that the equilibrium point $(0, 0)$ is asymptotically stable if the damping coefficient $B(t)$ remains larger than a strictly positive constant, which implies constant energy dissipation by the damper. Surprisingly this is not always true! Let's have a look at the following example:

$$\ddot{x} + (2 + e^t)\dot{x} + Kx = 0 \quad (4.6)$$

with initial condition $x(0) = 2$, $\dot{x}(0) = -1$, the above system has solution $x(t) = 1 + e^{-t}$ which goes to $x(\infty) = 1$ instead. In fact, additional constraints are needed in order to make the equilibrium of above system asymptotic stable. It can be shown [Slotine and Li] that one sufficient condition is to satisfy the following

$$\begin{aligned} B(t) &> a > 0 \\ \dot{B}(t) &\leq b \leq K \end{aligned} \quad (4.7)$$

where a, b are positive numbers.

Now we come back to our problem, that is a second-order system with time-varying spring coefficient

$$\ddot{x} + B\dot{x} + K(t)x = 0, \quad B > 0, K(t) > 0 \quad (4.8)$$

Without any additional constraints, it is easy to show that the system can be driven unstable by changing $K(t)$ even if it is bounded. For instance, a slightly damped mass-damper-spring system goes unstable if we set the spring constant to a large value whenever the mass moves towards the equilibrium point and a small value whenever the mass moves away from it. However, as we will see later, the asymptotic stability can be guaranteed if certain conditions are satisfied.

First, we introduce some stability concepts from general LTV system theory.

Definition: A linear dynamical equation

$$\begin{aligned} E : \quad \dot{X} &= A(t)X + D(t)U \\ Y &= C(t)X \end{aligned} \tag{4.9}$$

is said to be totally stable, or T-stable for short, if and only if for any initial state and for any bounded input, the output as well as all the state are bounded (refer to [33]).

It is clear total stability implies BIBO (bounded input/bounded output) stability. The following theorem states that with some conditions on $D(t)$ and $C(t)$, uniformly asymptotic stability implies total stability.

Theorem 4-1: Consider the dynamical equation

$$\begin{aligned} E : \quad \dot{X} &= A(t)X + D(t)U \\ Y &= C(t)X \end{aligned} \tag{4.10}$$

if the matrix $D(t)$ and $C(t)$ are bounded on $(-\infty, \infty)$, then the uniformly asymptotic stability of the zero state implies the system is T-stable (refer to [33]).

It is clear that for a LTI system, if its equilibrium point is asymptotically stable, then the system is T-stable.

Next we will prove the following useful theorem, which provides a sufficient condition for asymptotic stability for the master subsystem.

Theorem 4-2: Consider the second-order time-varying mass-damper-spring system

$$\ddot{x} + B\dot{x} + K(t)x = 0, \quad B > 0, K(t) > 0 \quad (4.11)$$

Suppose $K(t)$ is bounded by $K_{max} \geq K(t) \geq K_{min} > 0$ and

$$B^2 - 4K_{max} > 0 \quad (4.12)$$

Under these conditions, the system is uniformly asymptotically stable. Further the trajectory on phase plane can cross the \dot{x} axis at most once.

Remarks:

1. Since $K(t)$ is bounded by $K_{max} \geq K(t) \geq K_{min} > 0$, condition $B^2 - 4K_{max} > 0$ implies $B^2 - 4K(t) > 0$ for all time. Thus, at each time instant, the system can be thought as a overdamped, time-invariant, mass-damper-spring system.
2. This theorem makes no assumption on $\dot{K}(t)$.

Applying Theorem 4-1 and Theorem 4-2 to the master-slave system, we have the following:

Corollary Consider the master subsystem

$$M_m \ddot{x}_h + B_m \dot{x}_h + K_m(f_e)x_h = f_h, \quad B > 0, K_m(f_e) > 0 \quad (4.13)$$

where $K_m(f_e)$ is only a function of the contact force f_e and bounded by $K_{max} \geq K_m(f_e) \geq K_{min} > 0$. Suppose

$$B_m^2 - 4M_m K_{max} > 0 \quad (4.14)$$

Under these conditions, the equilibrium point is uniformly asymptotically stable. Further this system is T-stable; that is, any bounded input f_h and arbitrary initial condition result in bounded

states, and bounded output if the output takes the form of $Y = C(t)[x_h \quad \dot{x}_h]^T$ where $C(t)$ is bounded.

It is interesting to note that the rate of change of $K_m(f_e)$ does not affect the system asymptotic stability as long as its upper bound satisfies $B_m^2 - 4M_m K_{max} > 0$. In reality, the task impedance can be strongly nonlinear, e.g. at the transition between contact and free space motion. A quick contact with a hard surface could make the change of $K_m(f_e)$ very rapid, even nonsmooth. Additional nonlinearity comes from the master's position deadband. Nevertheless, stiffness feedback under the condition $B_m^2 - 4M_m K_{max} > 0$ can guarantee asymptotic stability no matter if the payload is passive or active, linear or nonlinear; no matter if there is a nonlinearity such as the master position deadband; no matter if there is a time delay in the communication line.

Proof of Theorem 4-2

<Part 1> First, we show that starting from any arbitrary initial state on the phase plane, after certain time, its trajectory must reach the x axis.

Assume the initial state is in quadrant IV. Since in this quadrant the velocity is negative, x will decrease all the time. After a certain time, there are at most two possibilities as shown in Figure 4.26.

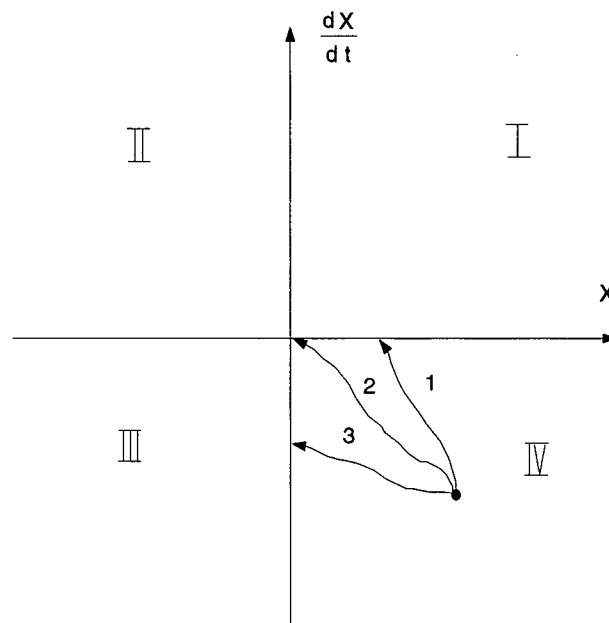


Figure 4.26 Trajectory in phase plane

1. Trajectory reaches the x axis with $x \geq 0$.
2. Trajectory reaches the \dot{x} axis with $\dot{x} < 0$.

We only need consider the second case $\dot{x} < 0$ and $x = 0$. It is clear the trajectory will go into quadrant 3. It can be treated later.

Assume that the initial state (x_0, \dot{x}_0) is in quadrant III. Since in this quadrant, velocity is still negative, x will decrease. Secondly, since we have $\ddot{x} = -B\dot{x} - K(t)x \geq K_{min}|x_0| > 0$ in this quadrant, \dot{x} will increase. Therefore, the trajectory reaches the x axis with $x < 0$ in finite time, as shown in Figure 4.27.

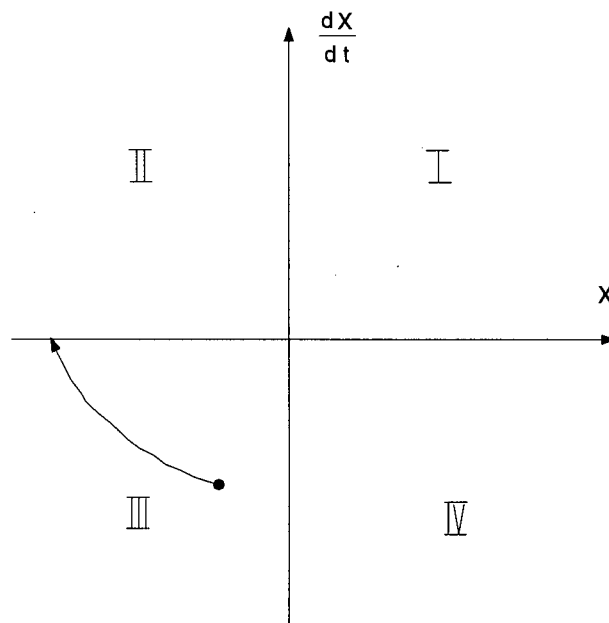


Figure 4.27 Trajectory in phase plane

The same analysis applies to the other two quadrants due to symmetry.

<Part 2> Next we show that any trajectory starting from x axis ($\dot{x} = 0$) goes to the origin asymptotically without crossing the \dot{x} axis.

We only need to consider the right half of the x axis due to symmetry.

Consider the time-invariant overdamped mass-damper-spring system

$$\ddot{x} + B\dot{x} + Kx = 0, \quad B > 0, K > 0 \quad (4.15)$$

where

$$B - 4K > 0 \quad (4.16)$$

We have the following two observations:

(Observation 1): Any trajectory starting from ($\dot{x} = 0$) goes to the origin asymptotically without crossing the \dot{x} axis.

Proof: The zero-input response of the system can be derived as follows:

$$\begin{aligned}x(t) &= ae^{\lambda_1 t} + be^{\lambda_2 t} \\ \dot{x}(t) &= a\lambda_1 e^{\lambda_1 t} + b\lambda_2 e^{\lambda_2 t}\end{aligned}\tag{4.17}$$

where λ_1, λ_2 are the roots of the characteristic equation, that is

$$\begin{aligned}\lambda_1 &= \frac{1}{2}(-B + \sqrt{B^2 - 4K}) \\ \lambda_2 &= \frac{1}{2}(-B - \sqrt{B^2 - 4K})\end{aligned}\tag{4.18}$$

a, b are two constants depending on initial state (x_0, \dot{x}_0)

$$\begin{aligned}a &= \frac{x_0(\lambda_1 + B) + \dot{x}_0}{\lambda_1 - \lambda_2} \\ b &= \frac{x_0(\lambda_2 + B) + \dot{x}_0}{\lambda_1 - \lambda_2}\end{aligned}\tag{4.19}$$

It is clear the system is asymptotically stable as $t \rightarrow \infty, x, \dot{x} \rightarrow 0$.

By way of contradiction, we assume that the trajectory reaches the \dot{x} axis at finite time $t = t_c$, that is

$$x(t_c) = ae^{\lambda_1 t_c} + be^{\lambda_2 t_c} = 0\tag{4.20}$$

By assumption we have $x_0 \neq 0, \dot{x}_0 = 0$, thus

$$e^{(\lambda_1 - \lambda_2)t_c} = -\frac{b}{a} = \frac{\lambda_1 + B}{\lambda_2 + B}\tag{4.21}$$

Since we know $\lambda_1 - \lambda_2 = \sqrt{B^2 - 4K} > 0$, the above equation implies

$$\frac{\lambda_1 + B}{\lambda_2 + B} > 1 \quad \text{or} \quad \lambda_1 < \lambda_2\tag{4.22}$$

which contradicts the fact that $\lambda_1 > \lambda_2$. Therefore, it is not possible for any trajectory to reach the \dot{x} axis in finite time.

(Observation 2): At any state in quadrant IV of the phase plane, the trajectory corresponding to the system with higher stiffness has higher tangent.

Proof: The tangent of a trajectory at state (x, \dot{x}) for the time-invariant mass-damper-spring system can be derived as

$$\text{Tangent}(K) = \frac{d\dot{x}}{dx} = \frac{\ddot{x}}{\dot{x}} = \frac{-B\dot{x} - Kx}{\dot{x}} \quad (4.23)$$

Thus we have

$$\text{Tangent}(K + \Delta) - \text{Tangent}(K) = \frac{-\Delta x}{\dot{x}} > 0 \quad (4.24)$$

in quadrant IV.

From the above two observations, we can sketch the trajectories which correspond to the systems with constant stiffness K_{max} and K_{min} respectively when starting from the same state P on positive \dot{x} axis, see Figure 4.28. The two trajectories can not intersect each other. Otherwise it contradicts observation 2.

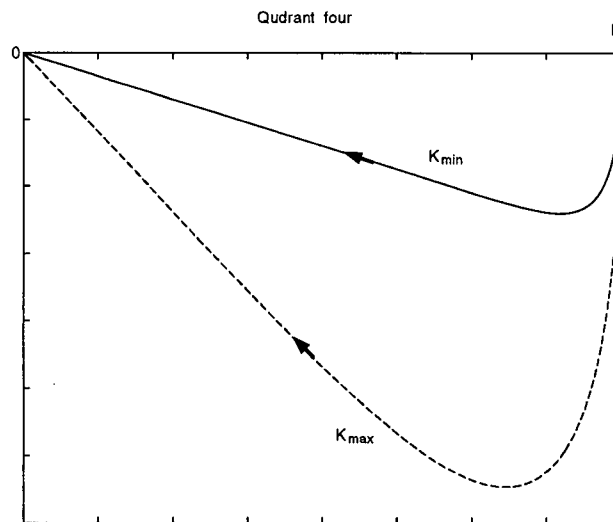


Figure 4.28 Trajectory in phase plane

Now consider the second-order time-varying mass-damper-spring system

$$\ddot{x} + B\dot{x} + K(t)x = 0, \quad B > 0, K(t) > 0 \quad (4.25)$$

which starts from the same initial state P . First, the trajectory of this time-variant system must be bounded by curve 1 and curve 2; otherwise, it will contradict Observation 2, see Figure 4.29. Second, since the velocity in quadrant IV is negative, thus, any trajectory will always move towards to the left. Therefore, we conclude that as $t \rightarrow \infty$, the trajectory will approach the origin. Therefore, the system is globally asymptotically stable. This completes the proof of Theorem 4-2.

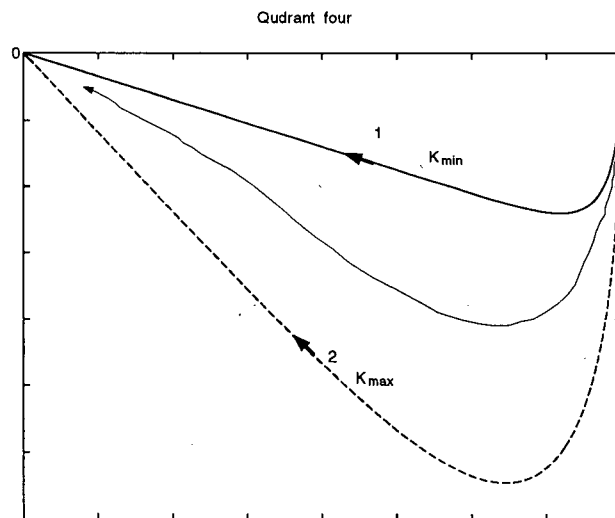


Figure 4.29 Trajectory in phase plane

Chapter 5 System Overview

The focus of our research is to implement real-time, force reflecting, resolved motion control for typical hydraulic mobile machines, an excavator and a feller-buncher. Previous work by Parker [3] employed the same approach to control a three degree-of-freedom (DOF) log-loader. Here, the results were extended to the manipulators with four and five DOF to further investigate the application of resolved motion control (rate v.s. position) and force reflecting control (direct force feedback v.s. stiffness feedback) for the control of the hydraulic mobile machines.

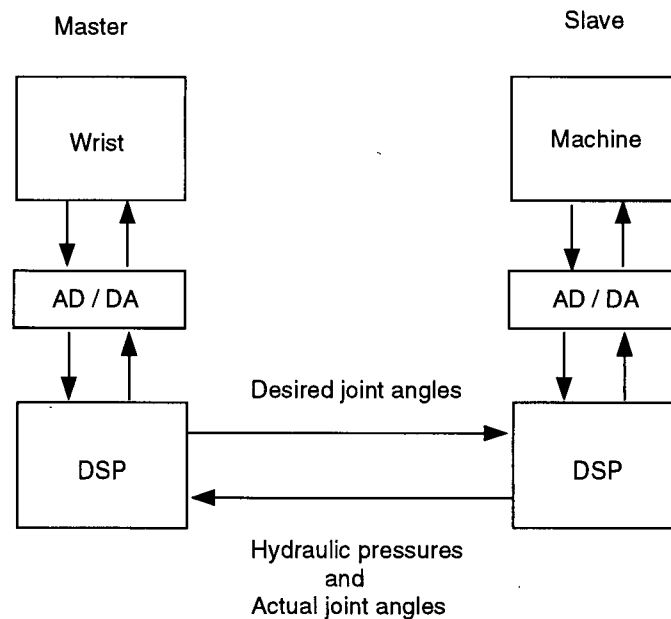


Figure 5.30 Overall system configuration

The complete teleoperator system can be divided into two parts, the master subsystem and the slave subsystem, as shown in Figure 5.30. A six DOF magnetically levitated joystick as a master is controlled by a local PID controller with programmable center of compliance. The

Joystick position is interpreted as a command to generate a desired machine endpoint position. Through an inverse kinematics transformation, the desired joint angles are computed and sent to the hydraulic machine controller for set-point control. The hydraulic cylinder pressures and actual joint angles are measured to calculate the endpoint force through inverse Jacobian transformation. This force is reflected to the master side either directly applied to the operator's hand or used to adjust the stiffness of the joystick.

5.1 Master — Maglev Joystick

The master plays a critical role in any master-slave teleoperator system. It serves as a man-machine interface, therefore has great influence on the overall system performance.

Various kinds of joysticks can be used as the input devices. Passive joysticks are popular due to the fact that they do not require actuators which makes them less expensive and less complicated to build and maintain. After force-reflection was introduced in teleoperation, great efforts have been spent in building ideal active joysticks which are capable of reproducing the desired force to the operator's hand while providing enough DOF for operation. Most designs use either hydraulic or electric servomotors. The nature of these actuators make it impossible to overcome problems such as friction and backlash which greatly affect the performance of the joystick.

The six DOF magnetically levitated joystick (Maglev Joystick) which is based on electrodynamic actuation, originally designed for coarse-fine manipulation, proves to be ideal to be used as a master for force-reflecting teleoperator system. Its novel design eliminate all mechanical linkages, and therefore friction and backlash.

5.1.1 System Configuration

A complete Maglev Joystick system [34] can be divided into four parts: a magnetically levitated joystick which consists of a fixed “stator” and a moving “flotor”, a signal conditioning box, a digital controller with an A/D and D/A interface and a current driver, as shown in Figure 5.31. The Maglev Joystick Assembly is shown in Figure 5.32.

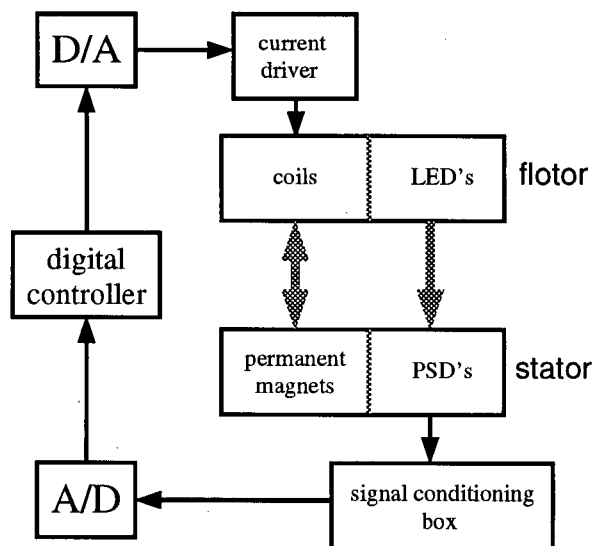
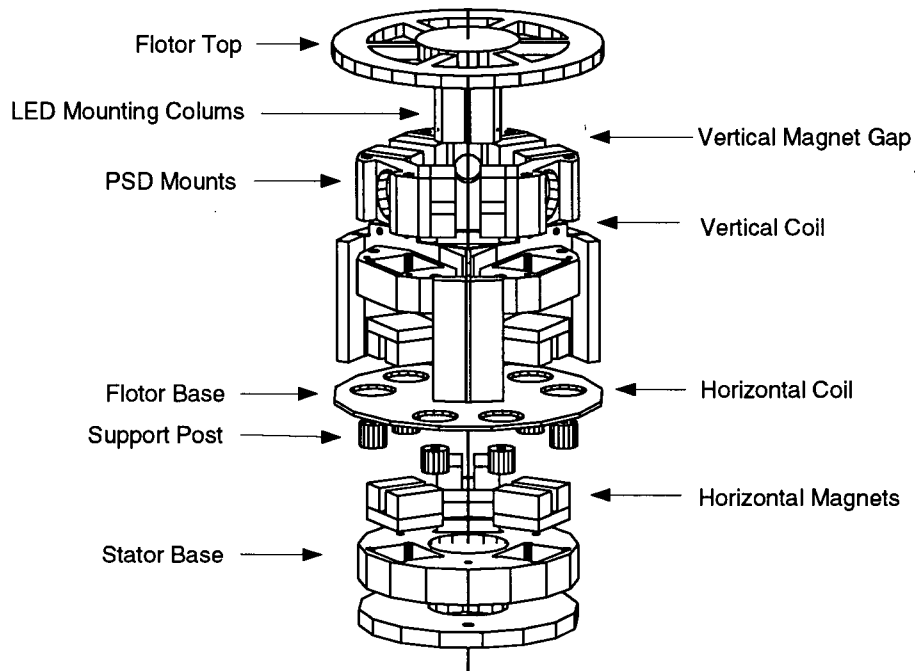


Figure 5.31 Maglev Joystick system configuration

Figure 5.32 Maglev Joystick assembly³

5.1.2 Sensor and actuator

The internal position measuring of the Maglev Joystick is accomplished by optical sensors which consist of light-emitting diodes (LED) and position-sensing devices (PSD). Three LED's mounted at the center of the flotor project narrow, coplanar, radial light beams 120° apart respectively onto the surfaces of the PSD's which are located at 120° intervals on the stator. Typical resolutions for such system are approximately $1 \mu m$ for translation and 0.001° for rotation.

Actuation for the Maglev Joystick is based on an electrodynamic, moving coil approach. Six coils and six pairs of permanent magnets mounted on flotor and stator respectively comprise six actuators which generate Lorentz forces to "fly" the flotor. The joystick workspace is limited by the size of the magnetic gap. A large workspace requires large magnets and high electric currents

³ Joystick design by S. E. Salcudean, AutoCAD drawing by C. T. Chen

which in turn increase the overall size of the wrist and could cause heating problems. The UBC Maglev Joystick has approximately $\pm 5 \text{ mm}$ translational motion and $\pm 7^\circ$ rotational motion from the nominal center. Two coordinate systems are defined: the stator coordinate frame, attached to the joystick stator, and the flotor coordinate frame, attached to the joystick flotor. The origin of the flotor coordinate frame is located at the intersection of the projection axes of the LED's. Due to the small motion range, the relation between the six coil currents and force-torque acting on the rigid flotor can be approximately expressed as linear transformation

$$\begin{bmatrix} {}^F f \\ {}^F \tau \end{bmatrix} = M I \quad (5.1)$$

where ${}^F f$ and ${}^F \tau$ are the force and torque vector with respect to and expressed in the flotor coordinate frame, $I = [I_1 \ I_2 \ I_3 \ I_4 \ I_5 \ I_6]^T$ is a vector of six coils currents and M is a well-conditioned 6×6 constant matrix.

5.1.3 Control about the Remote Center of Compliance

The control of the Maglev Joystick can be treated as the control of a free rigid body in space. By means of Remote Center of Compliance (RCC) control, we gain the ability to set the center of compliance of the rigid body anywhere in space. In [34], the center of compliance is assumed to be at the gravity center of the flotor. For the master-slave application, it is desirable to define the center of compliance of the master to be at the center of the handle.

In addition to the stator and flotor coordinate frames, we need to define two extra ones on the flotor: one called the tool frame which is at the remote center of compliance, the other called the gravity center frame which is at the center of gravity. They have the same orientation as the flotor frame, see Figure 5.33.

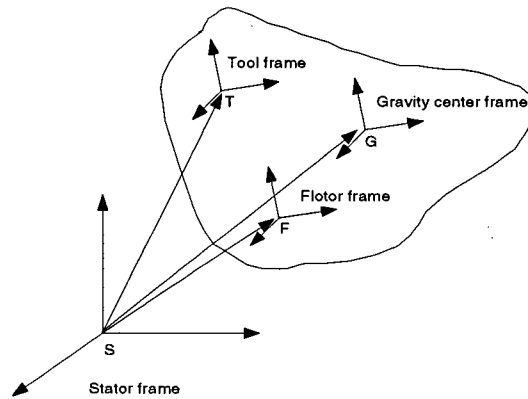


Figure 5.33 Frame assignment

We define the following symbols:

${}^G\omega$ = the flotor's angular velocity in gravity frame

GJ = flotor's inertia matrix in gravity frame

${}^G\tau$ = torque acting on the flotor with respect to gravity frame

${}^F\tau$ = torque acting on the flotor with respect to flotor frame (5.2)

Ff = force acting on the flotor in flotor frame

f = force acting on the flotor in stator frame

${}^G r_T$ = coordinates of point T in gravity frame

r_T = coordinates of point T in stator frame

${}^F r_G$ = coordinates of point G in flotor frame

Q = rotation matrix from stator frame to flotor frame (5.3)

m = mass of the flotor

g = gravity constant

For any vector $x = [x_1 \ x_2 \ x_3]^T$ a skew-symmetric matrix $x \times$ is defined as follows:

$$x \times \triangleq \begin{bmatrix} 0 & -x_3 & x_2 \\ x_3 & 0 & -x_1 \\ -x_2 & x_1 & 0 \end{bmatrix} \quad (5.4)$$

The rigid body dynamics can be described by two differential equations

$$\begin{aligned} {}^G \dot{\omega} &= -{}^G J^{-1} ({}^G \omega \times {}^G J {}^G \omega) + {}^G J^{-1} {}^G \tau \\ \ddot{r}_T &= \frac{f}{m} + g + Q {}^G \omega ({}^G \omega \times {}^G r_T) + \\ & \quad Q {}^G r_T {}^G J^{-1} ({}^G \omega \times {}^G J {}^G \omega) - Q {}^G r_T {}^G J^{-1} {}^G \tau \end{aligned} \quad (5.5)$$

where the first is for rotation, and the second is for translation.

Using Euler quaternions, the rotation can be described by a vector p , which is defined by

$$p = [\beta_0 \ \beta^T]^T = [\cos(\phi/2) \ \sin(\phi/2)s^T]^T \quad (5.6)$$

where s is the axis of rotation ($\|s\| = 1$) and ϕ is the angle of rotation.

The relations between the rotation matrix and Euler quaternions can be summarized as follows:

$$\begin{aligned} Q &= \exp(\phi s \times) = I + 2\beta_0 \beta \times + 2\beta \times^2 \\ \beta \times &= \frac{(Q - Q^T)}{2(1 + \text{tr}Q)^{1/2}} \\ \beta_0^2 + \beta^T \beta &= 1 \quad \beta_0 \geq 0 \end{aligned} \quad (5.7)$$

where $\text{tr}Q$ denotes the trace of Q .

Using the Euler quaternion representation and under the assumption of small angles and small angular velocities, the rigid body dynamic equations can be simplified as

$$\begin{aligned} \ddot{\beta} &= \frac{1}{2} {}^G J^{-1} {}^G \tau \triangleq u_1 \\ \ddot{r}_T &= \frac{1}{m} f + g - {}^G r_T \times {}^G J^{-1} {}^G \tau \triangleq u_2 \end{aligned} \quad (5.8)$$

Thus the dynamic equation can be easily transformed to decoupled second-order systems and controlled by the following feedback law:

$$u_1 = K_p(\beta_d - \beta) - K_v\dot{\beta} \quad (5.9)$$

$$u_2 = \tilde{K}_p(r_d - r_T) - \tilde{K}_v \dot{r}_T$$

where K_p , K_v , \tilde{K}_p and \tilde{K}_v are diagonal gain matrixes.

The current-force mapping is defined with respect to the flotor coordinate. The following transformation is performed to compute ${}^F\tau$ and Gf

$${}^Ff = Q^{-1}f \approx f \quad (5.10)$$

$${}^F\tau = {}^F r_G \times {}^Ff + {}^G\tau$$

Finally, the six coil currents required can be calculated as

$$I = M^{-1} \begin{bmatrix} {}^Ff \\ {}^F\tau \end{bmatrix} \quad (5.11)$$

where M^{-1} is a constant matrix which can be precomputed.

Previously, due to lack of inertial parameters, a simple PID control with gravity compensation was used. Experiments show the performance of such a controller degrades when the center of compliance is far away from the flotor center. Using parameter identification software developed in [35], the inertia matrix and the center of gravity of the joystick (with handle attached) were identified. Remote center of compliance control has been successfully implemented.

5.2 Slave — Hydraulic Mobile Machines

Two typical hydraulic mobile machines have been used as slaves for the study of force reflecting teleoperator systems. The CAT 215 excavator is a four DOF manipulator mainly used in general construction industry while the CAT 325 feller-buncher with five DOF used in the forestry industry. The machine joint angles are sensed using resolvers and hydraulic pressures are measured via pressure transducers. Both machines are outfitted with independent joint controllers due to previous work by P. D. Lawrence, D. Chan and S. Bachman at UBC.

5.3 Computing System

Based on a VME Bus structure, all the necessary processors, A/D and D/A boards can be hosted in one cage. The computing system configuration is shown in Figure 5.34.

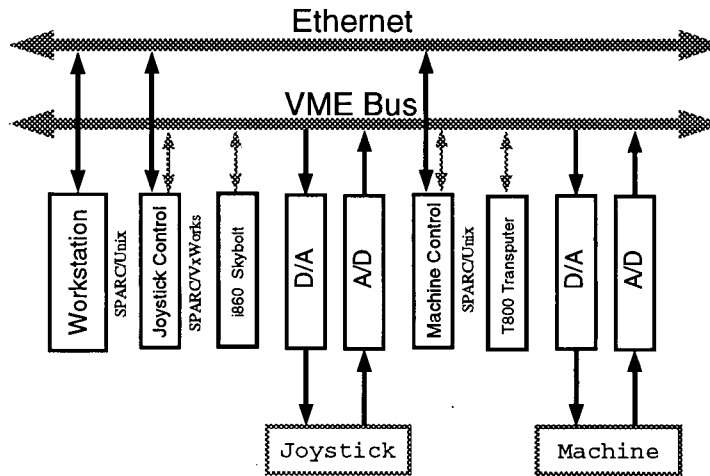


Figure 5.34 VME cage configuration

One SPARC 1E processor running the real-time multitasking operating system VxWorks and one Skybolt board take care of the computations of joystick control, slave path planning and force feedback. The Skybolt board which uses a 40 MHz i860 processor is a specially designed Math accelerator for Unix hosts. Now a new device driver makes it possible to directly interface with a VxWorks host to speed up VxWorks applications. The Skybolt, approximately 6 times as fast as a SPARC 1E, performs all the real-time computations while the SPARC 1E handles timer interrupts, collecting A/D data and sending D/A data. A shared memory block is defined at the Skybolt side to communicate with VxWorks across the VME Bus. The real-time control runs at 200 HZ. Another SPARC running Unix and a T800 Transputer are included in the same VME cage for the set-point control of hydraulic machines. The SPARC/Unix is the I/O host and the Transputer performs the real-time computations.

The SPARC/VxWorks board which is the host for the VME cage is connected to Ethernet allowing cross-development from a Unix host — Sun Workstation. This structure makes a user-friendly environment for software development. Useful tools such as Stethoscope and Vxgdb can be used for real-time data collection and program debugging.

Chapter 6 Machine Experiments

The master-slave multi-axes force-reflecting resolved motion control strategy was successfully implemented on a CAT-215 excavator and a CAT-325 feller-buncher. Machine experiments were carried out to investigate position versus rate control, stiffness versus force feedback control.

6.1 Endpoint Force Sensing

6.1.1 Modeling

Accurate force sensing is crucial for successful implementation of force feedback. In our experiments, the hydraulic transducers were mounted in the hoses close to the hydraulic pump. The hydraulic pressures were used to compute the joint torques. For a discussion of other force sensing methods, refer to [3] for details. Previously, Parker [3] used the Newton-Euler method to derive a model for a log-loader which is three DOF manipulator.

During free motion, the manipulator's joint torques are caused by the following factors: gravity of the links and the dynamic forces due to the machine motion. The dynamic equation for a manipulator is:

$$\tau = D(q)\ddot{q} + C(q, \dot{q})\dot{q} + g(q) \quad (6.1)$$

where $\tau = [\tau_1 \ \tau_2 \ \dots \ \tau_n]^T$ is the vector of generalized forces, $q = [q_1 \ q_2 \ \dots \ q_n]^T$ is the vector of generalized coordinates of the system. When the manipulator contacts the environment, the dynamic equation should be modified to include the effect of external force F , that is

$$\tau_i = D(q)\ddot{q} + C(q, \dot{q})\dot{q} + g(q) + J^T(q)F \quad (6.2)$$

where J is the manipulator Jacobian.

Thus in order to have an accurate measure of F , we need to know not only the joint torque τ , but also the dynamic model of the manipulator.

As discussed in [36], a key feature of rigid robot dynamics is its linearity in the parameters although the dynamic equation itself is highly nonlinear. The dynamic equation of a manipulator can be written in the following format, which is linear in the parameters

$$\tau = D(q)\ddot{q} + C(q, \dot{q})\dot{q} + g(q) = Y(q, \dot{q}, \ddot{q})P \quad (6.3)$$

where $Y(q, \dot{q}, \ddot{q})$ is an $n \times r$ matrix of known functions of joint variables and P is an r -dimensional vector of parameters which only depends on link mass, moments of inertia, etc. This property of linearity in parameters makes it easy to identify the dynamic model through a parameter estimation technique such as the Least-squares method.

It is possible to identify the complete model of a manipulator by using

$$\tau = D(q)\ddot{q} + C(q, \dot{q})\dot{q} + g(q) = Y(q, \dot{q}, \ddot{q})P \quad (6.4)$$

The joint velocities \dot{q} and accelerations \ddot{q} are required to obtain P . However, in practice, \ddot{q} is not available even if \dot{q} can be measured, and digital differentiation of \dot{q} is noisy. Secondly, even for a two link manipulator, the vector of parameters P contains nine components (see Spong [36]). The complete model of a four or five DOF manipulator would be much more complicated. Therefore, in our experiments, only the static case is modeled, that is

$$\tau = g(q) \quad (6.5)$$

and the contact force at end-effector is approximated by

$$F \approx (J^T(q))^{-1}(\tau_t - g(q)) \quad (6.6)$$

where τ_t is a vector of the joint torques computed from the hydraulic pressures, $g(q)$ can be obtained from the measured joint angles and the link parameters.

Thanks to the powerful symbolic computation package Maple, a computer program was written to derive the static model of manipulator automatically using the Euler-Lagrangian formulation. The procedure is straightforward: first, the forward kinematics is performed to locate the gravity center of each link, then the potential energy of the system is computed symbolically. Finally, the joint torques are derived by differentiating the potential energy, according to

$$\frac{\partial V}{\partial q} = \tau \quad (6.7)$$

There are several advantages of using a computer program to derive the manipulator model:

1. Speed: the Maple program can generate a dynamic model within 2–3 seconds.
2. Correctness: once the program is running, by changing the manipulator link parameters, such as link distance, length and twist, we can easily get the result for manipulators with different configurations, and guarantee its correctness.
3. Efficiency: the simple procedure can be applied to manipulators with any number of degrees of freedom, and is easy to debug. This can save tedious algebraic manipulation when dealing with robot with high DOF. Besides, Maple has many easy-to-use functions to either simplify the results or to shape them to the format you like. These all can be done within a few seconds.

We have also successfully derived the manipulator Jacobian for the excavator and the feller-buncher symbolically using the Maple program. This is very helpful in real-time applications.

Static Model of the Excavator

$$\tau = Y(q, \dot{q}, \ddot{q})P = \begin{bmatrix} 0 & 0 & 0 & 0 & 0 & 0 \\ C_{234} & S_{234} & C_{23} & S_{23} & C_2 & S_2 \\ C_{234} & S_{234} & C_{23} & S_{23} & 0 & 0 \\ C_{234} & S_{234} & 0 & 0 & 0 & 0 \end{bmatrix} P \quad (6.8)$$

where $\tau = [\tau_1 \tau_2 \tau_3 \tau_4]^T$, $P = [P_1 P_2 P_3 P_4 P_5 P_6]^T$, $S_{234} = \sin(\theta_2 + \theta_3 + \theta_4)$ etc.

Static Model of the Feller-buncher

$$\tau = Y(q, \dot{q}, \ddot{q})P = \begin{bmatrix} 0 & 0 & 0 & 0 & 0 & 0 & 0 \\ C_{234}C_5 & C_{234} & S_{234} & C_{23} & S_{23} & C_2 & S_2 \\ C_{234}C_5 & C_{234} & S_{234} & C_{23} & S_{23} & 0 & 0 \\ C_{234}C_5 & C_{234} & S_{234} & 0 & 0 & 0 & 0 \\ -S_{234}S_5 & 0 & 0 & 0 & 0 & 0 & 0 \end{bmatrix} P \quad (6.9)$$

where $\tau = [\tau_1 \tau_2 \tau_3 \tau_4 \tau_5]^T$, $P = [P_1 P_2 P_3 P_4 P_5 P_6 P_7]^T$, $S_{234} = \sin(\theta_2 + \theta_3 + \theta_4)$ etc.

Jacobian of the Excavator

The nonzero elements of the Jacobian are as follows:

$$\begin{aligned}
 J[0][0] &= d_2 \\
 J[2][0] &= -a_4 C_{234} - a_3 C_{23} - a_2 C_2 - a_1 \\
 J[4][0] &= 1.0 \\
 J[0][1] &= -a_4 S_{234} - a_3 S_{23} - a_2 S_2 \\
 J[1][1] &= a_4 C_{234} + a_3 C_{23} + a_2 C_2 \\
 J[5][1] &= 1.0 \\
 J[0][2] &= -a_4 S_{234} - a_3 S_{23} \\
 J[1][2] &= a_4 C_{234} + a_3 C_{23} \\
 J[5][2] &= 1.0 \\
 J[0][3] &= -a_4 S_{234} \\
 J[1][3] &= a_4 C_{234} \\
 J[5][3] &= 1.0
 \end{aligned} \tag{6.10}$$

where J is the manipulator's Jacobian with respect to frame \underline{C}_1 , $S_{234} = \sin(\theta_2 + \theta_3 + \theta_4)$

etc.

Jacobian of the Feller-buncher

The nonzero elements of the Jacobian are as follows:

$$\begin{aligned}
 J[0][0] &= -a_5 S_5 \\
 J[2][0] &= -a_1 - 0.5a_5 C_{234-5} - 0.5a_5 C_{2345} - a_2 C_2 + d_5 S_{234} - a_4 C_{234} - a_3 C_{23} \\
 J[4][0] &= 1.0 \\
 J[0][1] &= -a_2 S_2 - a_3 S_{23} - a_4 S_{234} - d_5 C_{234} - 0.5a_5 S_{234-5} - 0.5a_5 S_{2345} \\
 J[1][1] &= 0.5a_5 C_{234-5} + 0.5a_5 C_{2345} + a_2 C_2 - d_5 S_{234} + a_4 C_{234} + a_3 C_{23} \\
 J[5][1] &= 1.0 \\
 J[0][2] &= -a_3 S_{23} - a_4 S_{234} - d_5 C_{234} - 0.5a_5 S_{234-5} - 0.5a_5 S_{2345} \\
 J[1][2] &= 0.5a_5 C_{234-5} + 0.5a_5 C_{2345} - d_5 S_{234} + a_4 C_{234} + a_3 C_{23} \\
 J[5][2] &= 1.0 \\
 J[0][3] &= -a_4 S_{234} - d_5 C_{234} - 0.5a_5 S_{234-5} - 0.5a_5 S_{2345} \\
 J[1][3] &= 0.5a_5 C_{234-5} + 0.5a_5 C_{2345} - d_5 S_{234} + a_4 C_{234} \\
 J[5][3] &= 1.0 \\
 J[0][4] &= 0.5a_5 S_{234-5} - 0.5a_5 S_{2345} \\
 J[1][4] &= -0.5a_5 C_{234-5} + 0.5a_5 C_{2345} \\
 J[2][4] &= -a_5 C_5 \\
 J[3][4] &= -S_{234} \\
 J[4][4] &= C_{234}
 \end{aligned} \tag{6.11}$$

where J is the manipulator's Jacobian with respect to frame \underline{C}_1 , $S_{234} = \sin(\theta_2 + \theta_3 + \theta_4)$, $S_{234-5} = \sin(\theta_2 + \theta_3 + \theta_4 - \theta_5)$ etc.

6.1.2 Torque Computations

The hydraulic cylinder force can be computed from the hydraulic pressures and the cylinder geometry:

$$F_{cyl} = P_{in}A_{in} - P_{out}A_{out} \quad (6.12)$$

where P_{in} , P_{out} are the pressures at the piston head side and rod side respectively, A_{in} , A_{out} are the areas at the piston head side and rod side.

Link Name	Head Area in (in^2)	Rod Area in (in^2)
Boom	31.80	19.92
Stick	23.75	14.13
Bucket	15.90	9.96

Table 6.3 Piston geometry of the excavator

Link Name	Head Diameter in (mm)	Rod Diameter in (mm)
Boom	120.00	85.00
Stick	150.00	105.00
Tilt	150.00	105.00
Head	152.40	63.50

Table 6.4 Piston geometry of the feller-buncher

Referring to the excavator and feller-buncher schematics Figure 1.3 and Figure 1.5, there are only two types of mechanical linkage on these machines: two-bar linkage and four-bar linkage, see below:

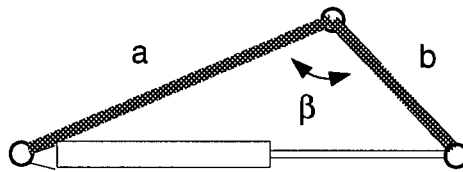


Figure 6.35 Two-bar mechanical linkage

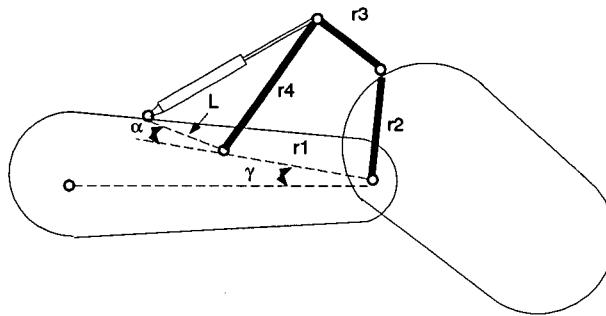


Figure 6.36 Four-bar mechanical linkage

Joint torques can easily be derived for a two-bar linkage as the following:

$$|\tau| = |F_{cyl}| \frac{ab|\sin \beta|}{\sqrt{a^2 + b^2 - 2ab \cos \beta}} \quad (6.13)$$

where F_{cyl} is the hydraulic cylinder force, β is the joint angle, a and b are the linkage lengths.

For the torque computation of a four-bar linkage, refer to [37] for detail.

Boom	Stick	Bucket
Two-bar Linkage	Two-bar Linkage	Four-bar Linkage
$a = 1999.8$ (mm)	$a = 720.2$ (mm)	$r1 = 324.9$ (mm), $r2 = 404.9$ (mm)
$b = 624.0$ (mm)	$b = 2443.6$ (mm)	$r3 = 484.9$ (mm), $r4 = 548.6$ (mm)
		$\gamma = 0.0468407$ (rad)
		$\alpha = 0.3469905$ (rad)
		$L = 1602.7$ (mm)

Table 6.5 Joint linkage geometry of the excavator

Boom	Stick	Tilt	Head
Two-bar Linkage	Two-bar Linkage	Four-bar Linkage	Two-bar Linkage
$a = 2281.6$ (mm)	$a = 901.2$ (mm)	$r1 = 481.3$ (mm)	$a = 634.0$ (mm)
$b = 911.2$ (mm)	$b = 2339$ (mm)	$r2 = 563.7$ (mm)	$b = 588.0$ (mm)
		$r3 = 640$ (mm)	
		$r4 = 685$ (mm)	
		$\gamma = 0.0728$ (rad)	
		$\alpha = 0.1831$ (rad)	
		$L = 2316.3$ (mm)	

Table 6.6 Joint Linkage geometry of the feller-buncher

6.1.3 Recursive Least-squares Link Parameter Estimation

There are several reasons for using a recursive estimation method. First, it is likely that some experimental data are corrupted due to factors such as temporary sensor or transmitter failure, etc. Since the number of observations is always limited, these outliers can have a strong effect on the estimated parameters. Thus it is important to evaluate the estimated parameter over the full range of observation so that the residuals can be examined to find out any "bad data" which is responsible for large residual values. In our case, these outliers can be eliminated, and the estimation procedure repeated. Secondly, from the plots, we can get information such as convergence. With this information, we can get some idea as to what degree of accuracy the estimated parameters have. In the case of nonconvergence, we can reexamine the whole procedure including the way the experiments were carried out, find the cause, then take appropriate measures. During the experiments, the hydraulic machines were commanded to move slowly from one configuration to another randomly while the joint angles and hydraulic pressures were recorded. Then, these data were subsampled for off-line estimation. The initial parameters and the covariance matrix were computed from the first 50 sets of data. The recursive Least-squares estimation results for the excavator and the feller-buncher are shown in Figure 6.37 — Figure 6.44 in which we call each set of data one "sample".

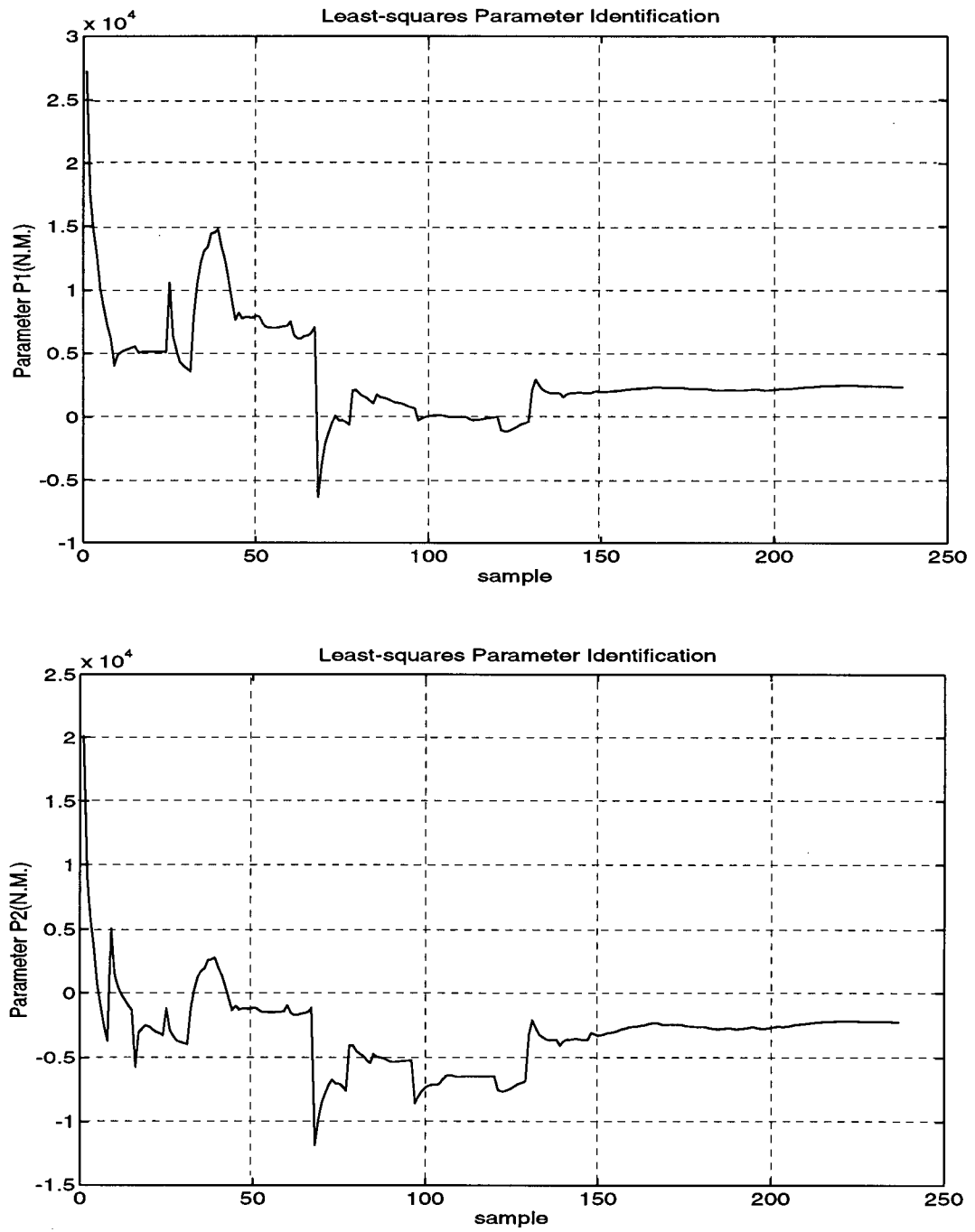


Figure 6.37 Excavator link parameter identification

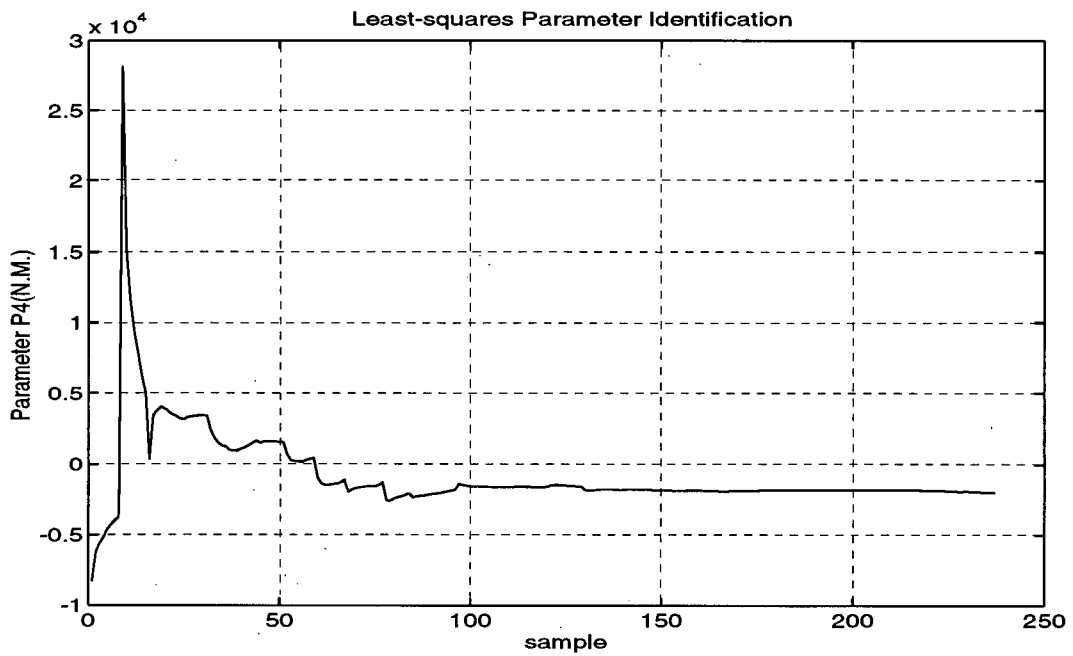
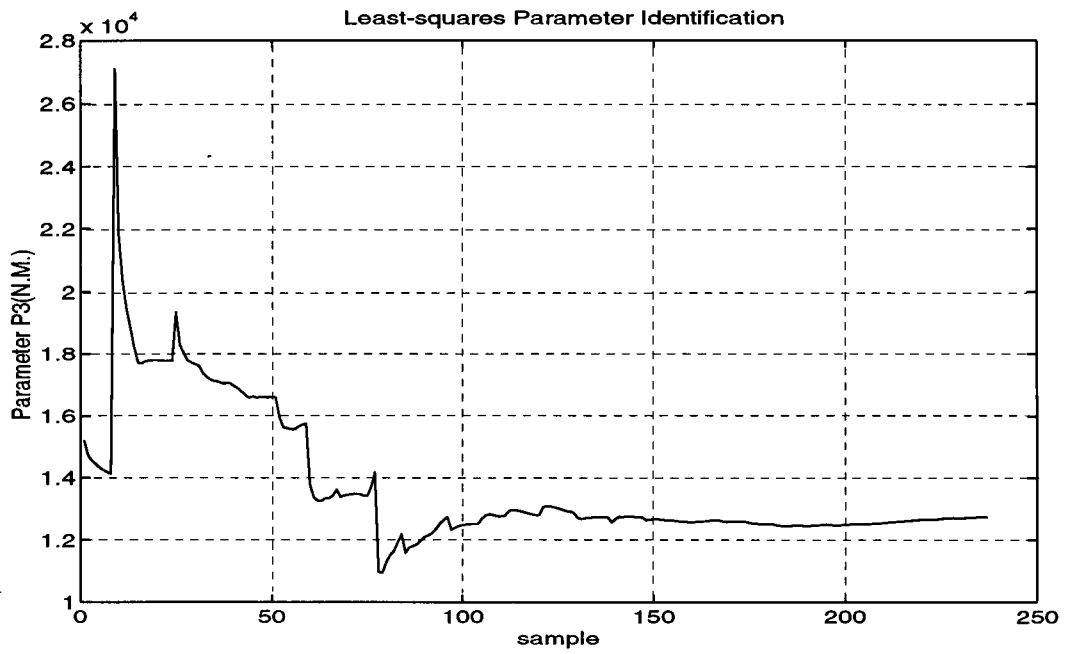


Figure 6.38 Excavator link parameter identification

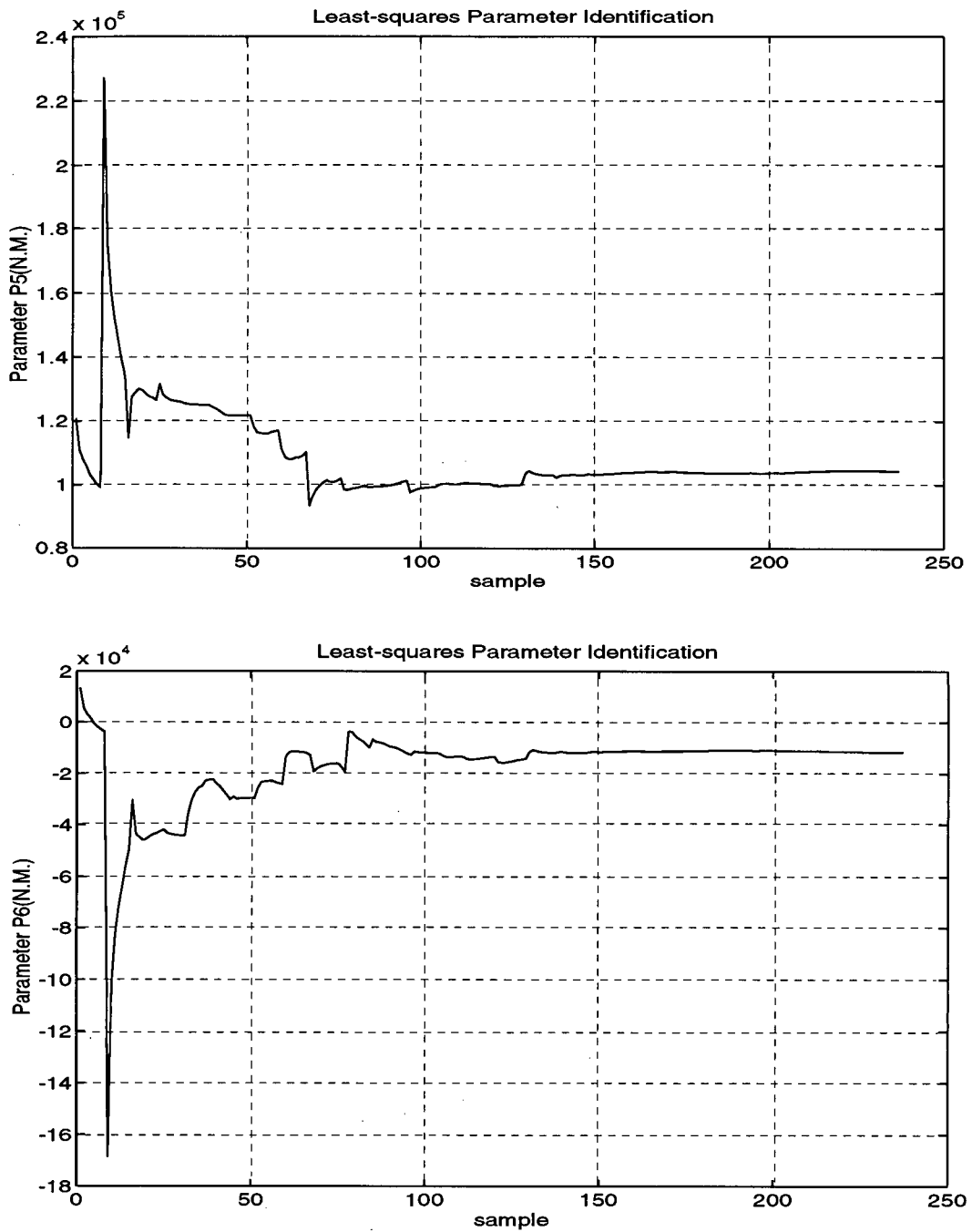


Figure 6.39 Excavator link parameter identification

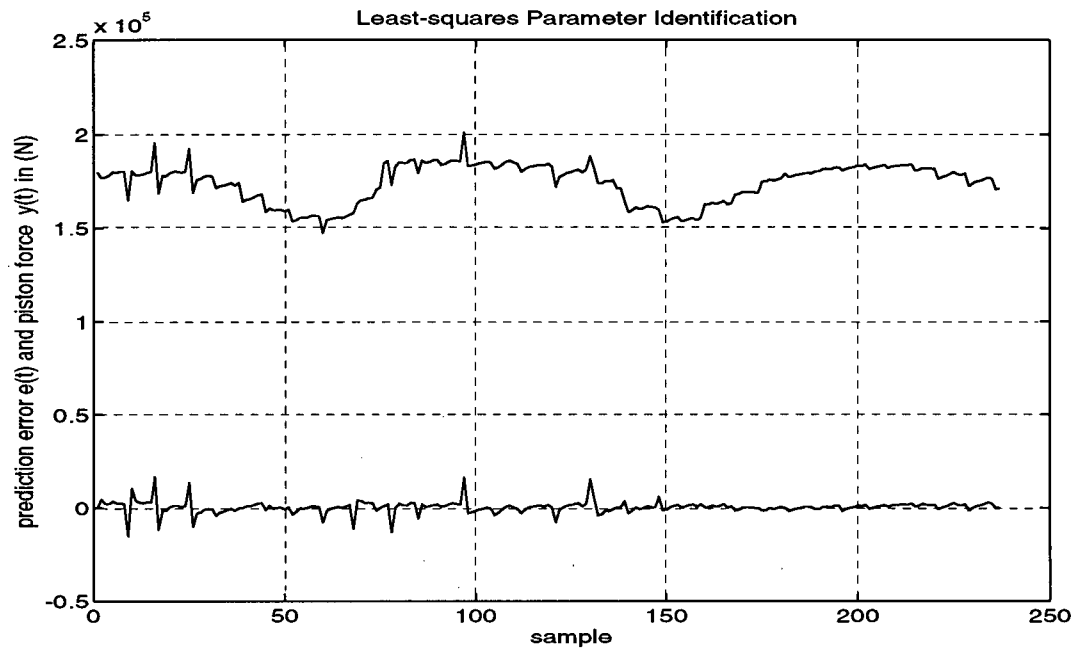


Figure 6.40 Excavator link parameter identification

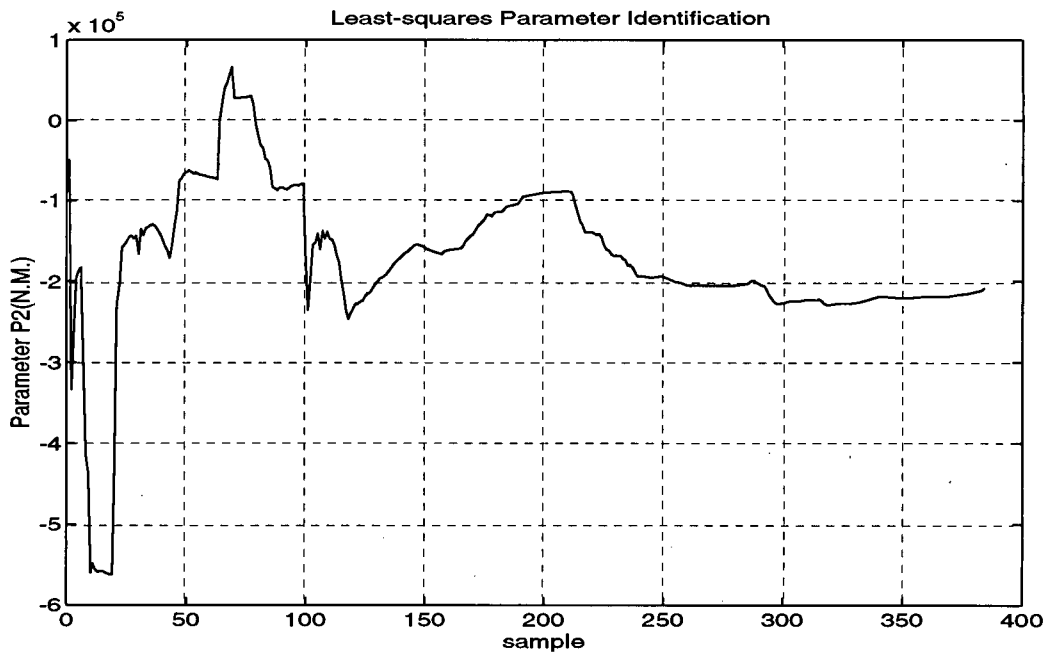
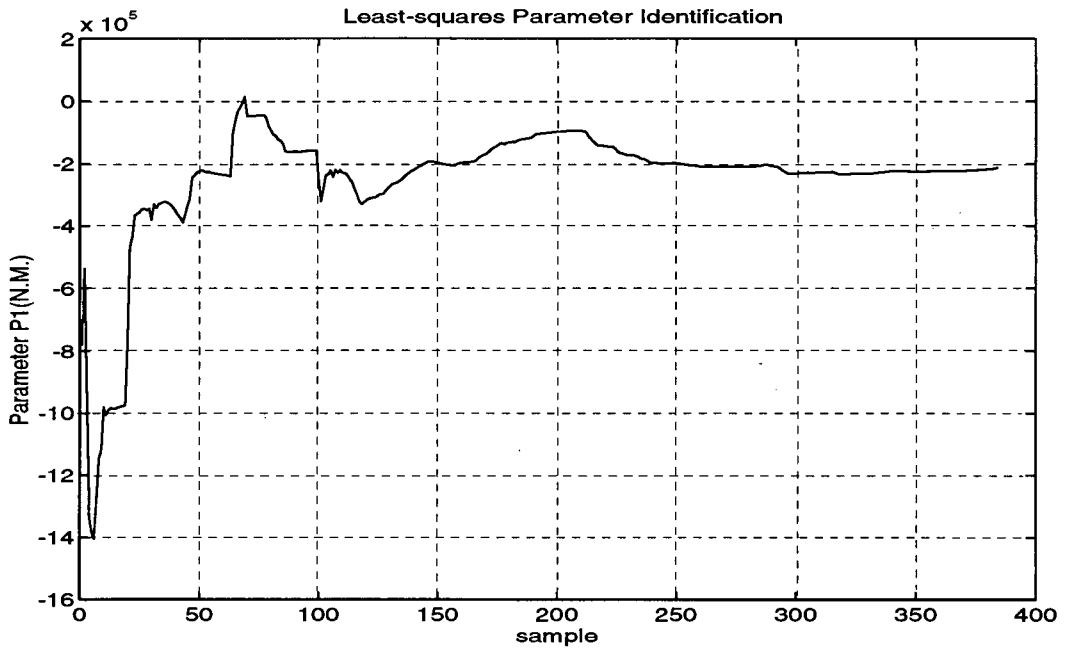


Figure 6.41 Feller-buncher link parameter identification

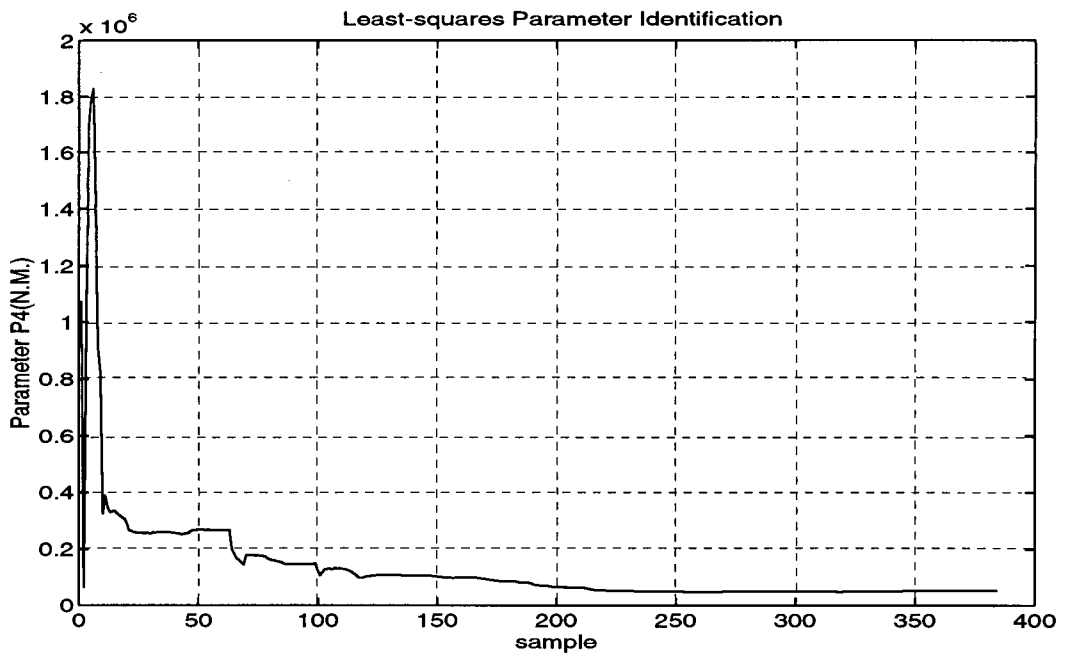
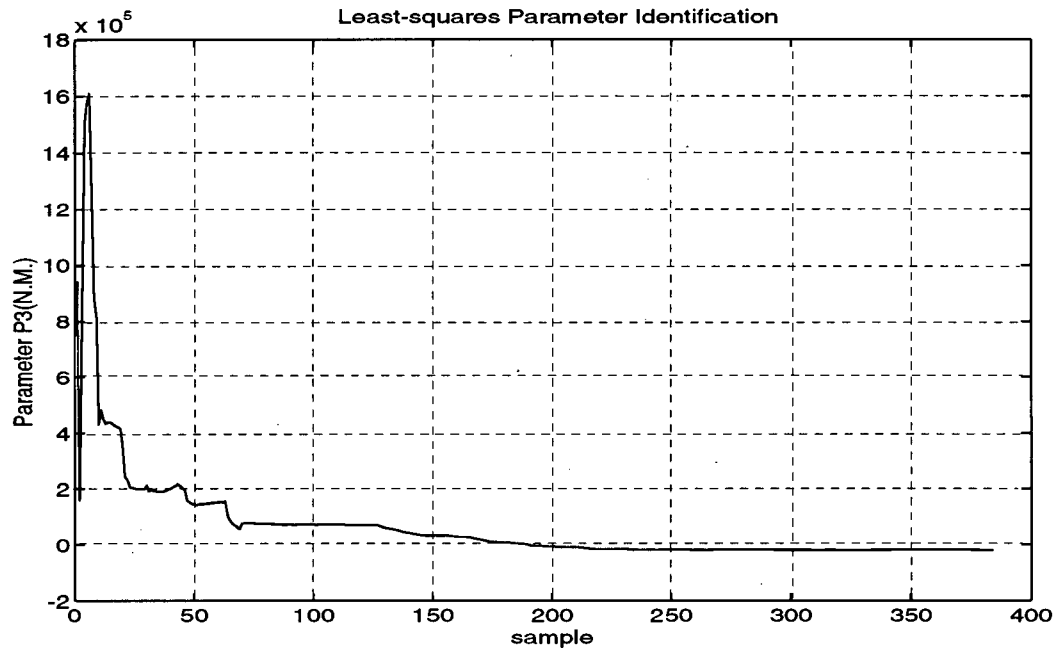


Figure 6.42 Feller-buncher link parameter identification

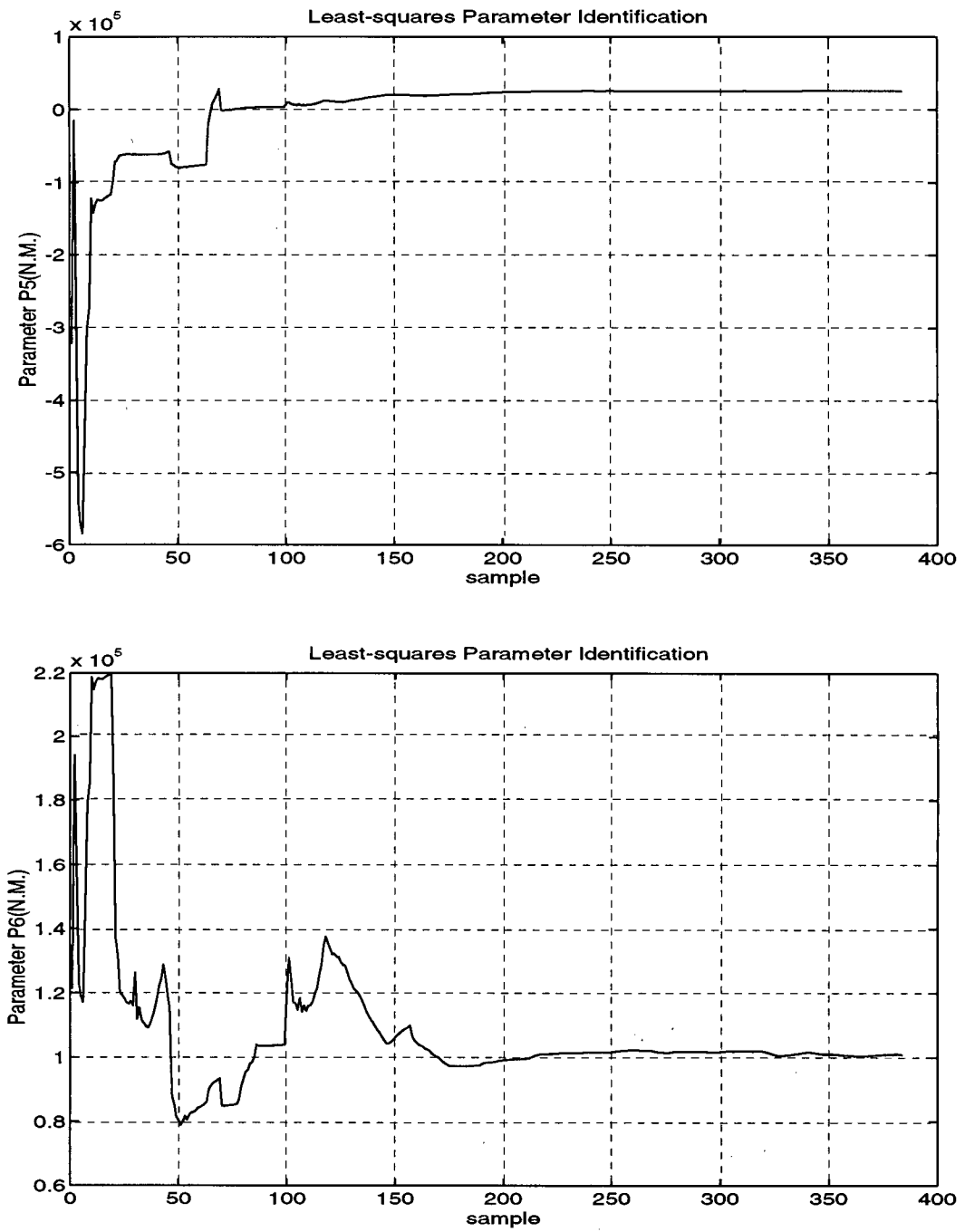


Figure 6.43 Feller-buncher link parameter identification

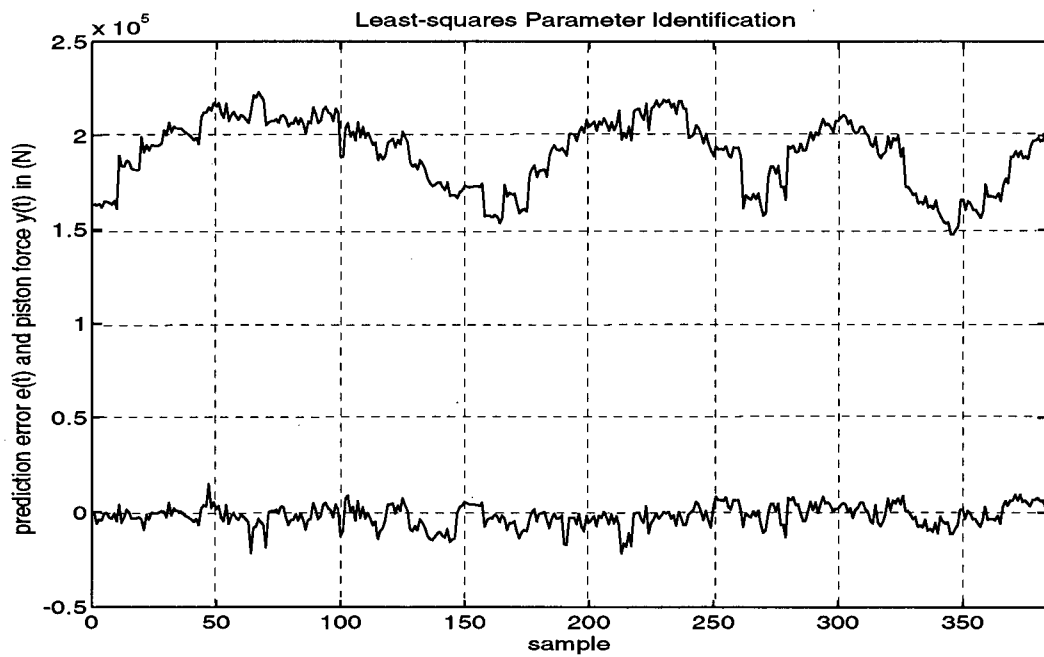
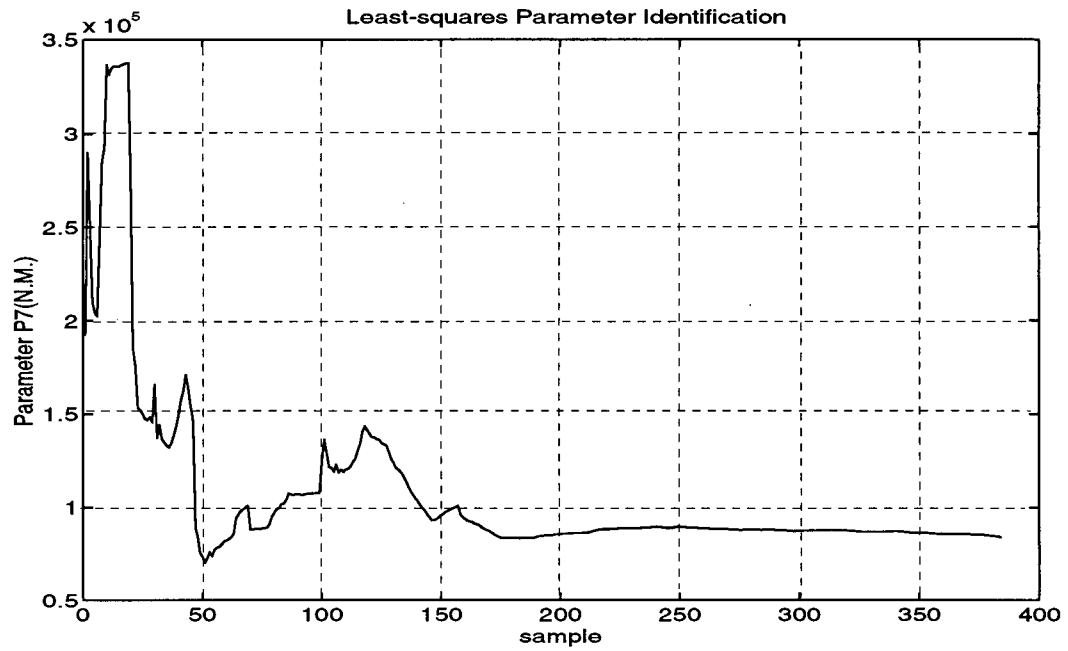


Figure 6.44 Feller-buncher link parameter identification

6.2 Excavator Experiments

The master-slaver force reflecting resolved motion control was first implemented on a four DOF manipulator — CAT 215 excavator. The machine was operated remotely from a nearby lab. The first set of experiments focused on resolved motion control — position versus rate. Hands-on experiences confirmed the results reported by Kim [8] that for a slow manipulator such as a hydraulic excavator, rate control is preferable. The mismatch of the fast joystick and the slow excavator could cause oscillation under position control. On the other hand, an operator can easily achieve a smooth operation when the machine is under rate control. While position control is important in some delicate operations such as peg-in-hole or microsurgery etc., the application of such control to hydraulic machines is not suitable at least from the operator's point of view. The second set of experiments were carried out to test different force reflection schemes, namely stiffness versus direct force feedback.

The following gains were selected for the joystick control during the experiments (see Figure 4.24):

Axis	Kp max	Kp nom	Kp min	Kd	Deadband
X	4.0	0.6	0.3	0.06	1.5
Y	4.0	0.6	0.3	0.06	1.5
Z	4.0	0.6	0.3	0.06	1.5
X Rotation	0.1	0.06	0.01	0.03	2000.0
Y Rotation	0.1	0.06	0.01	0.03	50.0
Z Rotation	0.1	0.06	0.01	0.03	2000.0

Table 6.7 Gain selections for the excavator experiments

In the above table, Kp(max) is the maximum stiffness value, Kp(nom) is the nominal stiffness value, Kp(min) is the minimum stiffness value (units: N/mm for translation and 100 Nm/rad for

rotation); K_d is the damping factor (units: N/mm/s for translation and 100 Nm/rad/s for rotation); The units for the joystick deadband are mm for translation and 0.0001rad for rotation.

The contact force for feedback is saturated by the following values:

Axis	X	Y	Z	X Rotation	X Rotation	X Rotation
F_max	50 (KN)	50 (KN)	50 (KN)	40 (KNm)	40 (KNm)	40 (KNm)

Table 6.8 Maximum feedback force for the excavator experiments

6.2.1 Resolved Motion Control

The machine was under rate control and operated remotely to achieve straight line motions. Figure 6.45 and Figure 6.46 show the bucket was commanded to go straightly up and down while keeping the bucket angle and radial displacement constant. Figure 6.47 and Figure 6.48 show the bucket was directed to come straightly out from and in towards the cabin while keeping the bucket angle and height constant. The joystick deadband is 1.5 mm. It is clear from these plots that the motion accuracy is high due to the fact inverse kinematics instead of Jacobian transformations were used and the joint angles of the excavator were under closed-loop control.

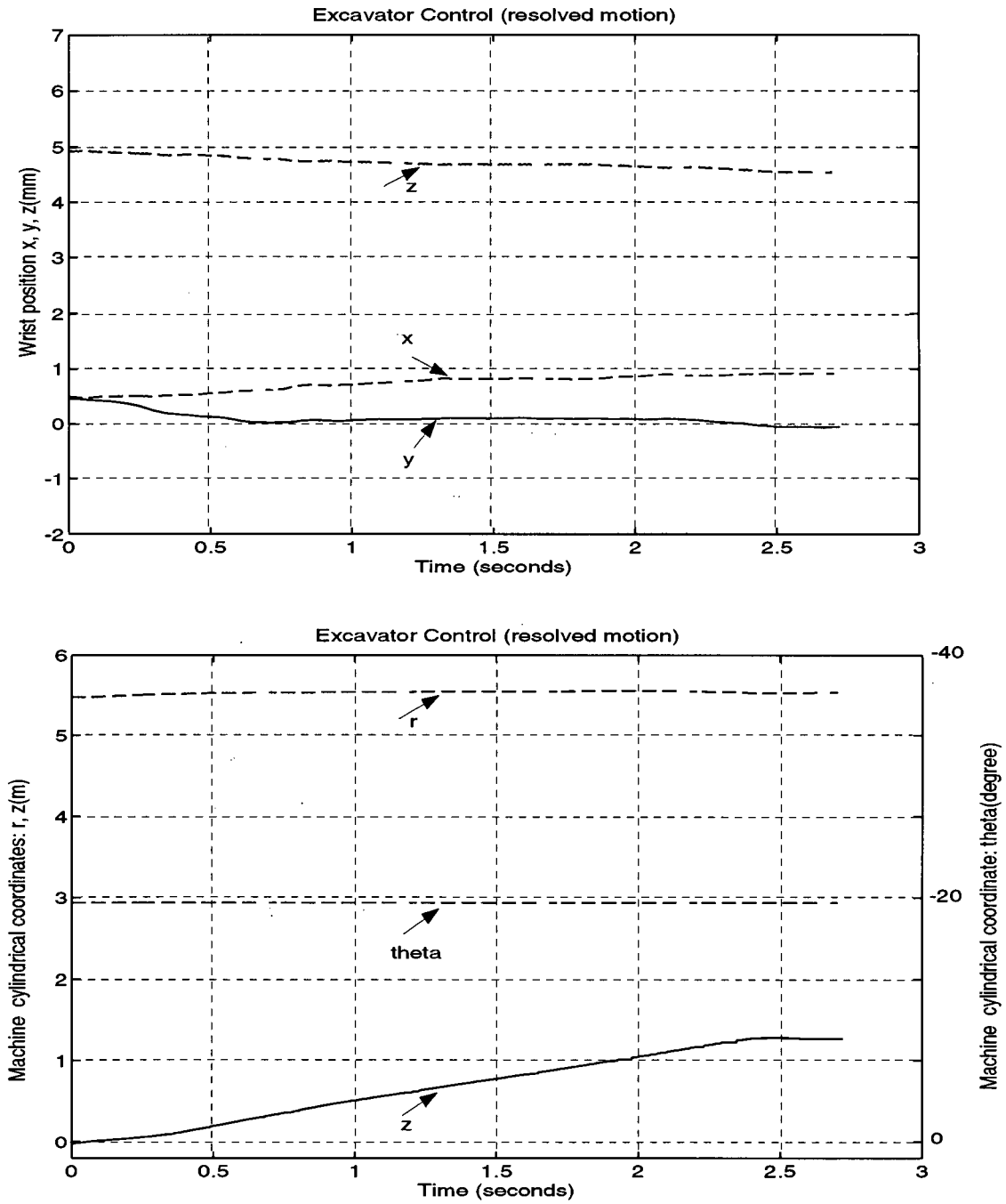


Figure 6.45 Excavator resolved motion control: bucket straight up

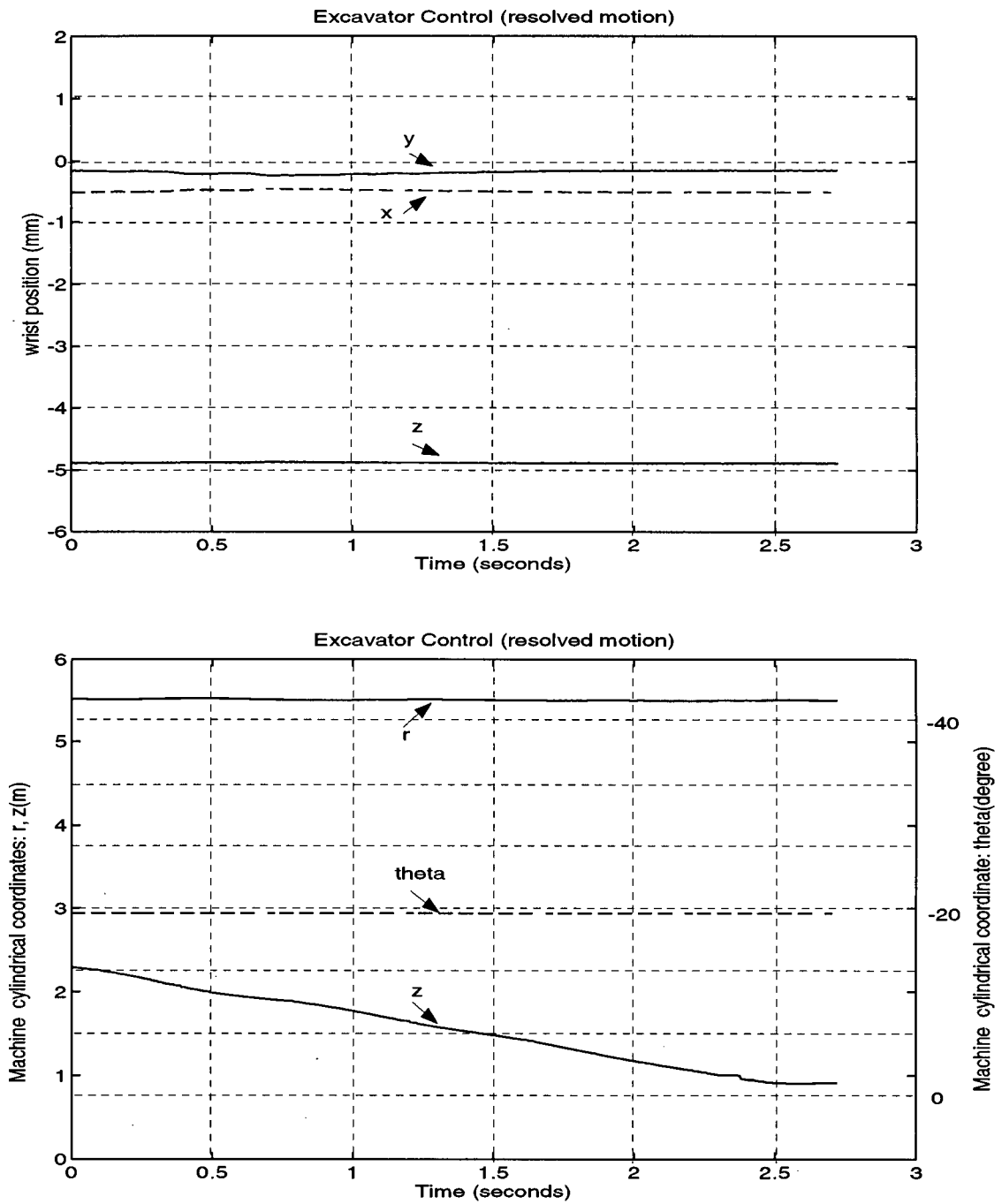


Figure 6.46 Excavator resolved motion control: bucket straight down

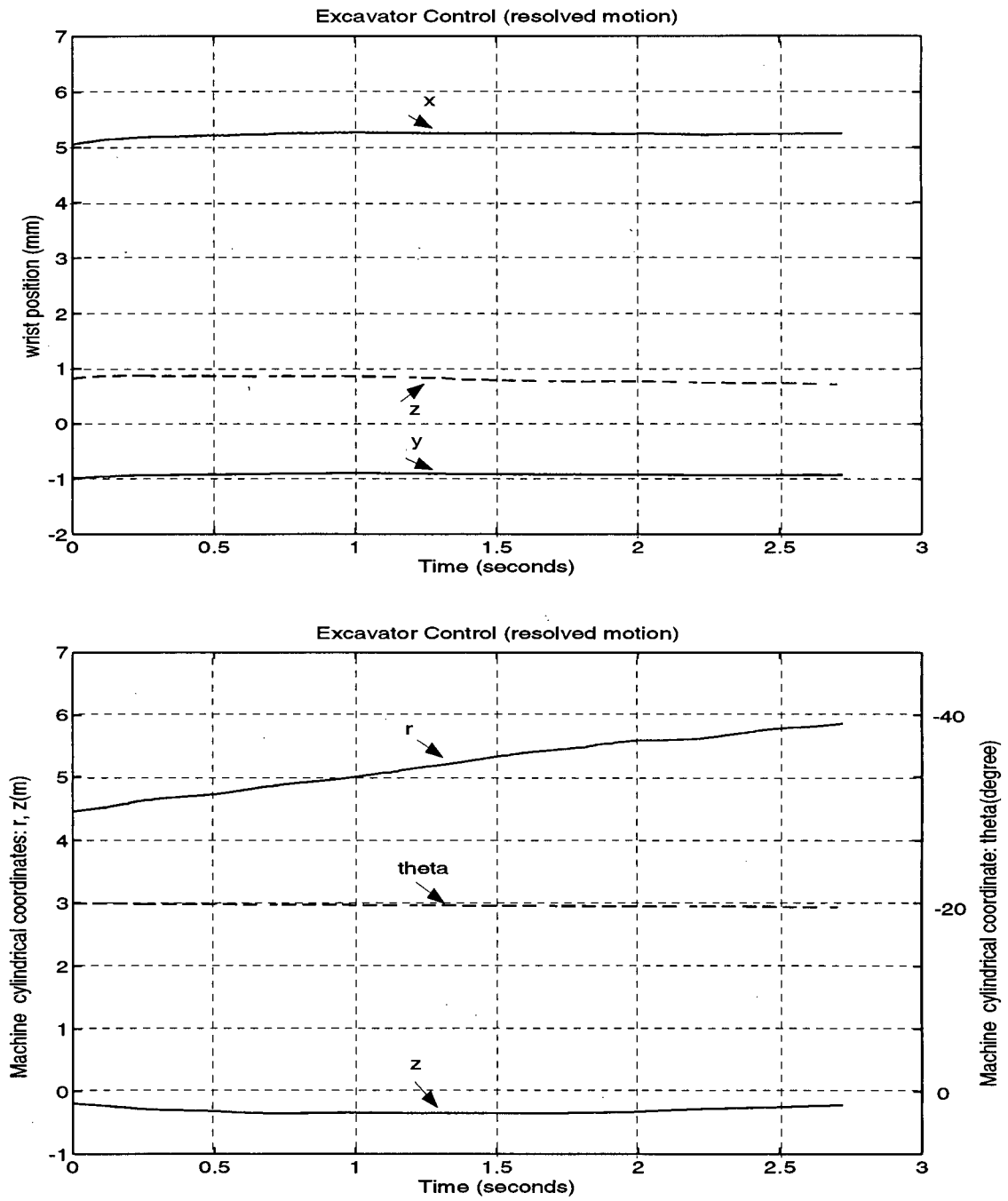


Figure 6.47 Excavator resolved motion control: bucket straight out

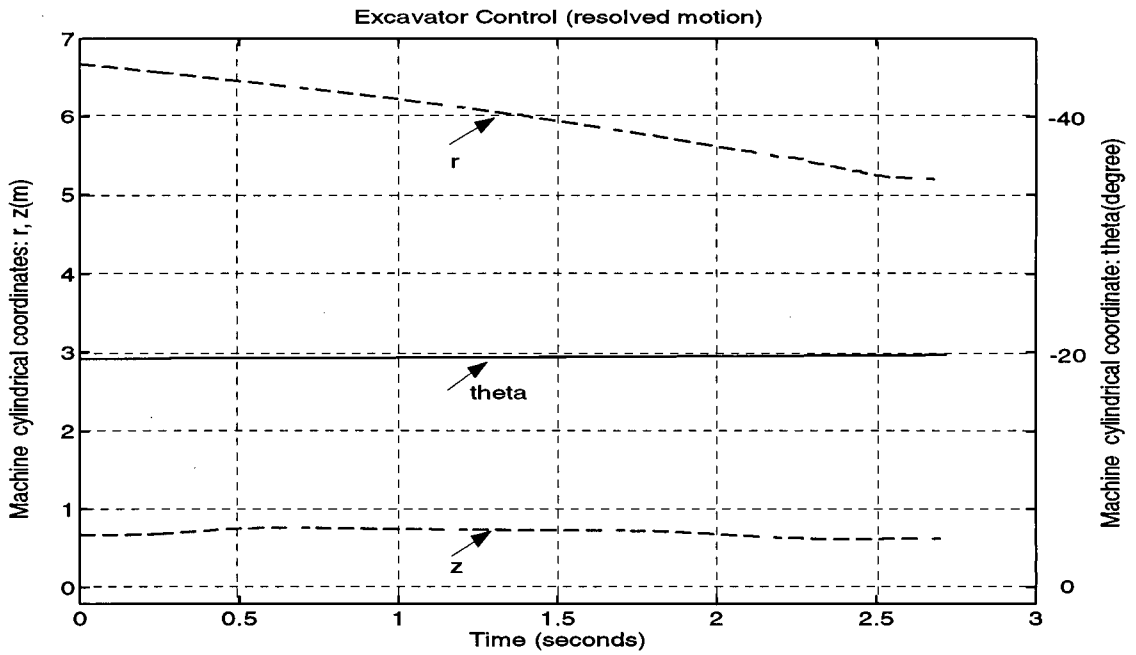
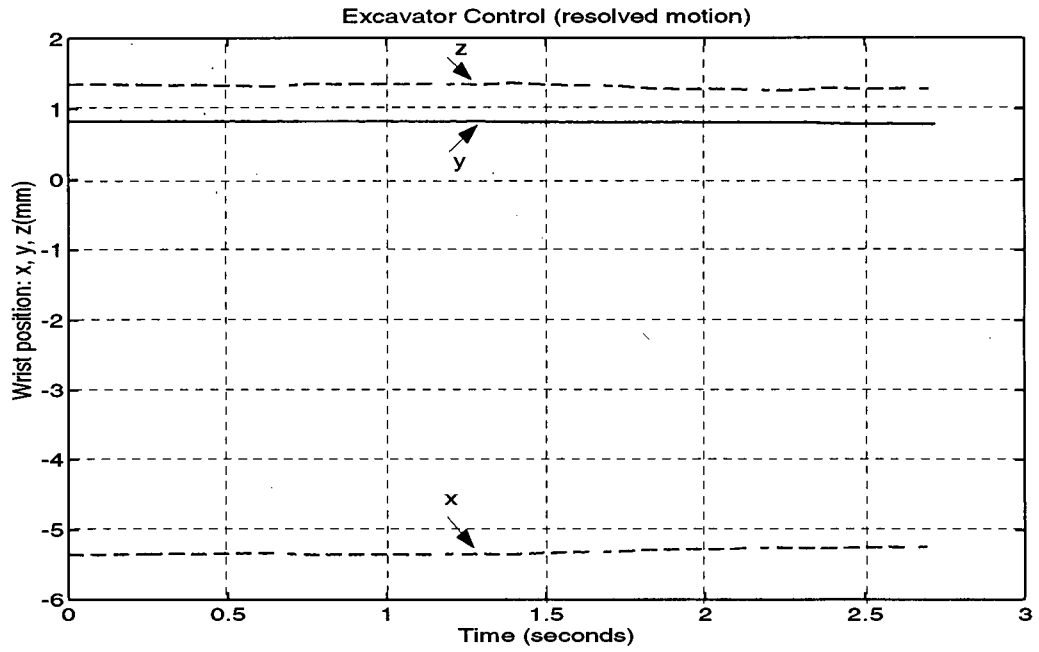


Figure 6.48 Excavator resolved motion control: bucket straight in

6.2.2 Applying a Desired Force

This experiment is to test the ability of an operator to apply a desired force to the environment via our force reflection master-slave teleoperator system. The operator sat in the lab and remotely commanded the excavator to contact the ground. At the beginning, he was allowed to look at the force display on the screen to relate the contact force to the kinesthetic feel at his hand. Then the operator was asked to apply a desired force to the ground depending solely on the information from the joystick. The operator's hand applied forces were measured using JR-3 force sensor. Two force reflection methods were tested — stiffness and direct force feedback. Results are shown in Figure 6.47 and Figure 6.48 respectively. Both methods achieved reasonably good results in terms of controlling the endpoint force. However, direct force feedback method is only possible when the amount of force feedback is severely restricted. Otherwise, stability problems can arise. In stiffness control (Figure 6.47), the operator's hand applied force is proportional to the wrist displacement along corresponding z axis. In direct force feedback (Figure 6.48) while the operator applied -4.5 Newton force to the wrist to counterbalance the feedback force there is almost no wrist displacement in z axis.

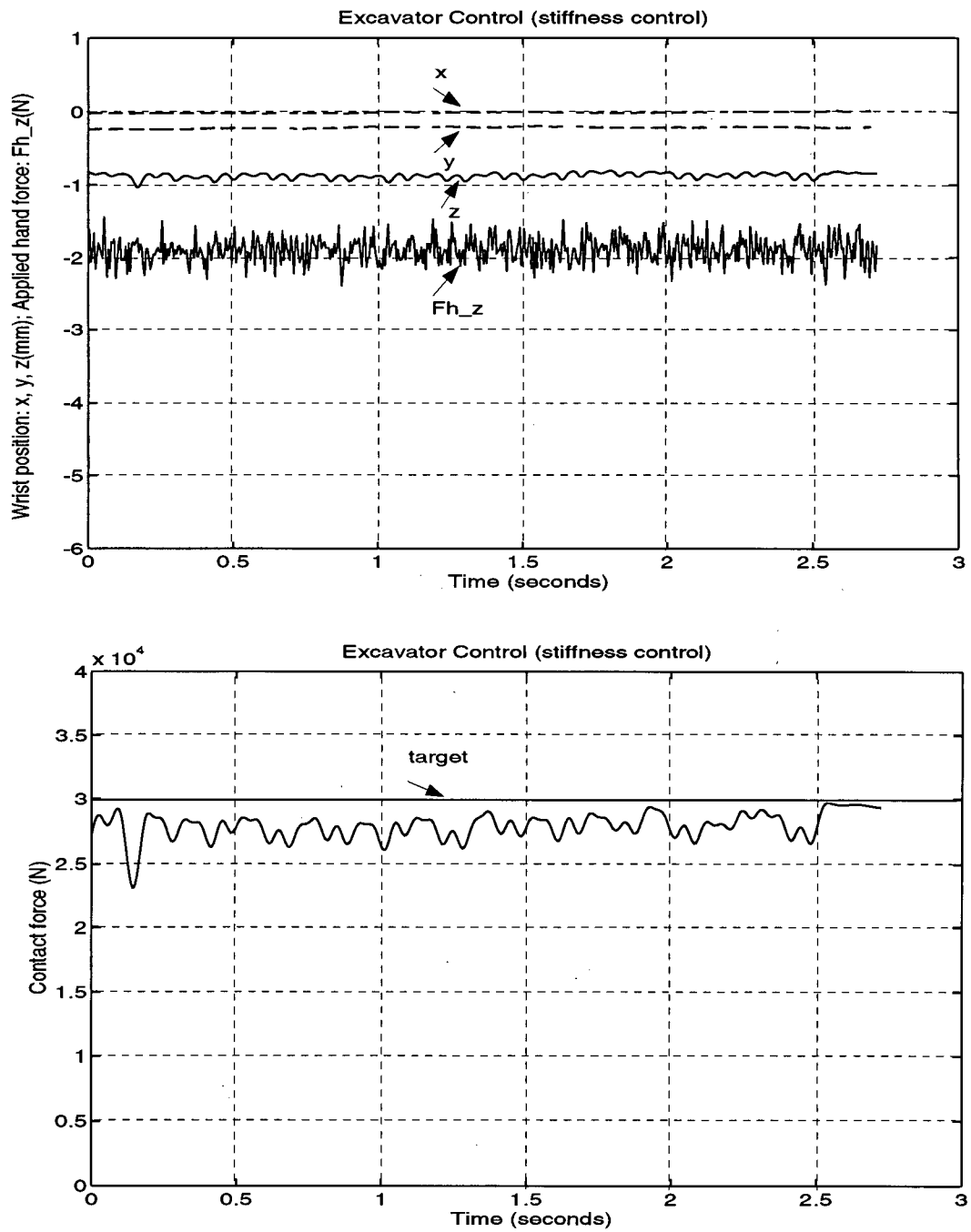


Figure 6.49 Excavator stiffness control: applying a desired force

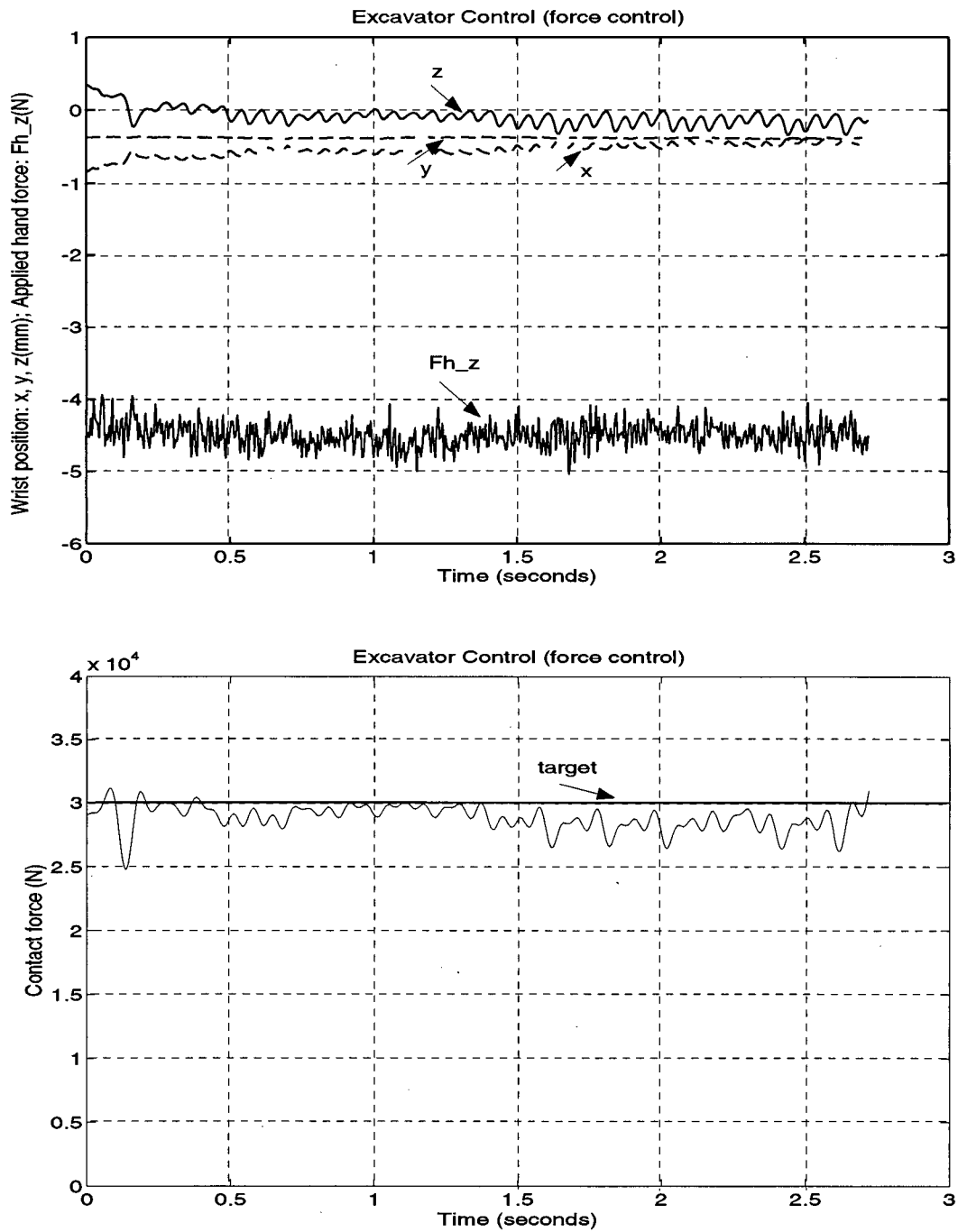


Figure 6.50 Excavator force control: applying a desired force

6.3 Feller-buncher Experiments

The master-slaver force reflecting resolved motion control was also implemented on a five DOF manipulator — CAT 325 feller-buncher. The master Maglev Joystick was mounted in the cabin during the experiments. Field tests such as tree-cutting were also carried out. Experiments show that while the sound of the engine and the motion of the machine do provide the operator with information to detect potential machine tip over, the most effective way is via force reflection which automatically pushes the joystick back into its position deadband. Similar to the excavator experiments, position control was found to be unsuitable for the control of the feller-buncher. Direct force feedback is possible only if the amount of feedback is severely limited.

The following gains were selected for the joystick control during the experiments (see Figure 4.24):

Axis	Kp max	Kp nom	Kp min	Kd	Deadband
X	8.0	4.0	3.00	0.06	1.5
Y	4.0	3.0	2.00	0.06	1.5
Z	9.0	4.0	3.00	0.06	1.5
X Rotation	0.8	0.45	0.30	0.04	350.0
Y Rotation	0.8	0.45	0.30	0.04	350.0
Z Rotation	0.26	0.25	0.24	0.04	2000.0

Table 6.9 Gain selections for the feller-buncher experiments

In the above table, Kp(max) is the maximum stiffness value, Kp(nom) is the nominal stiffness value, Kp(min) is the minimum stiffness value (units: N/mm for translation and 100 Nm/rad for rotation); Kd is the damping factor (units: N/mm/s for translation and 100 Nm/rad/s for rotation); The units for the joystick deadband are mm for translation and 0.0001rad for rotation.

The contact force for feedback is saturated by the following values:

Axis	X	Y	Z	X Rotation	X Rotation	X Rotation
F_max	30 (KN)	30 (KN)	30 (KN)	40 (KNm)	40 (KNm)	40 (KNm)

Table 6.10 Maximum feedback force for the feller-buncher experiments

Hydraulic mobile machines such as excavators and feller-bunchers often operate in harsh environments. Bumpy road conditions can cause undesired motion of the joystick. Thus it is desirable to have a stiff joystick. On the other hand, an operator may get tired from manipulating a stiff joystick during normal operation. Also, a stiff joystick could easily cause heating problem. Another problem often encountered when using multi-degree joysticks is coupling between joystick axes. A motion in one direction could easily cause an unexpected motion in another.

In order to solve these problems, a detent scheme was implemented in the digital PID controller, as shown in Figure 6.51.

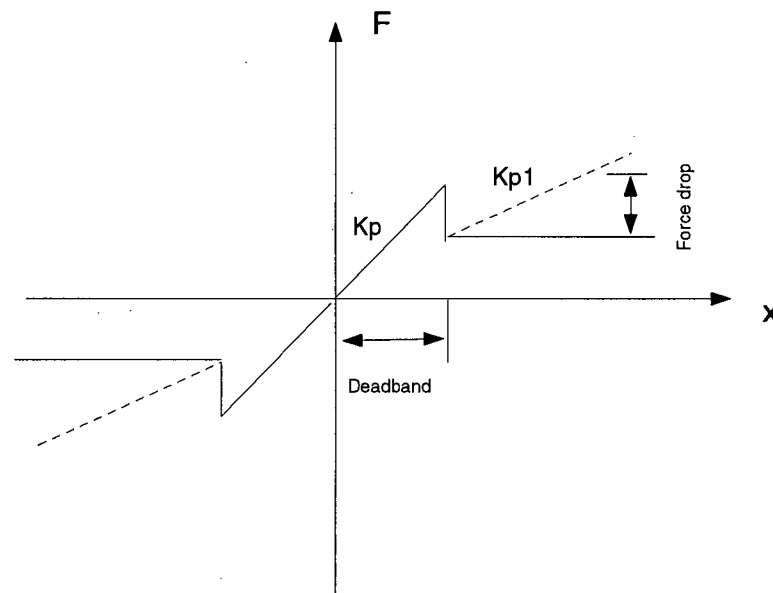


Figure 6.51 Detent implementation

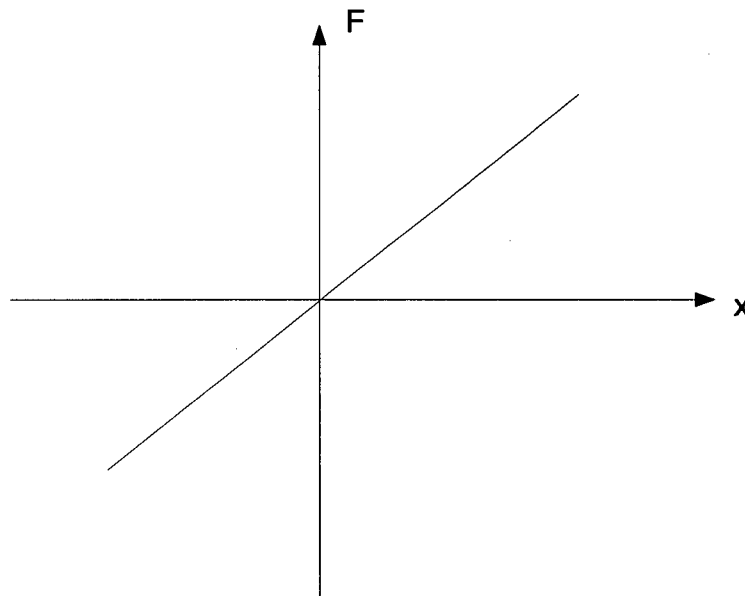


Figure 6.52 Conventional position control

For conventional position control (see Figure 6.52), the restoring force is a linear function of the position error. The bigger the position error, the higher the restoring force. In detent implementation, there are two slopes. Within the joystick position deadband, it is the same as the single slope approach. Outside this band, it has another slope which is lower than the first one. At the edge of the band, there is fixed amount of force drop. Clearly with this detent scheme, we can achieve high stiffness within the position deadband (desirable when machine travels) without having a high restoring force during normal operation which is outside the deadband. An operator can feel a “notch” when the joystick crosses the edge of the deadband. This is a good hint to the operator as to which area he is working in. As a result, decoupling between axes is achieved to a certain degree. Experiments show reduced restoring force outside the deadband makes normal operation easy which in turn reduces undesired motion in other axes.

	X	Y	Z	X Rotation	Y Rotation	Z Rotation
Force Drop	2.00 (N)	2.00 (N)	2.00 (N)	0.8 (NM)	0.8 (NM)	0 (NM)
Kp	4.0	3.0	4.0	0.45	0.45	0.25
Kp1	0.3	0.3	0.4	0.03	0.03	0.25

Table 6.11 Detent parameters for the feller-buncher experiments

In the above table, the units for stiffness are N/mm for translation and 100 Nm/rad for rotation

6.3.1 Desired Force Tracking

This experiment aimed to investigate the difference between teleoperation with and without force reflection in controlling the end point force. During the experiment, the operator controlled the machine inside the cabin. The contact force was collected and displayed on a computer screen to provide additional guide to the operator. First, the operator commanded the machine under stiffness feedback to contact a solid rock and tried to follow a desired force trajectory displayed to him as a graph on the computer screen shown in Figure 6.53. Next, the operator repeated the same experiment except that there was no force reflection present, see Figure 6.54. Experiments indicate that it is very hard to track a desired force trajectory without the use of force reflection. The results clearly demonstrate that the addition of force reflection to the teleoperator system greatly improves the ability of the operator to control the endpoint force.

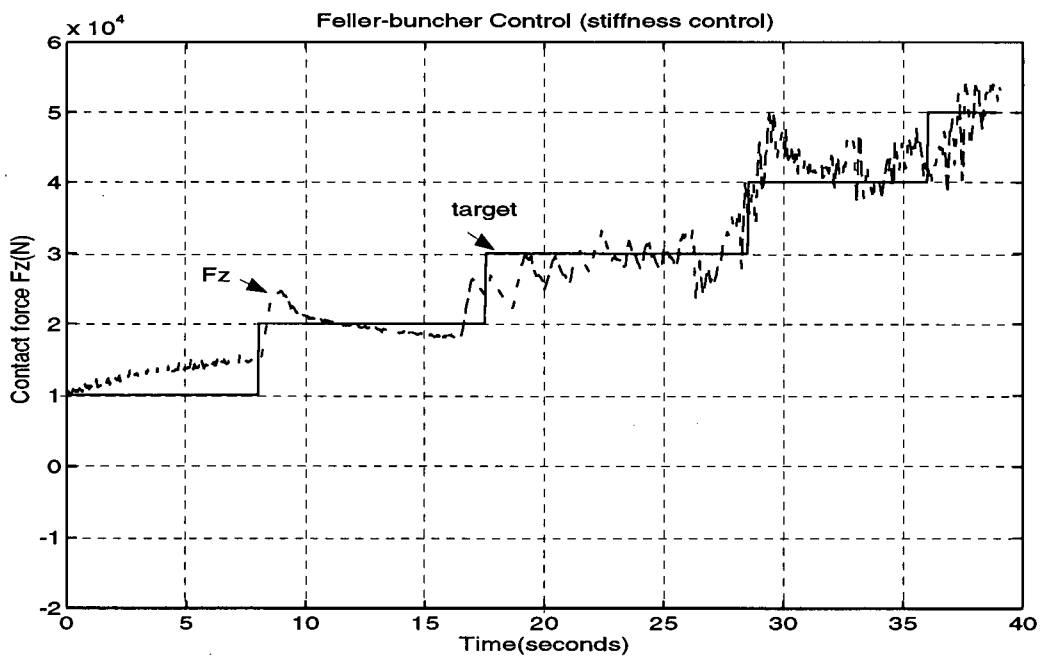
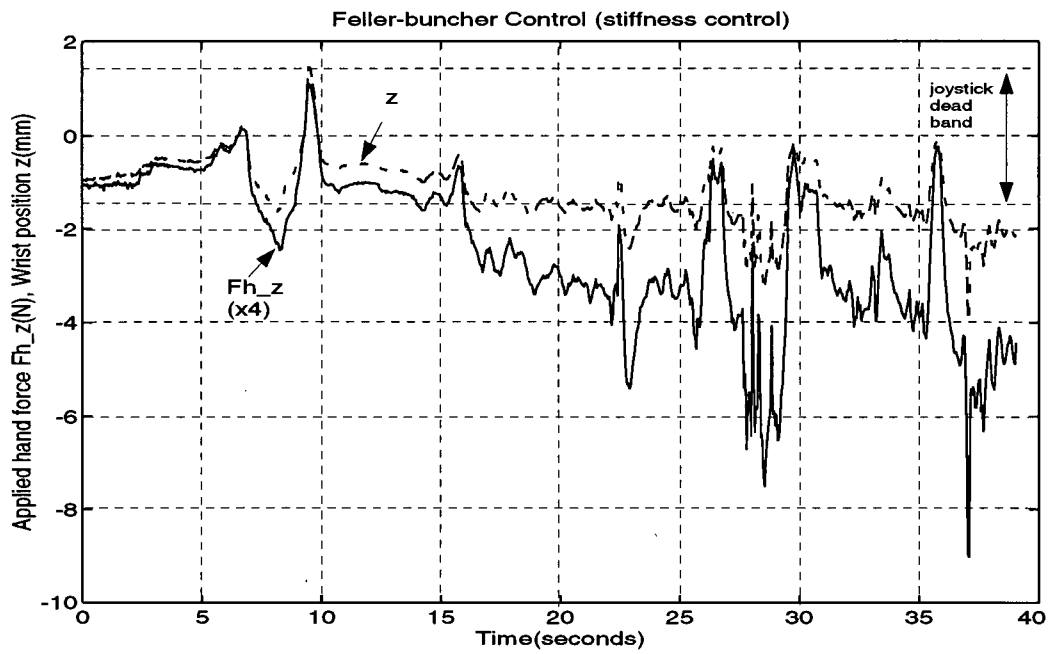


Figure 6.53 Feller-buncher stiffness control: force tracking

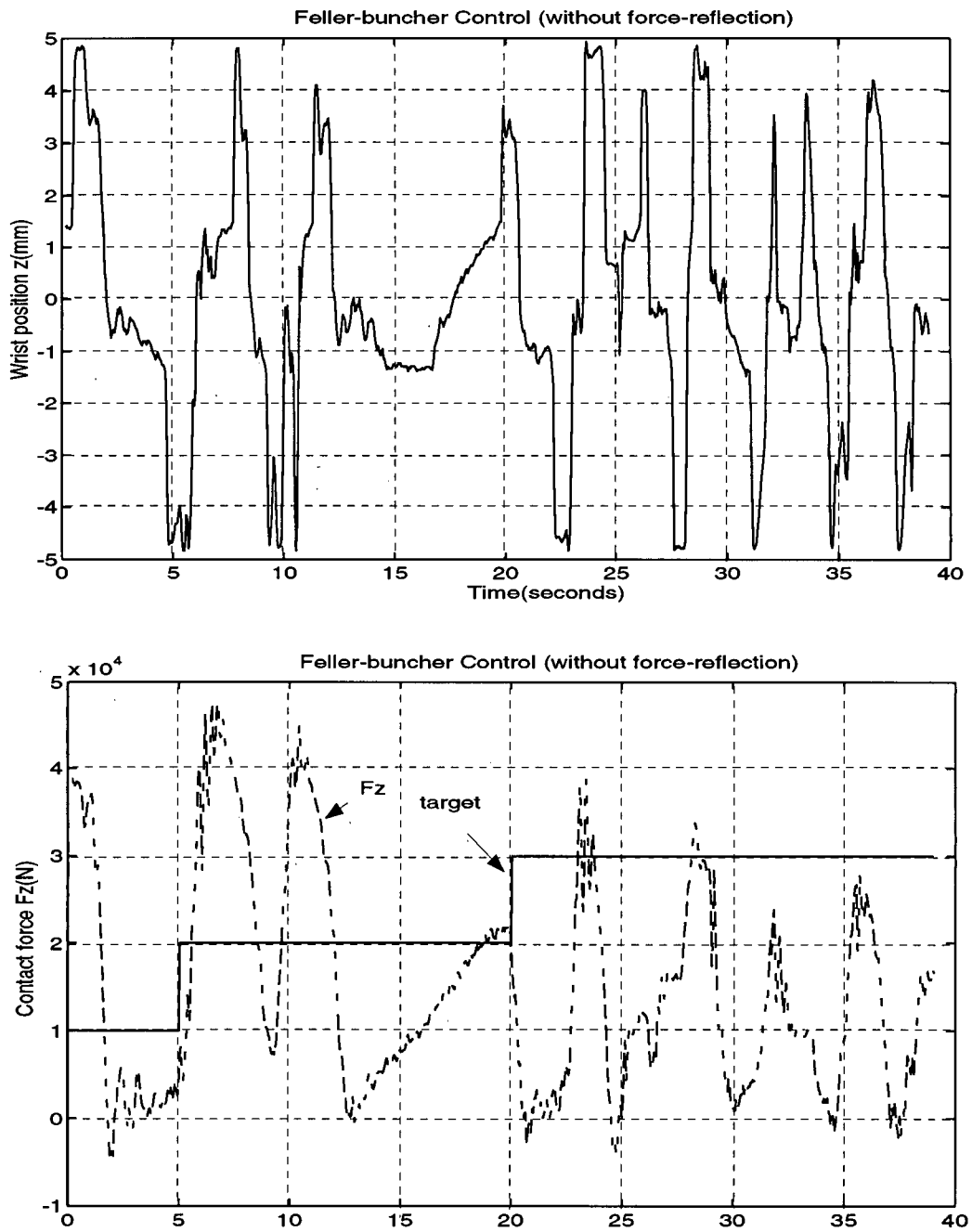


Figure 6.54 Feller-buncher control without force-reflection: force tracking

6.3.2 Complete Tree Cutting Process

Quantitative data for complete tree cutting process is shown in Figure 6.55. The operator first commanded the felling-head of the feller-buncher to approach a tree. The endpoint force increased rapidly after contact with the tree was made. Through the change of stiffness of the joystick, the operator could feel this contact kinesthetically, see the hand applied force (which is approximated by the centering force of the joystick) in Figure 6.55. While this was happening, the rotating saw started cutting the tree, and the grab arm on the felling-head closed and grabbed it. The cut tree was then laid to the side in bunches.

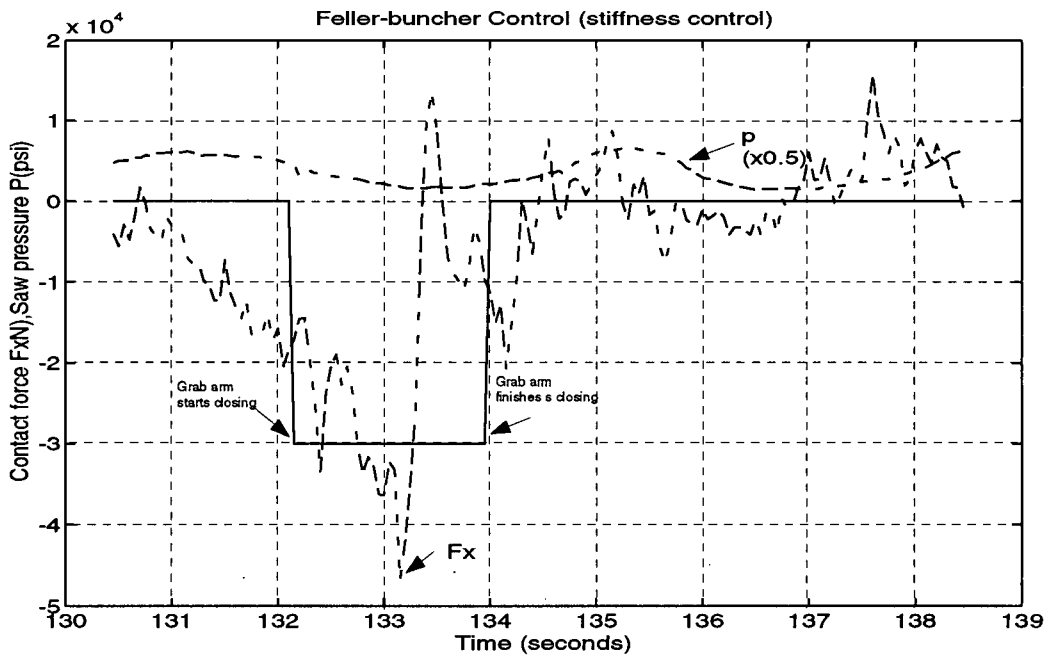
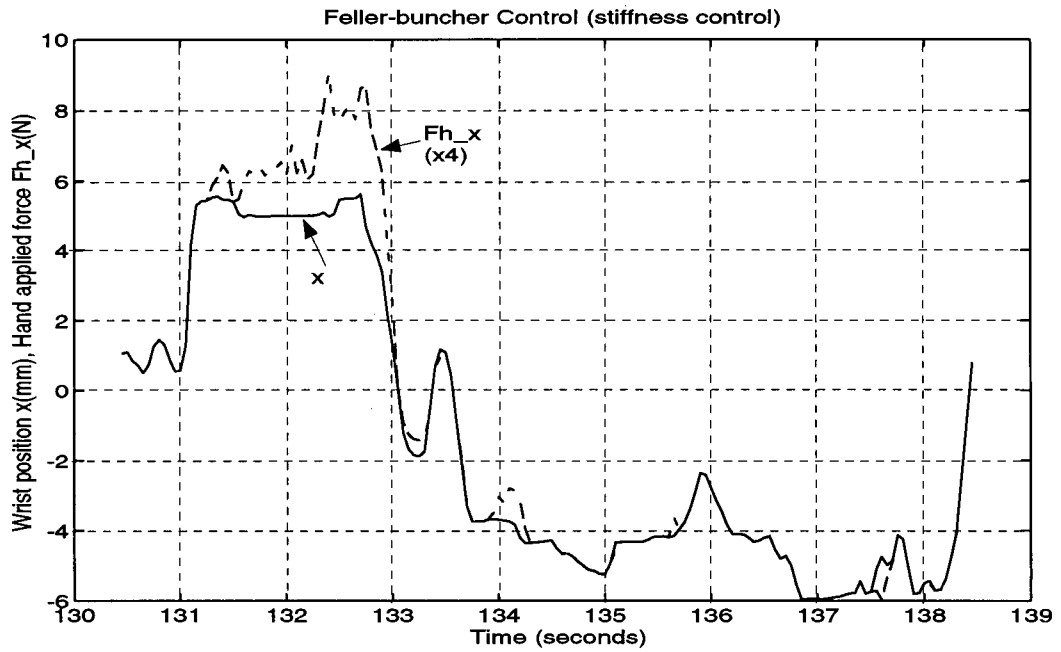


Figure 6.55 Feller-buncher stiffness control: tree cutting process

6.3.3 Practical Issues

For simplicity, only the static models of the manipulators were used for force computation. During free motion, the joint torques caused by the manipulators dynamics can introduce big computed-force error. Figure 6.56 — Figure 6.58 show the joint step responses of the feller-buncher, from which we can see that huge hydraulic pressures oscillations during free motion. Clearly, the static model of the manipulator without considering the actuator dynamics is not enough. One option is to completely model the manipulator dynamics. This might be hard in practice as well because there is large amount of friction present in the system. Other methods, such as direct force sensing via load cells, as suggested in [3], were not pursued due to the lack of time. Although the force resolution is not ideal, the experiments show that force reflection did help the operator to control the endpoint force effectively.

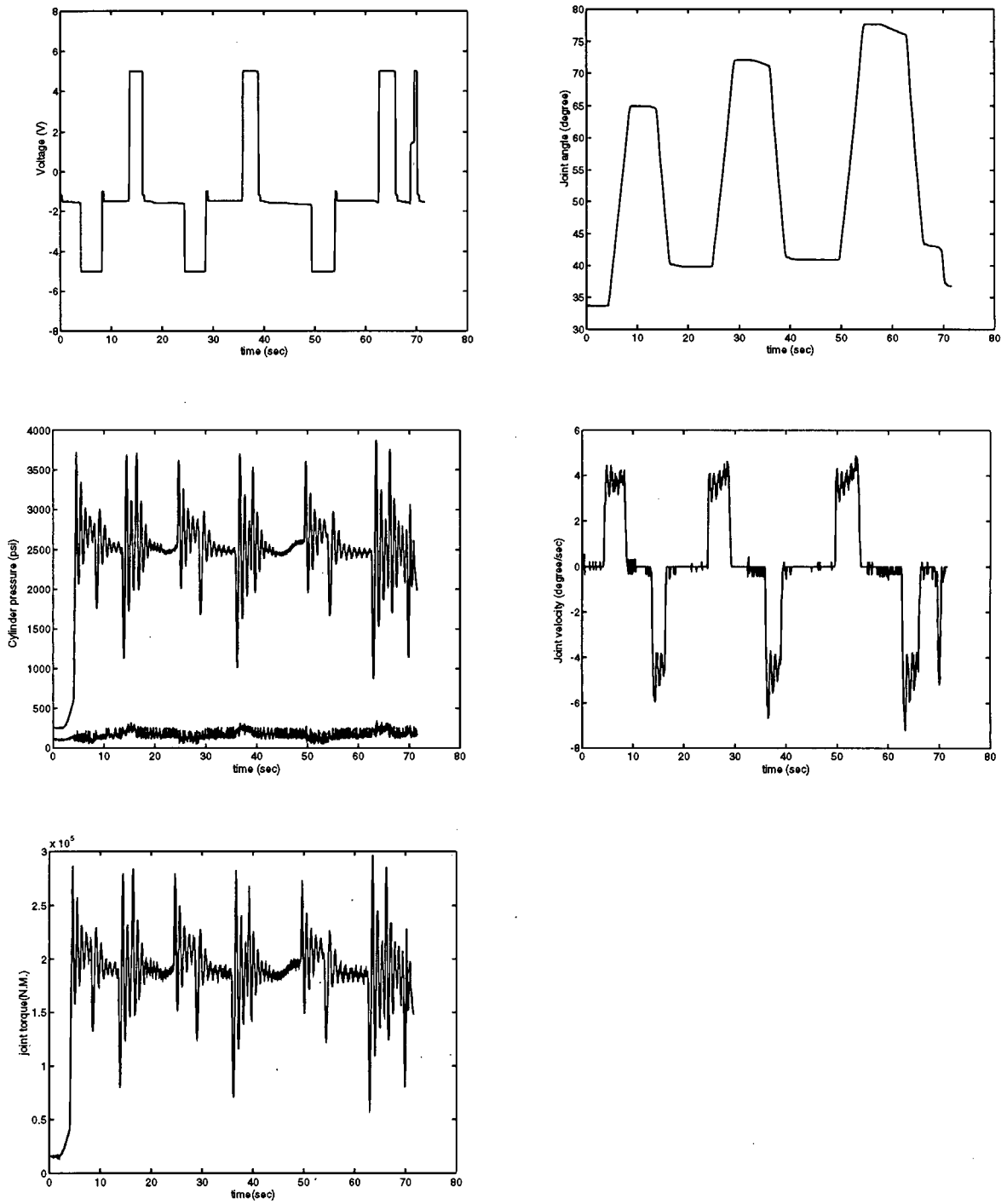


Figure 6.56 Feller-buncher step response: boom

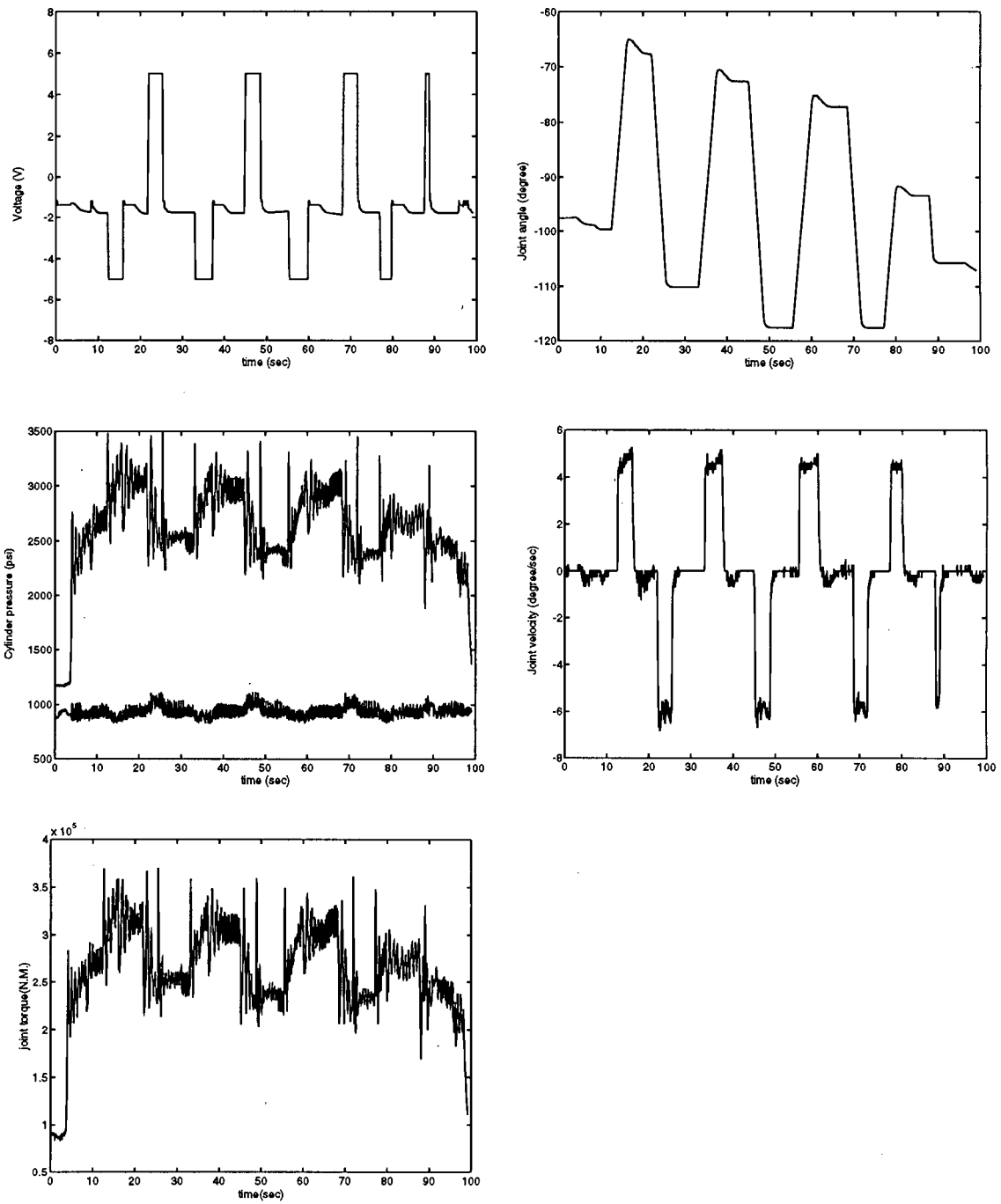


Figure 6.57 Feller-buncher step response: stick

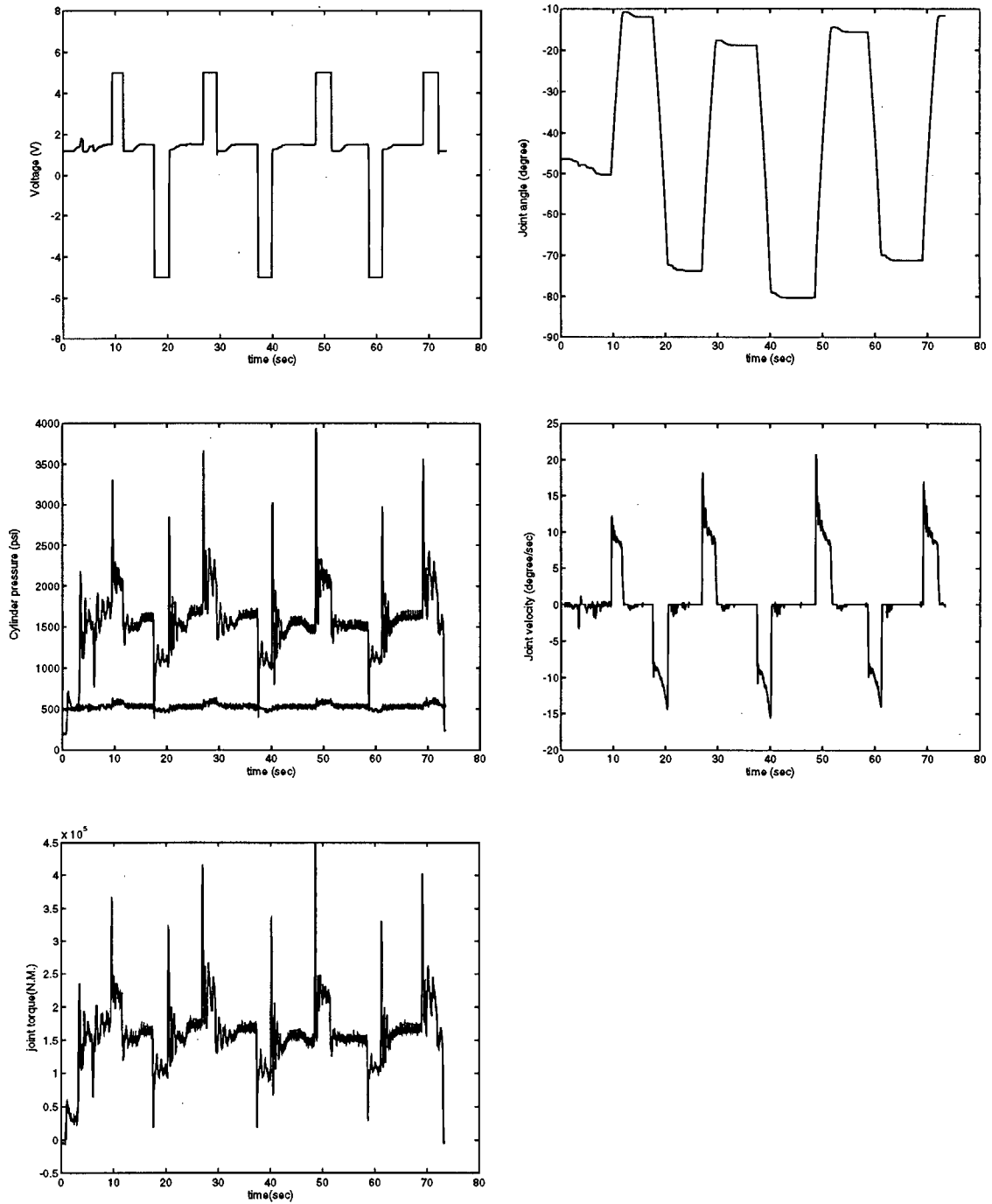


Figure 6.58 Feller-buncher step response: tilt

Chapter 7 Conclusions

Issues concerning the design and implementation of master-slave force-reflecting resolved motion control for hydraulic mobile machines are addressed in this thesis. A six DOF magnetically levitated joystick is employed as the teleoperator master which proves ideal for the application of force reflection. Machine experiments show rate control is preferable to position control for slow response slave manipulators such as excavators and feller-bunchers. Gravity torque cancellation for end-effector force sensing is effective, but not complete. The dynamic model of the manipulator is needed in order to eliminate the dynamic torque, especially during free motion. While direct force feedback under rate control can easily introduce instability, stiffness feedback provides a promising way in controlling the endpoint force.

7.1 Thesis Contributions

The major contributions of this thesis are as follows:

1. A new control structure is proposed to achieve “transparency” for teleoperator system under rate control.
2. A novel approach to stability analysis of the stiffness feedback strategy proposed in previous work is provided which, under certain condition, guarantees global asymptotic stability of the teleoperator system. The system could be either under rate or position control and could be subject to time-delay, nonlinearity and active environment.
3. Closed-form inverse kinematics solution of a five DOF manipulator — a feller-buncher — has been found to achieve resolved-motion of the manipulator’s end-effector within its workspace.

4. Remote Center of Compliance control was implemented for the Maglev Joystick.
5. Master-slave multi-axes force-reflecting resolved motion control was successfully implemented on a CAT-215 excavator and a CAT-325 feller-buncher. Machine experiments were carried out to demonstrate the ability to control forces using stiffness feedback.

7.2 Further Work

Present force resolution through pressure sensing is limited. It could be improved by either complete modeling of the manipulator's dynamics or using different force sensing technique such as load cells. Resolved motion control of the feller-buncher near the edge of workspace needs further study. Implementation of the proposed rate control structure which aims to achieve transparency needs to be carried out.

References

- [1] *STS-7 Press Information*. Rockwell International, 1983.
- [2] H. Kazerooni, "Human/robot interaction via the transfer of power and information signals: Parts i and ii," in *Proceedings of the IEEE International Conference on Robotics and Automation*, (Scottsdale, Arizona), pp. 1632-1649, 1989.
- [3] N. R. Parker, "Application of force feedback to heavy duty hydraulic machines," Master's thesis, University of British Columbia, October 1992.
- [4] P. D. Lawrence, B. Sauder, U. Wallersteiner, and J. Wilson, "Teleoperation of forest harvesting machines," in *Robotics in Forestry*, (Vaudreuil, Quebec), pp. 36-39, September 1990.
- [5] R. C. Goertz and Thompson, "Electrically controlled manipulator," *Nucleonics*, pp. 46-47, 1954.
- [6] N. M. Wong, "Implementaion of a force-reflection telerobot system with magnetically levitated master and wrist," Master's thesis, University of British Columbia, December 1992.
- [7] J. Jansen, R. Kress, and S. Babcock, "Controller design for a force-reflecting teleoperator system with kinematically dissimilar master and slave," *Robotics Research, ASME*, vol. 26, 1990.
- [8] W. S. Kim, F. Tendick, S. R. Ellis, and L. W. Stark, "A comparison of position and rate control for telemanipulations with consideration of manipulator system dynamics," *IEEE Tr. Robotics and Automation*, vol. RA-3, pp. 426-436, October 1987.
- [9] A. M. Sabatini, M. Bergamasco, and P. Dario, "Force feedback-based telemicromanipulation for rbot surgery on soft tissues," in *IEEE Engineering in Medicine and Biology Society 11th Annual Internatinal Conference*, 1989.
- [10] J. Yan, "A motion-scaling force-reflecting teleoperation system for microsurgery," Master's thesis, University of British Columbia, March 1994.
- [11] S. Lee and H. S. Lee, "An advanced teleoperator control system: Design and evaluation," in *Proceedings of the IEEE International Conference on Robotics and Automation*, (Nice, France), May 10-15 1992.
- [12] Y. Strassberg, A. A. Goldenberg, and J. K. Mills, "A new control scheme for bilateral teleoperation," *Robotics Research, ASME*, vol. 26, 1990.
- [13] B. Hannaford and R. Anderson, "Experimental and simulation studies of hard contact in force reflection teleoperation," in *IEEE International Conference on Robotics and Automation*, p. 584, 1988.
- [14] S. E. Salcudean, N. M. Wong, and R. L. Hollis, "Design and control of a force-reflecting teleoperation system with magnetically levitated master and wrist." August 26 1993.

- [15] R. J. Anderson and M. W. Spong, "Bilateral control of teleoperators with time delay," *IEEE Tr. Automatic Control*, vol. 34, pp. 494-501, May 1989.
- [16] C. A. Lawn and Blake Hannaford, "Performance testing of passive communication and control in teleoperation with time delay," in *Proceedings of the IEEE International Conference on Robotics and Automation*, vol. 13, 1993.
- [17] W. S. Kim, B. Hannaford, and A. K. Bejczy, "Force-reflection and shared compliant control in operating telemanipulators with time delay," *IEEE Tr. Robotics and Automation*, vol. 8, pp. 176-185, April 1992.
- [18] B. Hannaford, "Stability and performance tradeoffs in bi-lateral telemanipulation," in *Proceedings of the IEEE International Conference on Robotics and Automation*, pp. 1764-1767, 1989.
- [19] B. Hannaford, "A design framework for teleoperators with kinesthetic feedback," *IEEE Transactions on Robotics and Automation*, vol. 5, no. 4, 1989.
- [20] G. J. Raju, G. C. Verghese, and T. B. Sheridan, "Design issues in 2-port network models of bilateral remote teleoperation," in *Proceedings of the IEEE International Conference on Robotics and Automation*, pp. 1317-1321, 1989.
- [21] S. E. Salcudean, N. Wong, and R. Hollis, "A force-reflecting teleoperation system with magnetically levitated master and wrist," in *Proceedings of the IEEE International Conference on Robotics and Automation*, (Nice, France), May 10-15 1992.
- [22] D. A. Lawrence, "Designing teleoperator architecture for transparency," in *Proceedings of the IEEE International Conference on Robotics and Automation*, (Nice, France), May 10-15 1992.
- [23] Y. Yokokohji and T. Yoshikawa, "Bilateral control of master-slave manipulators for ideal kinesthetic coupling," in *Proceedings of the IEEE International Conference on Robotics and Automation*, (Nice, France), May 10-15 1992.
- [24] M. Ostoja-Starzewski and M. J. Skibniewski, "A master-slave manipulator for excavation and construction tasks," *Robotics and Autonomous Systems*, pp. 333-337, 1989.
- [25] R. Langreth, "Smart shovel," *Popular Science*, pp. 82-84, 108-109, 1992.
- [26] U. Wallersteiner, P. Stager, and P. Lawrence, "A human factors evaluation of teleoperator hand controllers," in *Proceeding of International Symposium Teleoperation and Control*, pp. 291-296, IFS Ltd., July 1988.
- [27] K. Sugimoto and J. Duffy, "Analysis of five-degree-of-freedom robot arms," *Journal of Mechanisms, Transmissions, and Automation in Design*, vol. 105/23, 1983.
- [28] D. Manocha and J. F. Canny, "Real time inverse kinematics for general 6r manipulators," in *Proceedings of the 1992 IEEE International Conference on Robotics and Automation*, 1985.
- [29] T. Yih and Y. Youm, "Matrix solution for the inverse kinematics of robots,"
- [30] A. A. Goldenberg, B. Benhabib, and R. G. Fenton, "A complete generalized solution to the inverse kinematics of robots," *IEEE Journal of Robotics and Automation*, vol. RA-1, no. 1, 1985.

- [31] A. Goldenberg and D. Lawrence, "A generalized solution to the inverse kinematics of robotic manipulators," *Journal of Dynamic Systems, Measurement, and Control*, vol. 107/103, 1985.
- [32] B. Hannaford, "Scaling, impedance and power flows in force reflecting teleoperation," *Robotics Research, ASME*, vol. 26, 1990.
- [33] C.-T. Chen, *Linear System Theory and Design*. CBS College Publishing, 1984.
- [34] R. L. Hollis, S. Salcudean, and A. P. Allan, "A six-degree-of-freedom magnetically levitated variable compliance fine-motion wrist: Design, modeling and control," *IEEE Tr. Robotics and Automation*, vol. 7, pp. 320-332, June 1991.
- [35] P. J. Hacksel, "Observer based velocity and environment force estimation for rigid body control," Master's thesis, University of British Columbia, October 1993.
- [36] M. W. Spong and M. Vidyasagar, *Robot Dynamics and Control*. John Wiley and Sons, 1989.
- [37] N. Sepehri, *Dynamic Simulation and Control of Teleoperated Heavy-Duty Hydraulic Manipulators*. PhD thesis, University of British Columbia, September 1990.